SYSTEMS BIOLOGY DERIVED MECHANISM OF BMP GRADIENT FORMATION

Joseph Zinski

A DISSERTATION

in

Cell and Molecular Biology

Presented to the Faculties of the University of Pennsylvania

in

Partial Fulfillment of the Requirements for the

Degree of Doctor of Philosophy

2017

Supervisor of Dissertation

_____

Mary Mullins, PhD

Professor, Vice Chair for Cell Biology

Graduate Group Chairperson

_____

Daniel Kessler, PhD

Professor of Cell & Developmental Biology, Chair of Cell and Molecular Biology

Dissertation Committee

Steve DiNardo, Professor of Cell & Developmental Biology, DSRB Chair

John Murray, Assistant Professor of Genetics

Matt Good, Assistant Professor of Cell and Developmental Biology

Christopher Fang-Yen, Wilf Family Term Assistant Professor of Bioengineering (BE)

Acknowledgements

I would like to thank first and foremost my mentor Mary for her unwavering support and positivity. She truly cares about each student she mentors and goes out of her way to help us develop as scientists. Even when nothing was working in the lab, I never felt lost or alone.

Thank you to Sam Warrick and Dan Zhou for all of their time spent with the fish and running endless KASP reactions. You are both capable researchers in your own right and I have no doubt you will find success in whatever field you choose. A special thanks to Sam for her constant positive attitude and fish husbandry skills.

Thank you to all Mullins and Granato lab members past and present, but most especially James Dutko who taught me all I know about molecular biology. James taught me how to be a model lab citizen and citizen of the world. I would also like to mention Francesca Tuazon, my lab sibling, and Ben Tajer, my crazy lab cousin. I wish Allison, Hannah, and Robyn the best of luck carrying on the BMP torch. I would also like to thank Megumi Hashiguchi, Bettina Schmid, Hannah Bell, Camille Syrette, Melissa Baxter, and Yvette Langdon for never hesitating to lend a hand.

A special thanks to Dave Cobb for making the fish facility accessible to me and Amy Kugath for always being there to help. Thank you to the entire fish facility staff for keeping all of our fish alive every day.

I would like to thank Lynn Goodstein and Jennifer Lease-Butts for helping me return to my studies after my injury at UConn, Steven Geary and Ranjan Srivastiva for giving me a chance to work in their labs, Willy Lensch for believing in me, Richard White for showing me I could work with zebrafish.

Outside of the lab I have been so fortunate to have the constant support of my family. I can not begin to thank my mother Joanne, father Ed, and sister Allison for the rides to conferences, help with supplies and emergencies, emotional support, and love. I would like to thank my uncle Joe for his constant interest in my work, emotional and financial support, and love. I would like to thank my grandfather Louis and grandmother Emma, who nurtured and celebrated my curious mind since the day I was born, and gave themselves whole-heartedly to myself and my family. I would also like to thank my other half Jasmin, whose presence in my life brings me joy every day. Without them, my journey this last 12 years would not have been possible.

I have also been fortunate to have the support of so many friends here who enrich my life with their intelligence, creativity, and humor. Thank you Alan, Scott, Will, Alex, Seth, Logan, Betsy, Jason, and Michael for the years of gaming and fun. Thank you to the Wednesday night crew, especially Julie, Samantha, Celine, and Lee for making Wednesday the best day of the week for 5+ years. I would especially like to thank Janelle for her friendship. She was and remains one of the most self-less and steady people I have ever met. She was the first person I met here and the hardest one to say goodbye to.

Finally, I would be remiss if I did not mention the aide I received from so many nursing students here at Penn, who helped keep my life running behind the scenes. Their compassion is a constant reminder to me of one of my favorite quotes by Albert Einstein:

> "A hundred times every day I remind myself that my life depends on the labors of others, living and dead, and that I must exert myself in order to give in the same measure as I have received and am still receiving…"

ABSTRACT

SYSTEMS BIOLOGY DERIVED MECHANISM OF BMP GRADIENT FORMATION

Joseph M. Zinski

Mary C. Mullins

A morphogen gradient of Bone Morphogenetic Protein (BMP) signaling patterns the dorsoventral (DV) axis of all vertebrates. This gradient is established by the extracellular interaction of the asymmetric expression of the BMP ligand and its extracellular regulators. Though the basic agonism and antagonism of BMP by these regulators has been established over the last two decades, the mechanism by which they come together to form a robust BMP signaling gradient remains poorly understood. The prevailing view in vertebrates for BMP gradient formation is through a counter gradient of BMP antagonists, often along with ligand shuttling to generate peak signaling levels. To delineate the mechanism in zebrafish, I created a quantitative method of measuring BMP signaling, and used it to precisely quantify the BMP activity gradient in wild-type and mutant embryos. We combined these data with a computational model-based screen to test hypotheses for gradient formation. Surprisingly, the analysis did not support a counter-gradient mechanism and rules out both a BMP shuttling mechanism, and a *bmp* transcriptionally-informed gradient mechanism. Instead a fourth model emerged, a source-sink mechanism, which relies on a restricted BMP antagonist distribution acting as a BMP sink that drives BMP diffusion and gradient formation. We measured Bmp2 diffusion and found that it supports the source-sink model, suggesting a new mechanism to shape BMP gradients during development. We have developing a way to quantify the BMP signaling gradient, a mathematical model incorporating the core extracellular BMP

regulators, and mathematical definitions for the different gradient mechanisms. In doing so, we have opened the door for future studies to add in additional BMP regulators to the model such as Bmper, Twisted Gastrulation and Sizzled, to identify and measure key biophysical parameters, and to address questions about how cells sense a BMP morphogen gradient and translate that signal into target gene expression.

Table of Contents

List of Figures

List of Tables

Preface

Our lab has been fortunate to have a productive collaboration with the lab of Dr. David Umulis from Purdue who I have worked with closely throughout the development of the story in Chapter 2. Notable contributions from Dr. Umulis and his lab members have been in the initial MATLAB implementation of a solver for the system of partial differential equations used for all of Chapter 2 by Wei Dou, using Coherent Point Drift to align embryos by Wei Dou, the fluorescent in situ for bmp2b done by Xu Wang, and the FRAP experiment for BMP-Venus done by Ye Bu.

We are currently collaborating with Tanya T. Whitefield on the development of the Bmper story in Chapter 3. Dr. Whitfield was responsible for bringing the ear defect in *bmper* mutant alleles to our attention, but I generated all data presented here-in.

Chapter 1: The extracellular regulation of BMP morphogen gradients

Subsection 1.1: Morphogen Gradients

Morphogen gradients pattern axonal pathways, the neural tube, the dorsal-ventral (DV) and anterior-posterior (AP) embryonic axes, as well as multiple organ systems (Bokel and Brand 2013, Briscoe and Small 2015, Cohen et al. 2013, Rogers and Schier 2011, Rushlow and Shvartsman 2012, Sansom and Livesey 2009, Schilling et al. 2012, Tuazon and Mullins 2015). Morphogens are defined as factors that form a spatially non-uniform distribution spanning multiple cell-lengths that instructs different cell fates at distinct levels. Their importance in specifying multiple cell fates in a gradient has spurred decades of research deciphering how they work. In 1970, Francis Crick proposed that such a gradient could be formed by a source of morphogen flowing to a sink that destroyed it (Crick 1970). We now know that the mechanisms by which morphogen gradients are established are diverse and complex, and that understanding these mechanisms is paramount to understanding developmental biology (Briscoe and Small 2015, Muller et al. 2013, Rogers and Schier 2011). Bone Morphogenetic Proteins (BMPs) act as morphogens repeatedly during development, including in patterning the embryonic DV axis, the neural tube, and the *Drosophila* wing disc (Bier and De Robertis 2015, Briscoe and Small 2015, Rogers and Schier 2011).

A morphogen gradient of BMP signaling patterns the dorsal-ventral (DV) axis of all vertebrates (Fig. 1.1) (Gourronc et al. 2007, Robertis 2008). Axis patterning in mice takes place from about E5.5-E8.5, 5 days after the transition from maternal to zygotic transcription (Beddington and Robertson 1999). In contrast, the DV axis of zebrafish is

patterned between 4 and 12 hours after fertilization, just hours after the initiation of zygotic trascription (De Robertis and Kuroda 2004, Schier and Talbot 2005, Tucker et al. 2008). In vertebrates, high levels of BMP signaling induce ventral tissue fates (such as epidermis and blood), intermediate levels induce lateral tissue (such as neural crest), while BMP signaling must be blocked for dorsal tissue development (such as notochord, hindbrain, and prechordal plate) (De Robertis and Sasai 1996, Little and Mullins 2006, Schier and Talbot 2005). It is postulated that cells all along the gradient sense the amount of BMP signal, which determines their DV tissue fate. Known to be directly activated by BMP signaling during DV patterning are *msx1b* (Esteves et al. 2014, Maeda et al. 1997, Tribulo et al. 2003), *p63* (Bakkers et al. 2002), *foxi1* (Hans et al. 2007), *XVent2* (Hata et al. 2000, Henningfeld et al. 2002, Karaulanov et al. 2004, Lee et al. 2002, Schuler-Metz et al. 2000), *XVent1* (Lee et al. 2011), *bambi* (Karaulanov et al. 2004), *tsg* (Karaulanov et al. 2004), *bmpr2* (Karaulanov et al. 2004), *smad6* (Karaulanov et al. 2004) and *smad7* (Karaulanov et al. 2004), and there are likely more yet to be identified.

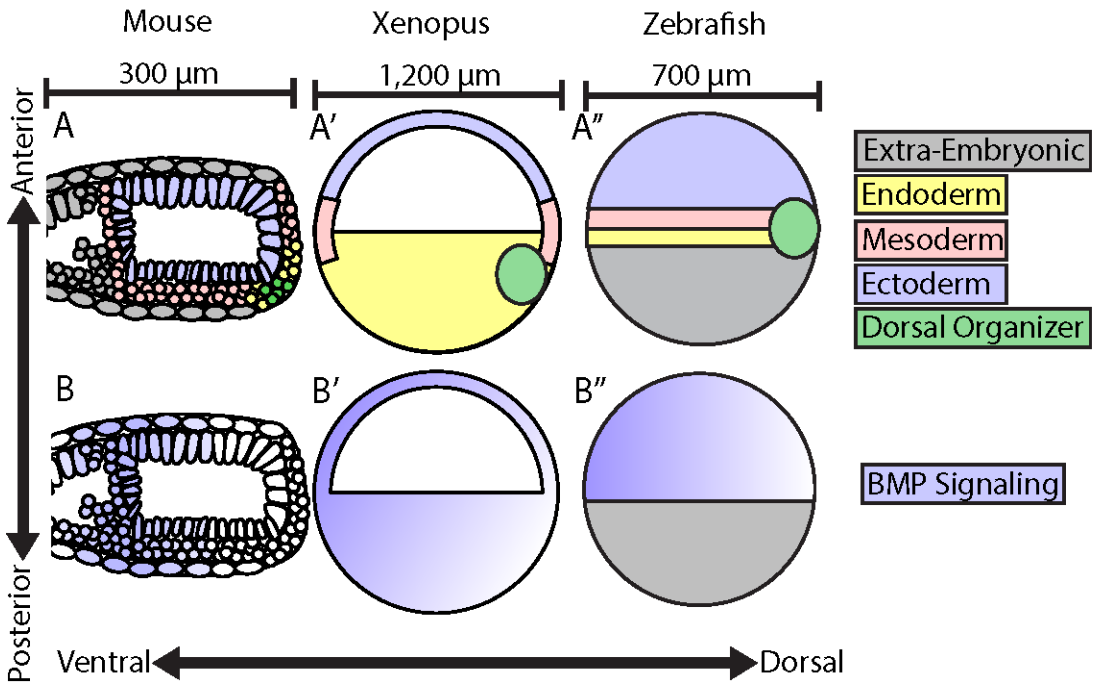

Figure 1.1: BMP signaling during vertebrate DV patterning. Lateral views of embryos at the onset of gastrulation during DV patterning (mouse embryos at E7.5, Xenopus embryos at stage 10, and zebrafish embryos at shield stage). (A-A') Location of the germ layers and dorsal organizer in each organism, (B-B') An approximation of the BMP signaling gradient in each organism.

It is unclear whether DV cell fate is specified by different thresholds of BMP signaling, different durations of BMP signaling, or some combination of the two. It is also unclear how many distinct domains/signaling thresholds are patterned by the gradient of BMP signaling. Deciphering these mechanisms has been hindered by the lack of quantitative measurements of BMP signaling and BMP target gene expression taken to date. The BMP signaling gradient has been visualized using antibodies against phosphorylated Smad5 in mouse (Di-Gregorio et al. 2007), zebrafish (Hashiguchi and

Mullins 2013, Ramel and Hill 2013, Tucker et al. 2008, Xue et al. 2014), and Xenopus (Cho et al. 2013, Kurata et al. 2001, Plouhinec et al. 2013, Schohl and Fagotto 2003) embryos, but these visualizations have only been qualitative. The development of quantitative readouts for target gene expression and BMP signaling could reveal how the BMP target genes read and respond to the BMP signaling gradient.

Subsection 1.2: The extracellular regulation of BMP signaling

The BMP signaling gradient is established by the asymmetric expression of BMP ligands, agonists, and antagonists, while the expression of the BMP receptors and *smads* are ubiquitous. In mouse, zebrafish, and Xenopus, the majority of the BMP ligands are expressed ventrally while the majority of the extracellular antagonists are expressed dorsally near and in the dorsal organizer (Fig. 1.2A) (Carron and Shi 2016, Kishigami and Mishina 2005, Little and Mullins 2006, Niehrs 2004). Also referred to as the Spemann-Mangold organizer in Xenopus and zebrafish or the Node in mouse, the dorsal organizer is the region where gastrulation movements begin. The dorsal organizer expresses a common suite of extracellular BMP antagonists and transcriptional repressors essential to repressing BMP signaling in the dorsal region of the embryo (Niehrs 2004, Nieto 1999, Thisse and Thisse 2015). BMP antagonists such as Chordin, Noggin, and Follistatin bind to BMP ligands in the extracellular space, preventing BMP signaling dorsally. These antagonists are opposed by the ventrally expressed metaloproteases Tolloid and Bmp1a, which cleave Chordin and release BMP ligand. A complicated network of other extracellular proteins regulate antagonist binding and decay, including Bmper, Tsg, Ont1, Sizzled, and Crescent, and these interactions are covered in detail in this section (Fig. 1.2A).

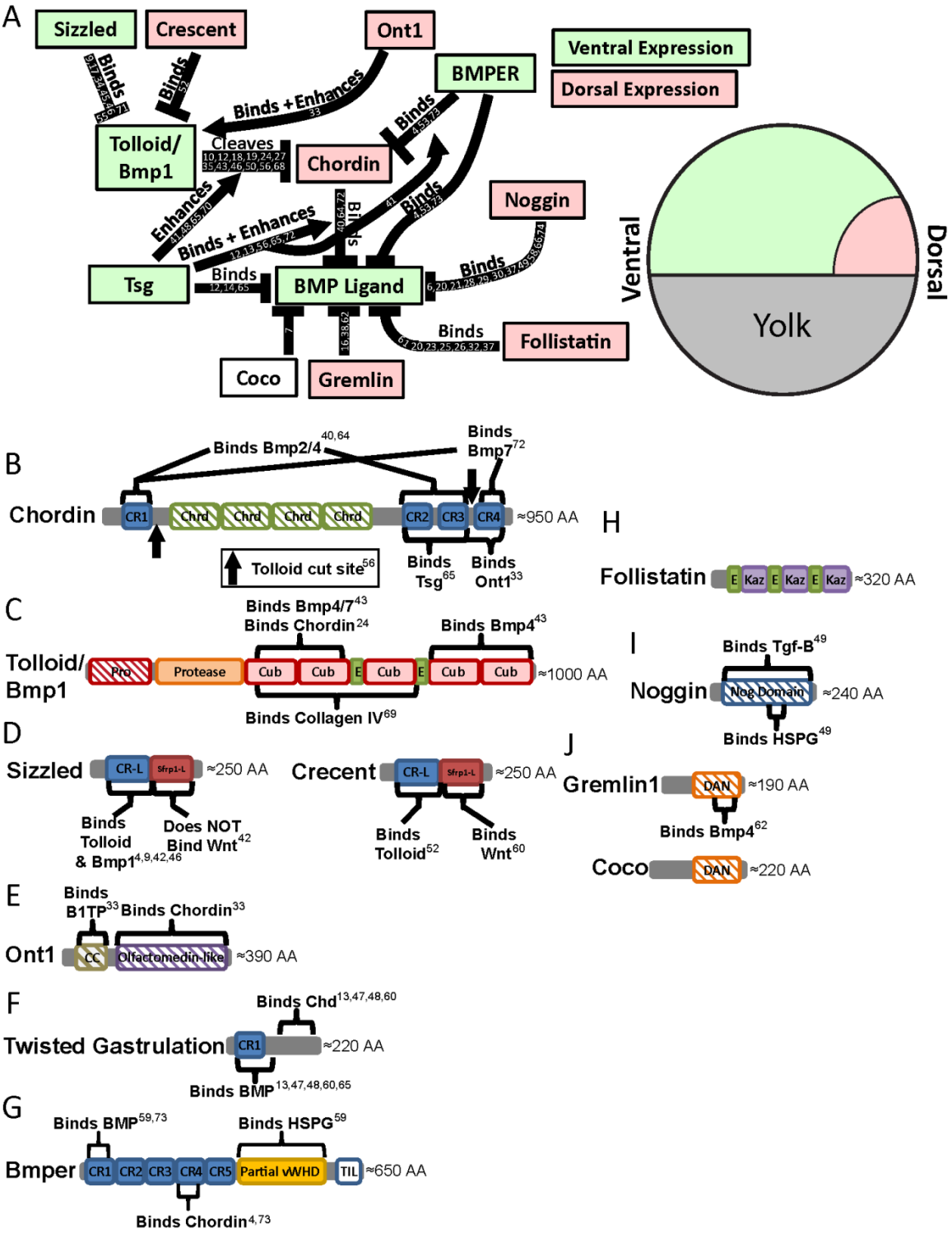

Figure 1.2: Extracellular agonism and antagonism of BMP and Nodal during axis patterning. *A*) References supporting and defining agonism and antagonism listed next

to each connector. Expression domain of each species during axis patterning denoted by box color. B) Conserved domains of each agonist and antagonist along with known binding domains. Note that additional known binding partners that don't have a known binding domain determined by a structure-function analysis may exist. References to structure-function analysis shown for each binding domain. AA=Amino acid, CR=Cystine-rich domain, Pro=Pro-domain, CC=Coil-coil domain, DAN=Differentially screening-selected gene Arbitrative in Neuroblastoma domain, Olfactomedin= Olfactomedin domain, TM=TransMembrane domain, Partial vWHD=Von Willebrand factor type D domain, Kaz=Kazal domain family Follistatin module, E=EGF domain, CUB= complement C1r/C1s-sea urchin epidermal growth factor-BMP1, Protease= Protease, Nog domain=Noggin domain, Sfrp-1L=secreted frizzled-related protein domain, Chrd=Chordin domain, TgfB-L=Tgf-B-Like domain, TIL= typsin inhibitor-like cysteine-rich domain.

References: 1. (Agius et al. 2000) 2. (Aykul and Martinez-Hackert 2016) 3. (Aykul et al. 2015) 4. (Ambrosio et al. 2008) 5. (Bates et al. 2013) 6. (Bayramov et al. 2011) 7. (Bell 2003) 8. (Belo et al. 2000) 9. (Bijakowski et al. 2012) 10. (Blader 1997) 11. (Blitz et al. 2000) 12. (Blitz et al. 2003) 13. (Chang C. et al. 2001b) 14. (Chang Chenbei et al. 2003) 15. (Chen and Shen 2004) 16. (Church et al. 2015) 17. (Collavin 2003) 18. (Connors SA. et al. 1999) 19. (Connors S. A. et al. 2006) 20. (Dal-Pra et al. 2006) 21. (Degenkolbe et al. 2013) 22. (Feldman et al. 2002) 23. (Geng et al. 2011) 24. (Geach and Dale 2008) 25. (Glister et al. 2004) 26. (Glister et al. 2015) 27. (Goodman et al. 1998) 28. (Jay Groppe and Affolter 1998) 29. (Groppe et al. 2002) 30. (Groppe et al. 2003) 31. (Harms and Chang 2003) 32. (Iemura et al. 1998) 33. (Inomata et al. 2008) 34. (Inomata et al. 2013)

35. (Jasuja et al. 2006) 36. (Katsu et al. 2012) 37. (Khokha M. K. et al. 2005) 38. (Kisonaite et al. 2016) 39. (Larrain et al. 2000) 40. (Larrain et al. 2000) 41. (Larrain et al. 2001) 42. (Lee et al. 2006) 43. (Lee et al. 2009) 44. (Marques et al. 2004) 45. (Miller-Bertoglio et al. 1999) 46. (Muraoka et al. 2006) 47. (Oelgeschlager et al. 2000) 48. (Oelgeschlager 2003) 49. (Paine-Saunders et al. 2002) 50. (Stefano Piccolo Eric Agius, Bin Lu, Shelley Goodman, Leslie Dale, and Eddy M. De Robertis 1997) 51. (Piccolo et al. 1999) 52. (Ploper et al. 2011) 53. (Rentzsch et al. 2006) 54. (Cha et al. 2006) 55. (Salic et al. 1997) 56. (Scott et al. 1999) 57. (Scott et al. 2001) 58. (Seemann et al. 2009) 59. (Serpe et al. 2008) 60. (Shibata et al. 2005) 61. (Sidis et al. 2006) 62. (Sun et al. 2006) 63. (Tanegashima et al. 2004) 64. (Troilo et al. 2014) 65. (Troilo et al. 2016) 66. (Viviano et al. 2004) 67. (Vonica and Brivanlou 2007) 68. (Wardle et al. 1999) 69. (Winstanley et al. 2015) 70. (Xie and Fisher 2005) 71. (Yabe T. 2003b) 72. (Zhang J. L. et al. 2007a) 73. (Zhang J. L. et al. 2010) 74. (Zimmerman et al. 1996) 75. (Cheng et al. 2004)

Name	BMP Agonist or Antagonist	Dorsal or Ventral Exression	Mechanism	Organism	Binding Affinities	Ref
Tolloid	Agonist	Ventral	Cleaves Chd	human, zebrafish, frog, mouse	[2]Bmp7=Binds [2]Bmp4≈ 20 nM [1]Chd≈10 nM [1]Szl=19 nM [3]Collagen IV=Binds	[1]Lee et al. 2006; [2]Lee et al. 2009; [3]Winstanley et al. 2015
Bmp1	Agonist	Ventral	Cleaves Chd	human, zebrafish, frog, mouse	[2]Bmp4=16 nM [1]Szl=14 nM [3]Ont1=Binds	[1]Bijakowsky et al. 2012; [2]Lee et al. 2009; [3]Inomata et al. 2008
BMP Ligands	Agonist	Ventral	Signals Through Type I and Type II Receptors to activate Smad1/5/8	human, zebrafish, frog, mouse	See Inhibitors [1]HSPG=Binds	[1]Jasuja et al. 2004
Twisted Gastrulation	Agonist and Antagonist	Ventral	Enhances chd cleavage by Tld/Bmp1a; Enhances the binding of Chd to BMP; Binds and inhibits BMP; Has another yet-unknown Chd-independent BMP agonist function	human, zebrafish, frog, mouse	[1]Bmp7=28 nM [2,3]Bmp4=2.5 nM [1]Bmp2=50 nM [1]Gdf5=53 nM [5]HSPGs=NB [2,3,6]Chd=3 nM [4]Bmper=Binds [6]Tld=NB	[1]Zhang et al. 2007; [2]Oelgeschlager et al. 2000, 2003; [3]Chang et al. 2001; [4]Ambrosio et al. 2008; [5]Jasuja et al. 2004; [6]Troilo et al. 2016
Bmper	Agonist and Antagonist	Ventral	Binds and Inhibits Chd; Binds and inhibits BMP	human, zebrafish, frog, mouse	[7]Bmp9=Binds [2,5]Bmp7=3.5-7 nM [1,2]Bmp4=2.0 nM [2,4,5]Bmp2=1.2-22 nM [1,2,4]Chd=1.4-175 nM [2,3]HSPGs=Binds [5]Gdf5=34 nM [6]LRP1=Binds [1]Tsg=Binds	[1]Ambrosio et al. 2008; [2]Rentzsch et al. 2006; [3]Serpe et al. 2008; [4]Zhang et al. 2010; [5]Zhang et al. 2007; [6]Pi et al. 2012; [7]Yao et al. 2012;
Sizzled	Antagonist	Ventral	Inhibits Chd Cleavage by Tld/Bmp1a	zebrafish, frog	[1]Bmp1=14 nM [2]Tld=19 nM	[1]Bijakowsky et al. 2012; [2]Lee et al. 2006;
ADMP	Agonist	Dorsal	Signals Through Type I and Type II Receptors to activate Smad1/5/8	zebrafish, frog	See Inhibitors	

Name	BMP Agonist or Antagonist	Dorsal or Ventral Exression	Mechanism	Organism	Binding Affinities	Ref
Ont1	Agonist and Antagonist	Dorsal	Enhances Chd cleavage by Tld/Bmp1; Binds to BMP ligand and Chd	Xenopus	[1]Chd=Binds [1]Bmp4=Binds	[1]Inomata et al. 2008
Chordin	Antagonist	Dorsal	Binds and Inhibits BMP	human, zebrafish, frog, mouse	[2,7]BMP7=8-46 nM [1,2,12]Bmp4=0.3-5.8 nM [3,7]BMP2=12-37 nM [4]Tld≈10 nM [3,5,6]Bmper=1.4-175 nM [8]HSPG=Binds [9]Tsg1=3 nM [10]Ont1=Binds [11]Integrins=Binds	[1]Picollo et al. 1996; [2]Trolio et al. 2014; [3]Rentzsch et al. 2006; [4]Lee et al. 2006; [5]Zhang et al. 2010; [6]Ambrosio et al. 2008;[7]Zhang et al. 2007; [8]Jasuja et al. 2004; [9]Troilo et al. 2016; [10]Inomata et al. 2008; [11]Larrain et al. 2000; [12]Larrain et al. 2003
Noggin	Antagonist	Dorsal	Binds and Inhibits BMP, Nodal, and Activin	human, zebrafish, frog, mouse	[5]ADMP=Binds [1]BMP10=NB [1]Bmp9=NB [2,7]BMP7=Binds [2,5,7]BMP4=0.02 nM [2]BMP2=Binds [3,4,6]HSPGs=Binds [1,8]GDF5=2 nM [5]Activin=Binds [5]Xnr2=Binds [5]Xnr4=Binds [5]Wnt8=Binds	[1]Seemann et al. 2009; [2]Zimmerman et al. 1996; [3]Nesterenko et al. 2015; [4]Viviano et al. 2004; [5]Bayramov et al. 2011, [6]Paine-Saunders et al., 2002; [7]Groppe et al. 1998,2003; [8]Degenkolbe et al. 2013
Follistatin	Antagonist	Dorsal	Binds 2:1 and Inhibits BMP[1]	human, zebrafish, frog, mouse	[5]Bmp15≈30 nM [6,7,8]Bmp7=35 nM [7,8]Bmp6=5.4 nM [6,7,8,11]Bmp4=2.9-23 nM [10]Bmp2=136 nM [2,9]HSPG=5-56 nM [10]GDF11=4.95 nM [3,4,7,8]Activin=0.02-0.28 nM [6]tgf-b=NB	[1]Thomsen et al. 2005; [2]Nakamura et al. 1991; [3]Chang et al. 2002; [4]Schneyer et al. 1994; [5]Otsuka et al. 2001; [6]Iemura et al. 1998; [7]Glister et al. 2004,2015; [8]Sidis et al. 2006; [9]Zhang et al. 2012; [10]Takehara-Kasamatsu et al. 2007. [11]Geng et al 2011

Name	BMP Agonist or Antagonist	Dorsal or Ventral Exression	Mechanism	Organism	Binding Affinities	Ref
Crescent	Antagonist	Dorsal	Inhibits Chd Cleavage by Tld/Bmp1a[1]; Can also inhibit Wnt5a/8/11[2]	frog	[1]Bmp1a=11 nM [2]Wnt11=Binds [2]Wnt8=Binds [2]Wnt5a=Binds	[1]Ploper et al. 2011; [2]Shibata et al., 2005
Coco/Dand5	Antagonist	Animal	Coco enhances tgf-B signaling, but inhibits Nodal, BMP, and Activin	zebrafish, frog, mouse, human	[1,2]Bmp4=Binds [2,3]Xnr1=Binds [2]Wnt8=Binds [2]Activin=Binds [3]Derriere=Binds	[1]Deglencerti et al. 2015; [2]Bell et al. 2003; [3]Vonica and Brivanlou 2006;
Gremlin-1	Antagonist	Dorsal	Binds and Inhibits BMP	human, zebrafish, frog, mouse	[3]Bmp7=88 nM [3]Bmp6=76 nM [3,6]Bmp4=28 nM [3]Bmp2=32 nM [1]BMP2=5.6 nM [2]HSPGs=20 nM [5]Gdf5=Binds [4]VEGFR1=47 nM	[1]Kisonaite et al. 2016; [2]Chiodelli et al. 2011; [3]Church et al. 2015; [4]Mitola et al. 2010; [5]Dionne et al. 2001; [6]Sun et al. 2006

Table 1.1: The expession, binding, and function of the extracellular BMP Agonists and Antagonists active during Zebrafish and/or Xenopus DV patterning.

Subsection 1.3: The antagonism of BMP by Chordin: an overview

The extracellular BMP antagonist Chordin and its homologs are essential to proper regulation of BMP signaling in mouse, fish, and frog development. Chordin is the central node of a network of regulators that modulate Chordin function in the extracellular space. Chordin inhibits BMP signaling by binding BMP ligand, rendering BMP ligand unable to bind its receptors (Fig. 1.2A, Table 1.1) (Stefano Piccolo Yoshiki Sasai, Bin Lu, Eddy M. De Robertis 1996, Troilo et al. 2014, Zhang J. L. et al. 2007a). Chordin is expressed in dorsal tissues, including the dorsal organizer, throughout early development (Abe et al. 2014, Abe et al. 2016, Bachiller 2003, Bachiller et al. 2000, Branam et al. 2010, Kuroda et al. 2004, Miller-Bertoglio et al. 1997, Ramel and Hill 2013, Schulte-Merker et al. 1997, Shimizu et al. 2000, Xue et al. 2014). In zebrafish, the loss of *chordin* causes a modest expansion of ventral mesodermal and ectodermal structures such as blood and tail and a concomitant reduction of dorsal structures such as the somites, eyes, and brain (Fisher et al. 1997, Matthias Hammerschmidt 1996, Schulte-Merker et al. 1997). A similar expansion of ventral mesodermal markers and ventral structures is seen in Xenopus embryos deficient for Chordin (Oelgeschlager et al. 2003). In mice, the loss of *chordin* alone does not induce as severe a phenotype, causing an expansion of the allantois at the expense of the embryonic mesoderm, along with mild pharyngeal and bone defects (Bachiller 2003).

Other BMP antagonists play partially redundant roles to Chordin. In both zebrafish and Xenopus, the loss of the BMP antagonists Noggin and Follistatin further ventralize embryos lacking *chordin,* suggesting these three antagonists act together to inhibit BMP signaling during DV patterning (Dal-Pra et al. 2006, Khokha M. K. et al.

2005). These genes have not yet been knocked out altogether in mice. In all of these organisms, other genes similar to *chordin* are present that, like *chordin*, contain conserved CXXCXC and CCXXC motifs and antagonize BMP signaling (Garcia Abreu et al. 2002). These genes are referred to as *chordin-like* genes (Garcia Abreu et al. 2002). While one *chordin-like* gene has been suggested to act redundantly with *chordin* during gastrulation in fish, the limited early expression of *chordin-like* genes in mice and Xenopus suggests they only play a role later in development (Branam et al. 2010, Nakayama et al. 2001, Nakayama et al. 2004, Pfirrmann et al. 2015).

Chordin binds to BMP via multiple conserved Cysteine rich repeats known as CR domains or Von Willebrand Type C domains (Fig. 1.2B) (Larrain et al. 2000, Zhang J. L. et al. 2007a). One molecule of Chordin binds one dimer of BMP ligand (Stefano Piccolo Yoshiki Sasai, Bin Lu, Eddy M. De Robertis 1996, Troilo et al. 2014, Zhang J. L. et al. 2007a). Chordin curves around the BMP dimer, binding one half with its CR1 domain and the other with its CR2/CR3/CR4 domains (Troilo et al. 2014). Chordin is also able to bind numerous other BMP extracellular modulators. The CR2-CR3 domains of Chordin bind the BMP extracellular modulator Twisted Gastrulation (Tsg) (Table 1.1, Fig. 1.2B) (Troilo et al. 2016). Chordin binds the BMP extracellular modulator Bmper (CV2) and HSPGs via undetermined domains (Fig. 1.2B, Table 1.1) (Ambrosio et al. 2008, Jasuja et al. 2004, Lee et al. 2006, Zhang J. L. et al. 2010).

Given that Chordin can bind so many extracellular BMP modulators, it is unsurprising that these modulators regulate the stability and activity of Chordin. The stability of the Chordin protein is regulated by the highly homologous metalloproteases Tolloid (also called Xolloid in Xenopus) and Bmp1, as well as the metalloprotease

inhibitors Sizzled and Crescent (Fig. 1.2A) (De Robertis and Moriyama 2016). Tolloid and Bmp1 cleave Chordin in two locations rendering it unable to inhibit BMP ligand effectively (Fig. 1.2B black arrows) (Blader 1997, Blitz et al. 2000, Connors SA. et al. 1999, Connors S. A. et al. 2006, Geach and Dale 2008, Jasuja et al. 2006, Muraoka et al. 2006, Stefano Piccolo Eric Agius, Bin Lu, Shelley Goodman, Leslie Dale, and Eddy M. De Robertis 1997, Wardle et al. 1999). Tolloid and Bmp1 function is abrogated by the proteinase inhibitors Sizzled and Crescent (Fig. 1.2 A-D) (Bijakowski et al. 2012, Collavin 2003, Inomata et al. 2013, Miller-Bertoglio et al. 1999, Muraoka et al. 2006, Ploper et al. 2011, Salic et al. 1997, Yabe T. 2003b). Ont1 acts as a scaffold to enhance the cleavage of Chordin by Tolloid and Bmp1 (Fig. 1.2 A,E) (Inomata et al. 2008).

Tsg and Bmper regulate BMP activity by binding independently to Chordin and to BMP ligand, or by binding both Chordin and BMP in a tripartite complex. Tsg can enhance the cleavage of Chordin by Tolloid and Bmp1 by binding Chordin and pulling CR domains 2-4 away from the BMP ligand, thus making CR domain 2-4 more accessible to cleavage (Fig. 1.2A,B,F, Table 1.1) (Larrain et al. 2001, Little and Mullins 2004, Troilo et al. 2016, Xie and Fisher 2005). Tsg can inhibit BMP signaling by binding to and enhancing the binding of Chordin to BMP ligand, as well as by binding BMP ligand itself (Fig. 1.2A,F, Table 1.1) (Blitz et al. 2003, Chang C. et al. 2001a, Scott et al. 2001, Troilo et al. 2016, Zhang J. L. et al. 2007a). Bmper similarly is able to both enhance and inhibit BMP signaling. Bmper enhances BMP signaling by binding Chordin, and inhibits BMP signaling by binding to BMP ligand (Fig. 1.2A,G, Table 1.1) (Ambrosio et al. 2008, Rentzsch et al. 2006, Zhang J. L. et al. 2010). Together, this

network of extracellular factors regulate BMP signaling by modulating activity and stability of the antagonist Chordin.

Subsection 1.4: Tolloid and Bmp1 antagonize Chordin

Tolloid and Bmp1 are metalloproteases that regulate Chordin stability by cleaving Chordin at two locations near the N- and C-terminal region of the protein (Fig. 1.2B) (Blader 1997, Muraoka et al. 2006, Scott et al. 1999, Stefano Piccolo Eric Agius, Bin Lu, Shelley Goodman, Leslie Dale, and Eddy M. De Robertis 1997, Wardle et al. 1999). The cleavage of Chordin blocks the ability of Chordin to bind and inhibit BMP ligand (Larrain et al. 2000, Lee et al. 2006, Stefano Piccolo Eric Agius, Bin Lu, Shelley Goodman, Leslie Dale, and Eddy M. De Robertis 1997). Though the cleavage of Chordin by Tolloid leaves the individual BMP binding domains (CR domains) intact, which are still able to bind BMP (Troilo et al. 2014), these fragments: bind BMP with a lower affinity than full-length Chordin (Larrain et al. 2000), are cleared from the extracellular space faster (Kelley et al. 2009, Larrain et al. 2001, Xie and Fisher 2005), and can be competed away by the extracellular BMP agonist Twisted Gastrulation (Larrain et al. 2001). The first two "Complement 1r/s, Uegf and BMP1" (CUB) domains and Epidermal Growth Factor (EGF) domain of Tolloid are needed for effective cleavage of Chordin (Canty et al. 2006, Geach and Dale 2008), as the CUB domains bind to BMP ligand, and may also be responsible for its high affinity to Chordin (Fig. 1.2C, Table 1.1) (Geach and Dale 2008, Lee et al. 2006, Lee et al. 2009). The first three CUB domains are also needed for Tolloid to bind Collagen IV (Winstanley et al. 2015), which enhances Chordin cleavage by Tolloid (Fig. 1.2A,C, Table 1.1) (Winstanley et al. 2015).

Bmp1 and Tolloid enhance BMP signaling and thus promote the formation of ventral cell fates in the developing embryo (Table 1.1). In zebrafish and Xenopus, *tolloid* and *bmp1* are first ubiquitously expressed in the early gastrula before becoming ventrally restricted in the mid to late gastrula (Table 1.1) (Connors SA. et al. 1999, Dale et al. 2002, Goodman et al. 1998, Jasuja et al. 2006). In zebrafish, the loss of either *bmp1* or *tolloid* alone only mildly dorsalizes the most posterior portions of the embryo, while the loss of both leads to a severe loss of all ventral tissues (Blader 1997, Connors SA. et al. 1999, Connors S. A. et al. 2006, Jasuja et al. 2006, Muraoka et al. 2006). A similar level of dorsalization is seen in frogs injected with dominant-negative *bmp1* or *tolloid* RNA (Blitz et al. 2000, Geach and Dale 2008, Stefano Piccolo Eric Agius, Bin Lu, Shelley Goodman, Leslie Dale, and Eddy M. De Robertis 1997, Wardle et al. 1999). In the early mouse gastrula, *bmp1* and *tolloid* are expressed ubiquitously, while *tolloid-like1* is expressed laterally and *tolloid-like2* is expressed anteriorly (Scott et al. 1999). However, mice mutant for *bmp1* and *tolloid* show no early DV patterning phenotype, possibly due to functional redundancy between Tolloid, Bmp1a, and the Tolloid-like proteins (Pappano et al. 2003, Suzuki et al. 1996).

Subsection 1.5: Sizzled and Crescent antagonize Tolloid and Bmp1

Sizzled and Crescent, relatives of the secreted Frizzled Receptor (Sfrp) family, competitively inhibit the metalloprotease action of Bmp1 and Tolloid (Fig. 1.2A) (Ambrosio et al. 2008, Bijakowski et al. 2012, Lee et al. 2006, Muraoka et al. 2006, Ploper et al. 2011). Like other Sfrps, Crescent is able to bind Wnt ligand (Fig. 1.2D, Table 1.1) (Pera and De Robertis 2000, Ploper et al. 2011, Shibata et al. 2005). In contrast, Sizzled is not able to bind Wnt ligand or inhibit Wnt signaling (Fig. 1.2D) (Lee

et al. 2006). The N-Terminal Cysteine-Rich Frizzled domain of both Sizzled and Crescent tightly binds to the active site of Tolloid and Bmp1, inhibiting the ability of Tolloid and Bmp1 to bind and cleave Chordin (Fig. 1.2A,D) (Ambrosio et al. 2008, Bijakowski et al. 2012, Lee et al. 2006, Muraoka et al. 2006, Ploper et al. 2011). This contrasts the human and mouse Sfrp proteins which cannot inhibit Tolloid- or Bmp1-mediated proteolysis of Chordin (Bijakowski et al. 2012, Kobayashi et al. 2009). Crescent and Frzb were recently found to greatly enhance the diffusion of Wnt in Xenopus embryos, transporting Wnts and allowing them to signal at considerable distances from where they are secreted (Mii and Taira 2009).

By inhibiting Tolloid and Bmp1, Sizzled and Crescent increase the amount of Chordin that can block BMP signaling, thus promoting dorsal cell fate specification in the early embryo (Table 1.1). *sizzled* is expressed ventrally and its expression depends on BMP signaling (Table 1.1), acting as a negative feedback inhibitor during DV patterning (Fig. 1.2A, Table 1.1). In contrast, *crescent* is expressed dorsally in Xenopus (Table 1.1) (Lee et al. 2006, Pera and De Robertis 2000, Ploper et al. 2011, Yabe S. I. 2003a). Loss of *sizzled* causes an expansion of ventral mesodermal and ectodermal cell fates, which depends on the presence of Tolloid/Bmp1 (Collavin 2003, Lee et al. 2006, Matthias Hammerschmidt 1996, Miller-Bertoglio et al. 1999, Yabe T. 2003b). This dependence and that loss of *sizzled* does not further ventralize *chordin* mutant embryos, shows that Sizzled acts entirely by inhibiting Tolloid/Bmp1 degradation of Chordin during axis patterning (Lee et al. 2006, Miller-Bertoglio et al. 1999). The loss of *crescent* ventralizes Xenopus embryos, while the injection of *crescent* RNA dorsalizes them (Pera and De Robertis 2000, Ploper et al. 2011). Despite the important role Sizzled and Crescent play

during zebrafish and Xenopus DV patterning, mammals do not have *sizzled* or *crescent* homologs (Kuraku and Kuratani 2011), and the related members of the Sfrp family do not appear to inhibit Chordin metalloprotease activity (Bijakowski et al. 2012, Kobayashi et al. 2009).

sizzled stands out as an antagonist of BMP signaling that is expressed ventrally in a similar domain to the BMP ligand (Lee et al. 2006, Yabe T. 2003b). *sizzled* transcription is regulated by BMP signaling (Table 1.1) (Inomata et al. 2013, Lee et al. 2006), thereby forming a negative feedback loop with BMP signaling. It has been postulated that this feedback loop provides stability to the system. If BMP signaling were to only upregulate BMP agonists and downregulate antagonists, the system could be easily thrown out of balance. The negative feedback of Sizzled helps BMP limit its own expression domain through a transcriptional autoregulatory loop, stabilizing the system (Collavin 2003, Inomata et al. 2013). There is also evidence that this negative feedback loop helps to properly shape the BMP gradient properly in different sized embryos, a phenomenon referred to as scaling (Inomata et al. 2013).

Subsection 1.6: The antagonism and agonism of BMP by Twisted Gastrulation

Twisted Gastrulation is a small but multi-functional extracellular modulator capable of promoting or antagonizing BMP signaling depending on embryonic context (Fig. 1.2A). Tsg is capable of antagonizing BMP signaling in either the absence or presence of Chordin (Fig. 1.2A). In the absence of Chordin, Tsg inhibits BMP signaling by binding the BMP ligand with an affinity ranging between 2.5-50 nM depending on the ligand (Table 1.1) (Chang C. et al. 2001a, Oelgeschlager 2003, Oelgeschlager et al. 2000,

Troilo et al. 2016, Zhang J. L. et al. 2007a). Tsg binds BMP ligand with its N-Terminal CR domain (Fig.1.2F) (Oelgeschlager 2003, Zhang J. L. et al. 2007a). Tsg can also antagonize BMP signaling by forming a ternary complex with BMP and Chd, thereby enhancing the binding of Chordin to BMP ligand (Fig. 1.2F) (Chang C. et al. 2001b, Oelgeschlager 2003, Oelgeschlager et al. 2000, Scott et al. 2001, Troilo et al. 2016, Zhang J. L. et al. 2007a). Consistent with this, the overexpression of *tsg* antagonizes BMP signaling in the absence or presence of Chordin (Blitz et al. 2003, Chang C. et al. 2001a, Little and Mullins 2004, Troilo et al. 2016). Conversely, in the presence of both Chordin and the metalloprotease Tolloid, Tsg acts as a BMP agonist by enhancing the degradation of Chordin by Tolloid (Fig. 1.2A) (Scott et al. 2001, Troilo et al. 2016, Xie and Fisher 2005). Tsg also enhances the binding of extracellular BMP modulator Bmper to Chordin (Fig. 1.2A) (Ambrosio et al. 2008). Therefore, Tsg can enhance or inhibit BMP signaling depending on the presence and concentration of BMP ligand, Chordin, Bmper, and the metalloproteases Tolloid and Bmp1.

Despite the numerous mechanisms by which Tsg can antagonize BMP signaling, Tsg may act predominantly as a BMP agonist during early patterning. In Xenopus, *tsg* is ventrally expressed in a similar domain as BMP ligand during DV patterning (Table 1.1) (Oelgeschlager et al. 2000). In mice, *tsg* is expressed in the anterior visceral endoderm and the primitive streak in the late blastula and throughout the mesoderm in the early gastrula (Zakin and De Robertis 2004). In fish and frogs, the loss of *tsg* causes a substantial retraction of ventral gene markers, an expansion of dorsal somites, and loss of tail structures (Blitz et al. 2003, Little and Mullins 2004). Despite the strong conservation between fish, frog, and mouse *tsg* genes, the loss of *tsg* in mice does not alter early

patterning, manifesting only as subtle defects in the vertebrae and thymus (Nosaka et al. 2003, Zakin and De Robertis 2004). However, the loss of *tsg* in conjunction with one allele of *bmp4* caused forebrain, eye, and further skeletal defects suggesting that *tsg* acts as a BMP agonist in mice as well (Zakin and De Robertis 2004). Though Tsg has been shown in some contexts to act as a BMP agonist *in vivo*, it is still likely that Tsg exerts different effects on BMP signaling in different embryonic contexts.

Subsection 1.7: The antagonism and agonism of BMP by Bmper

Like Tsg, Bmper (also known as Crossveinless-2) is a multi-functional extracellular modulator capable of promoting or antagonizing BMP signaling depending on embryonic context. Bmper can antagonize BMP signaling in the absence or presence of Chordin, but can only act as an agonist when Chordin is present (Fig. 1.2A, Table 1.1). Bmper acts as a BMP agonist by binding to Chordin, reducing its ability to bind and inhibit BMP (Fig. 1.2G, Table 1.1) (Ambrosio et al. 2008, Rentzsch et al. 2006, Zhang J. L. et al. 2010). Bmper interacts with the extracellular matrix by binding HSPGs (Fig. 1.2G, Table 1.1) (Serpe et al. 2008), and this interaction is thought to enhance BMP signaling during vertebral field patterning by concentrating BMP ligand in the vertebral body where *bmper* is expressed (Zakin et al. 2010, Zakin et al. 2008). Paradoxically, Bmper also increases Chordin protein levels in the vertebral body, suggesting Chordin, Bmper, and BMP ligand may form a ternary complex. Alternatively, Bmper may be sequestering Chordin extracellularly facilitating the release of BMP from Chordin. Additional studies are needed to fully resolve the mechanism by which Bmper enhances BMP signaling. The antagonism of BMP signaling by Bmper is clear. Bmper binds directly to the BMP ligand (Fig. 1.2G, Table 1.1), and thus interferes with the interaction

of the BMP ligand and its Type I receptor (Ambrosio et al. 2008, Rentzsch et al. 2006, Zhang J. L. et al. 2010). In cell culture, the BMP-Bmper complex binds to LRP1 and is endocytosed more rapidly than BMP alone, suggesting Bmper may also antagonize BMP ligand by clearing it from the extracellular space (Table 1.1) (Pi et al. 2012). Tsg enhances the ability of Bmper to bind BMP ligand and inhibit signaling (Fig. 2A) (Ambrosio et al. 2008), and it is possible that Bmper and Tsg act synergistically as suggested by their genetic interaction in mouse kidney and vertebral field formation (Ikeya et al. 2010, Zakin et al. 2008).

Bmper acts as either a BMP agonist or antagonist depending on developmental context and organism. During fish DV patterning, Bmper enhances BMP signaling by acting as a competitive inhibitor of Chordin, and the loss of *bmper* dorsalizes the embryo (Rentzsch et al. 2006, Zhang J. L. et al. 2010). Conversely, during Xenopus DV patterning Bmper inhibits BMP signaling by binding BMP ligand directly, and the loss of *bmper* ventralizes the embryo (Ambrosio et al. 2008). In both systems, overexpression of *bmper* dorsalizes the embryo by binding directly to the BMP ligand (Moser et al. 2003, Rentzsch et al. 2006, Zhang J. L. et al. 2010). In mice, the loss of *bmper* has no effect on axis patterning, instead causing skeletal and kidney defects later in development (Ikeya et al. 2006). The loss of *bmper* and *tsg* together does not affect axis patterning either (Ikeya et al. 2008, Zakin et al. 2008).

Subsection 1.8: The Noggin and the Follistatin family antagonize BMP

Noggin, Follistatin, and Follistatin-like are extracellular BMP inhibitors that bind to BMP ligand and inhibit BMP ligand-receptor interaction. Noggin self-dimerizes to

form a butterfly shaped complex capable of binding some, but not all, BMP ligands with a high affinity (Fig. 1.2A,I, Table 1.1) (Bayramov et al. 2011, Groppe et al. 2002, Groppe et al. 2003, Jay Groppe and Affolter 1998, Zimmerman et al. 1996). Noggin can also bind the BMP related GDFs, and to a lesser extent ADMP, Wnt8, and Activin (Table 1.1) (Bayramov et al. 2011, Degenkolbe et al. 2013, Seemann et al. 2009). Knockdown studies suggest that the binding of Noggin to Wnt8, and Activin/Nodal plays a role during embryonic patterning in Xenopus (Bayramov et al. 2011). Noggin also strongly binds HSPGs (Fig. 1.2I), and this interaction is thought to limit Noggin dimer mobility in the extracellular space (Inomata et al. 2013, Nesterenko et al. 2015, Paine-Saunders et al. 2002, Viviano et al. 2004). Follistatin similarly binds numerous BMPs, GDFs, and Activins (Fig. 1.2A) (Geng et al. 2011, Glister et al. 2004, Glister et al. 2015, Iemura et al. 1998, Nakamura et al. 1991, Otsuka et al. 2001, Schneyer et al. 1994, Sidis et al. 2006, Takehara-Kasamatsu et al. 2007). Unlike Noggin, Follistatin does not self-dimerize, though two Follistatin proteins can bind to a single BMP dimer (Thompson et al. 2005). Like Noggin, Follistatin strongly binds HSPGs, which may limit its diffusivity in the extracellular space (Table 1.1) (Nakamura et al. 1991, Zhang F. et al. 2012). Interestingly, Follistatin-Activin complexes bind HSPGs more tightly than Follistatin or Activin alone (Zhang F. et al. 2012).

Noggin, Follistatin, and Follistatin-like proteins act as BMP antagonists during axis patterning, promoting dorsal fates by binding BMP ligand. *noggin*, *follistatin*, and *follistatin-like* are expressed in the dorsal organizer during axis patterning (Table 1.1) (Bachiller 2003, Bachiller et al. 2000, Dal-Pra et al. 2006, Khokha M. K. et al. 2005). Interestingly, the loss of either *noggin* or *follistatin* or both *noggin* and *follistatin* together

has little effect on embryonic DV patterning (Dal-Pra et al. 2006, Geng et al. 2011, Khokha M. K. et al. 2005, Lana-Elola et al. 2011, Matzuk et al. 1995, McMahon et al. 1998, Stafford et al. 2014, Sylva et al. 2013). Only in the absence of *chordin* does the loss of *noggin* and *follistatin* further ventralize zebrafish and Xenopus embryos, indicating that these three proteins act partially redundantly to promote dorsal cell fates (Dal-Pra et al. 2006, Khokha M. K. et al. 2005). The *chordin;noggin;follistatin* loss of function phenotype is not yet known for mice, but double mutants for *chordin* and *noggin* fail to form forebrain (Bachiller et al. 2000). It is possible that additional BMP antagonists such as Gremlin, Cerberus, and Chordin-like also function redundantly to compensate for the loss of Chordin, Noggin, and Follistatin during axis patterning.

Subsection 1.9: Dan Family proteins Gremlin and Coco antagonize BMP and Nodal

Coco and Gremlin are 'Differentially screening-selected gene Arbitrative in Neuroblastoma' (DAN) family extracellular proteins capable of inhibiting BMPs as well as other ligands such as Activin, Wnt, and Nodal (Fig. 1.2J, Table 1.1). Coco binds and inhibits Activin, BMP, Nodal, and Wnt ligands, but also enhances canonical Tgf-β signaling (Bates et al. 2013, Bell 2003, Deglincerti et al. 2015) by interacting with its receptor Alk-5 (Fig. 1.2A,J, Table 1.1) (Deglincerti et al. 2015). Gremlin binds and inhibits numerous BMP ligands as well as Gdf5 (Fig. 1.2A,J, Table 1.1) (Church et al. 2015, Dionne et al. 2001, Kisonaite et al. 2016, Sun et al. 2006). Interestingly, Gremlin also belongs to the Cysteine knot superfamily, which includes Vascular Endothelial Growth Factor (VEGF) (Vitt et al. 2001). Due to its similarity to VEGF, Gremlin can activate VEGF receptors and promote angiogenesis (Mitola et al. 2010). Gremlin binds

strongly to HSPGs, likely limiting its effective diffusivity (Table 1.1) (Chiodelli et al. 2011).

Coco inhibits endoderm and mesoderm formation during AP patterning by inhibiting Activin and Nodal signaling (Bates et al. 2013, Bell 2003). Coco also helps establish the fate of the right side of the embryo by inhibiting Nodal signaling (Schweickert et al. 2010, Vonica and Brivanlou 2007). Mice lacking *gremlin* suffer malformed limbs, lungs, and kidneys (Khokha MK. et al. 2003, Michos et al. 2004). The phenotype for the loss of *gremlin1* has not been determined in zebrafish or Xenopus, but it is expressed dorsally during axis patterning in fish (Nicoli et al. 2005).

Chapter 2: Systems biology derived source-sink mechanism of BMP gradient formation

Subsection 2.1: Introduction: the mechanism of BMP gradient formation during DV patterning

While much is known about the binding interaction and basic function of the extracellular BMP regulators, how these regulators come together to form the BMP signaling gradient that patterns the DV axis in vertebrates is poorly understood. In contrast, the DV gradient has been well studied in Drosophila, revealing a complex mechanism referred to as 'shuttling' centered around the BMP antagonist Sog, a homologue of vertebrate Chordin (Eldar et al. 2002, Guillermo Marques 1997, Holley S. et al. 1996, Peluso et al. 2011, Shilo et al. 2013, Shimmi et al. 2005, Umulis et al. 2010). The mechanism was revealed by visualizing the BMP signaling gradient using an antibody against phosphorylated-Mad protein, which is phosphorylated by the Type I receptors in response to BMP signaling.

A key part of the shuttling mechanism is the ability of Sog to act not only as a BMP antagonist during DV patterning, but also as an agonist. During Drosophila DV patterning, Sog acts as an agonist by binding to and moving BMP ligand via facilitated diffusion to regions of Tolloid activity (Fig 2.1A). Tolloid then cleaves Sog, which releases BMP thus increasing peak BMP levels, a process altogether known as shuttling (Fig. 2.1A) (Eldar et al. 2002, Guillermo Marques 1997, Holley S. et al. 1996, Peluso et al. 2011, Shilo et al. 2013, Shimmi et al. 2005, Umulis et al. 2010). The shuttling mechanism is essential to *Drosophila* DV patterning, where Sog shuttles BMP ligand

from lateral regions to dorsal regions (Fig. 2.1A) (Eldar et al. 2002, Guillermo Marques 1997, Holley S. et al. 1996, Peluso et al. 2011, Shilo et al. 2013, Shimmi et al. 2005, Umulis et al. 2010). This shuttling mechanism is required to steepen the BMP signaling gradient and specify the dorsal-most cell fates in the *Drosophila* embryo (Eldar et al. 2002, Guillermo Marques 1997, Holley S. et al. 1996, Peluso et al. 2011, Shilo et al. 2013, Shimmi et al. 2005, Umulis et al. 2010). The shuttling of BMP ligand by Chordin has also been suggested to play a role in DV patterning in Echinoderms (Lapraz et al. 2009) and Nematostella (Genikhovich et al. 2015).

It is unclear whether Chordin shuttles BMP in patterning vertebrate tissues. In *Xenopus*, the shuttling of a particular BMP ligand, ADMP, by Chordin was reported to play a role in DV axial patterning in the scaling of embryos (Ben-Zvi et al. 2008, Reversade and De Robertis 2005). In the mouse, Chordin has been suggested to shuttle BMP ligand from where it is expressed in the intervertebral disc to its site of signaling in the vertebral body (Zakin et al. 2010). Mathematical models of zebrafish and *Xenopus* DV patterning have predicted that Chordin may shuttle BMP ligand (Ben-Zvi et al. 2008, Zhang Y. T. et al. 2007b). The transcriptional profiles of zebrafish BMP components at the onset of gastrulation resembles that of the *Drosophila* embryo (Dutko and Mullins 2011, O'Connor et al. 2006). In *Drosophila*, *sog* is expressed ventral-laterally while the BMP ligand *dpp* is expressed dorsally (Fig. 2.1A). Vertebrates have undergone a DV axis inversion with respect to arthropods (De Robertis and Sasai 1996, Gerhart 2000, Sander and Schmidt-Ott 2004, TC. 1995), thus *chordin* is expressed dorsally while *bmp* ligands are expressed ventrally (Fig. 2.1A,B). However, whether Chordin acts as a BMP agonist

by shuttling BMP ligand during DV patterning in zebrafish or other vertebrates has not been determined.

In vertebrates, the mechanism by which the BMP ligands and antagonists shape this gradient is unclear. Several potential mechanisms have been proposed: 1) an inverse gradient of BMP antagonists imparts the shape of the BMP signaling gradient (Fig. 2.1C) (Blitz et al. 2000, Connors SA. et al. 1999, Little and Mullins 2006, Thomsen 1997), 2) BMP antagonists generate the peak BMP signaling levels by shuttling BMP ligand to these regions (Fig. 2.1B,D) (Ben-Zvi et al. 2008, Shilo et al. 2013, Zhang Y. T. et al. 2007b), 3) the gradient shape mirrors the shape of the *bmp* expression domain (Fig. 2.1E) (Ramel and Hill 2013), and 4) the gradient is generated by BMP diffusing from its ventral source to a dorsal sink of BMP antagonists (Fig. 2.1F). These mechanisms are not mutually exclusive and multiple may act in combination.

To identify the mechanism of BMP signaling gradient formation in the zebrafish embryo, we established a robust quantitative imaging analysis to directly measure the BMP signaling readout. We integrated the results with a mathematical modeling approach, using the experiments to inform our model selection. The modeling provided information on key parameters to measure to identify the mechanism by which the BMP signaling gradient is formed. We used phosphorylated Smad5 protein as a direct read-out for BMP signaling in both WT and *chordin* mutant embryos. We quantified nuclear phosphorylated-Smad5 (P-Smad5) fluorescent intensity across the entire embryo at single-cell resolution at different stages of development. Combining the P-Smad5 data with a computational model-based screen showed that shuttling of BMP during DV patterning does not shape the gradient, and that a gradient of *bmp* transcript cannot

account for the gradient of BMP signaling activity. From these results, we conclude that the signaling gradient patterning the vertebrate DV axis is generated by either a source-sink or counter-gradient mechanism. To discern between these mechanisms, we developed and measured the diffusion rate of a BMP2-Venus fusion protein in the zebrafish blastula and found that it is relatively mobile, which supports a source-sink mechanism. Our results suggest that significant differences exist between the biophysical parameters of conserved proteins in zebrafish and *Drosophila* DV patterning. Through quantification and modeling, we present a new view of the mechanism that the BMP antagonists and ligand use to establish the BMP signaling gradient patterning the DV axis in zebrafish.

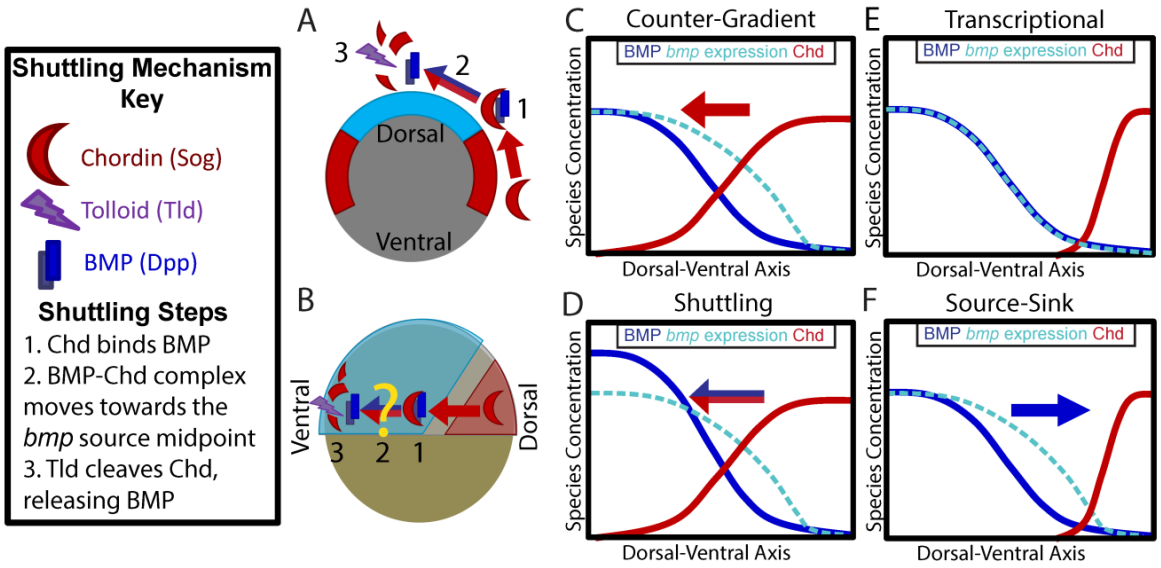

Figure 2.1: Potential Mechanisms of BMP Morphogen Gradient Formation. (A) Cross-sectional view of the Drosophila embryo depicting Sog shuttling Dpp (the fly BMP ligand) dorsally. (B) Lateral view of the zebrafish embryo depicting Chordin (Chd) shuttling BMP ventrally. (C) Counter-Gradient: Chd diffuses ventrally to form a counter-

gradient repressing BMP. (D) Shuttling: BMP bound to Chd is shuttled ventrally, where it is released by Tolloid cleavage. (E) Transcriptional: BMP stays where it is produced, mirroring the *bmp* expression gradient. (F) Source-sink: BMP diffuses from its source of ventral production to a sink of dorsal Chd.

Results

Subsection 2.2: Quantifying the Wild Type Signaling Gradient

To measure the BMP signaling gradient, we quantified the levels of the BMP signal transducer P-Smad5 across the entire embryo at single cell resolution. Smad5 is directly phosphorylated by the BMP type I receptor in response to BMP signaling, and P-Smad5 has been shown to linearly correlate with the concentration of BMP ligand in the *Drosophila* wing disc and S2 cells (Bollenbach et al. 2008, Serpe et al. 2008). Fixed embryos were whole-mount immunostained for P-Smad5 and imaged using a Line Scanning Confocal Microscope (Fig. 2.2A-E). We developed a mounting and imaging protocol that minimized photo-bleaching, light scattering, and refractive index mismatch (see methods). We wrote a Matlab algorithm to identify all 8000+ nuclei centerpoints in each embryo in 3 dimensions, to remove populations unresponsive to P-Smad5 such as yolk syncytial nuclei and dividing cells (see methods), and to extract the P-Smad5 intensities associated with each nucleus (Fig. 2.2A'-E'). Embryos were aligned by coherent point drift (see methods) to a reference embryo to create ensembles of embryos suitable for statistical analysis (Andriy Myronenko 2010). We used a band of cells around the margin of the embryo (Fig. 2.2F') to plot profiles from the dorsal-most to the ventral-

most points to compare P-Smad5 gradient profiles between stages and between wild-type and mutant embryos (Fig. 2.2F).

Our quantitative analysis revealed that the BMP gradient during DV patterning is quite dynamic. BMP signaling patterns prospective head and rostral trunk DV axial tissues during late blastula to mid-gastrula stages at ~5 to 7 hours post fertilization (hpf) in zebrafish (Hashiguchi and Mullins 2013, Kwon et al. 2010, Tuazon and Mullins 2015, Tucker et al. 2008). We quantified the BMP signaling gradient at 30-minute intervals across this period. We found that the ventral-most 30˚ undergoes about a 2-fold intensification from 4.7 to 6.7 hpf (Fig. 2.2F). This is accompanied by a 3 to 5 fold increase in the slope of the gradient in ventrolateral regions of the embryo (0-75 degrees) over this 2-hour period (Fig. 2.2G). Moreover, the lateral region encompassing the high slope (>0.5 A.U./degree) expands from a size of 20˚ to 75˚, meaning that by 6.7 hpf, nearly half the embryo falls within this high slope region. This contrasts with *Drosophila* DV patterning, where an initial broad, low-slope distribution of P-Mad is refined into a steep peak of BMP signaling covering only the dorsal-most 8% of the embryo (11 cell lengths) (Sutherland et al. 2003, Wang and Ferguson 2005). This intensification of P-Mad is very rapid in *Drosophila* DV patterning, where P-Mad increases about 3 fold in the 30 minutes between stages 5 and 6 (Ross et al. 2001, Sutherland et al. 2003, Wang and Ferguson 2005), a process that we found is much slower in the zebrafish embryo: a 2-fold increase over a 2 hour period.

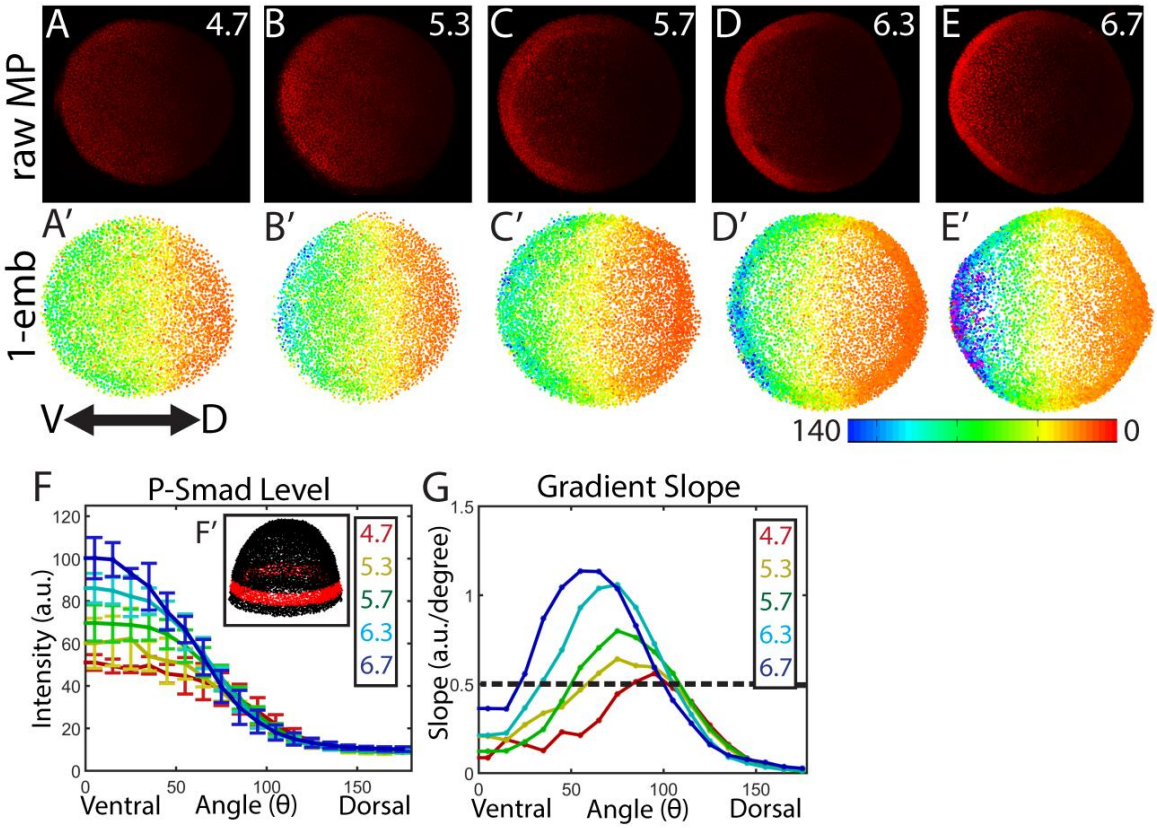

Figure 2.2: Dynamics of the WT P-Smad5 gradient across head and trunk patterning. (A-E) Animal views of maximum projections of P-Smad stained individual embryos. (A'-E') Animal views of nuclear intensities of all nuclei from the embryos shown above. (F) Average marginal intensities for 4.7-6.7 hpf (4.7: N=3, 5.3: N=4, 5.7: N=13, 6.3: N=11, 6.7: N=4). Error bars indicate standard deviation. (G) Slope of the P-Smad gradients shown in panel F. Dotted line separates high slope (>0.5 a.u./deg) regions from low slope regions.

Subsection 2.3: A Computational Model-Based Screen of Zebrafish the BMP Signaling Gradient

We then performed a computational model-based screen to investigate which gradient-forming mechanisms (Fig. 2.1C-F) would fit the WT P-Smad5 gradient profiles (Fig. 2.2). To do so, we first needed to determine the expression domains of *bmp*, *chordin*, *noggin*, and *tolloid* to use for the computational model. We based our domains on our own measurements (Fig. 2.3) as well as past groups' in situ hybridizations for *bmp* (Furthauer et al. 2004, Ramel and Hill 2013), *chordin* (Miller-Bertoglio et al. 1997), *tolloid* (Connors SA. et al. 1999), and *noggin* (Dal-Pra et al. 2006). *chordin* and *noggin* expression domain sizes were measured to be 75 and 40 degrees in width, respectively, based on quantification of animal-pole views of wholemount *in situ* hybridizations (Fig. 2.3A-C). We also estimated the size of the *bmp* expression domain via wholemount *in situ* hybridizations (Fig. 2.3D). However, *bmp2b* expression appeared to be graded and not as easily measured as *chordin* and *noggin*. Our collaborator Xu Zhang instead measured the relative shape of the *bmp2b* expression gradient via fluorescent in situ hybridization on cross-sections through the entire DV marginal domain at 5.7 hpf (Fig. 2.3F-H). She quantified the relative intensity of our fluorescent *bmp2b in situ* (Fig. 2.3I black line), and I used it to estimate the BMP production domain in our model (Fig 2.3I blue line).

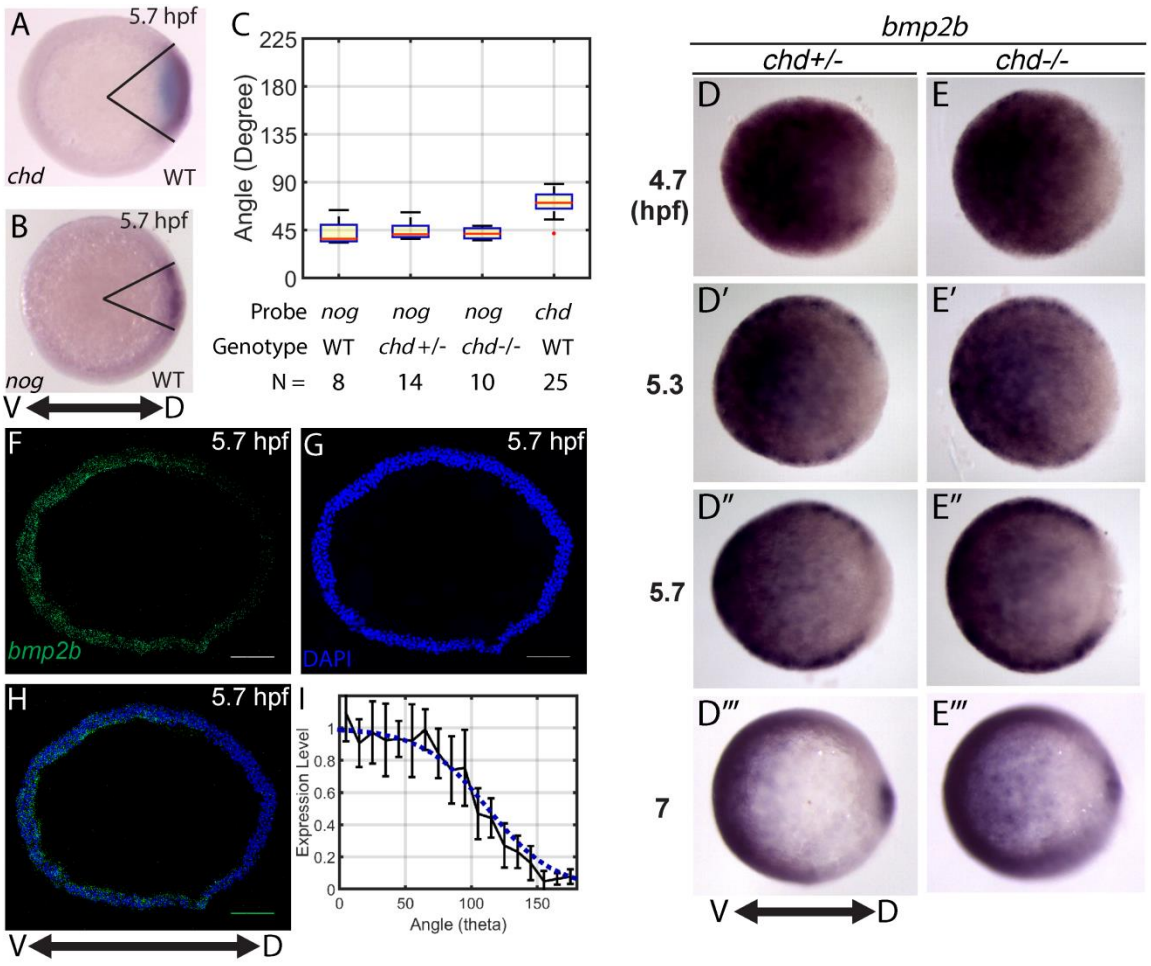

Figure 2.3: Measuring the bmp2b, chordin, and noggin expression domains. Animal pole views of wholemount in situ hybridizations of the expression of (A) chd (N=25), and (B) nog (N=8) in WT embryos. (C) Measured domain size of chd and nog domains via wholemount in situ hybridization in WT and chd mutant embryos. (D-D’’’) bmp2b in chd +/- embryos at 4.7 (N=10), 5.3 (N=15), 5.7 (N=20), and 7 hpf (N=16), and (E-E’’’) bmp2b expression in chd -/- embryos at 4.7 (N=6), 5.3 (N=16), 5.7 (N=13), and 7 hpf (N=12). (F-H) Fluorescent in situ hybridization (FISH) signal of bmp2b from a marginal slice at 5.7 hpf with a DAPI nuclear stain. Scale bars=100µm. (I) Quantification of FISH of bmp2b expression from ventral to dorsal (black line, N=5) compared to the BMP

production gradient used in the mathematical model (blue dotted line). Error bars indicate standard deviation.

We then developed a system of partial differential equations to model the interactions of BMP, Chordin, Noggin, and Tolloid. BMP, Chordin, Noggin, BMP-Chordin, and BMP-Noggin were modeled as diffusible species, while Tolloid was treated parametrically according to its domain of expression (Fig. 2.4A, 4.2A). The zebrafish gastrula was reduced to a 1-dimensional half-circumference with a length of 700 μm. Domains of production of BMP, Chordin, and Noggin were estimated as described in Fig. 2.3. The dissociation constants for Bmp-Chordin and BMP-Noggin were set to 1 and 0.1 nM respectively, based on previously reported analysis (Stefano Piccolo Yoshiki Sasai, Bin Lu, Eddy M. De Robertis 1996, Troilo et al. 2014, Zhang J. L. et al. 2007a, Zimmerman et al. 1996). All remaining parameters (ie. the diffusion coefficients, production rates, decay rates, on and off binding rates) were varied over 4 orders of magnitude encompassing all biologically feasible values (Table 2.1).

Parameter	Units	Symbol	Lower Bound	Upper Bound
BMP Production Rate	nM/s	η_B	10^{-2}	10^{2}
BMP Decay Rate	1/s	decB	10^{-1}	10^{-5}
BMP Diffusivity	$\mu m^2/s$	D_B	10^{-2}	10^{2}
Chd Production Rate	nM/s	η_C	10^{-2}	10^{2}
Chd Decay Rate	1/s	decC	10^{-1}	10^{-5}
Chd Diffusivity	$\mu m^2/s$	D_C	10^{-2}	10^{2}
Nog Production Rate	nM/s	η_N	10^{-2}	10^{2}
Nog Decay Rate	1/s	decN	10^{-1}	10^{-5}
Nog Diffusivity	$\mu m^2/s$	D_N	10^{-2}	10^{2}
BMP-Nog Decay Rate	1/s	decBN	10^{-1}	10^{-5}
BMP-Nog Diffusivity	$\mu m^2/s$	D_{BN}	10^{-2}	10^{2}
BMP-Chd Decay Rate	1/s	decBC	10^{-1}	10^{-5}
BMP-Chd Diffusivity	$\mu m^2/s$	D_{BC}	10^{-2}	10^{2}
Chd Degradation by Tld	1/s	λ_C	10^{0}	10^{-4}
BMP-Chd Degradation by Tld	1/s	λ_{BC}	10^{0}	10^{-4}
Length of the Embryo	µm	-	700	700
Length of the Chd domain (from dorsal)	µm	-	145	145
Length of the Nog domain (from dorsal)	µm	-	78	78
Length of the Tolloid domain (from ventral)	µm	-	400	400
Dissociation Constant of BMP-Chd	nM	-	1	1
Dissociation Constant of BMP-Nog	nM	-	0.1	0.1
Time	min	t	130	130

Table 2.1: List of the parameter ranges used in the computational model-based screen. Values range between the upper and lower bound. Note that the dissociation constant of BMP-Chd and BMP-Nog was held constant, but the on- and off- rates were allowed to vary.

The equations are solved for the developmental window from ~3.5 hpf to ~5.7 hpf, since *bmp* and *chordin* are first expressed after the mid-blastula-transition at 3 hpf (Koos and Ho 1999, Leung 2003, Shimizu et al. 2000, Solnica-Krezel and Driever 2001).

The equations were simulated 1,000,000 times, each time with different randomly selected parameters. Each parameter combination was then re-simulated without Chordin or Noggin to predict the BMP signaling gradient in a *chordin* or *noggin* loss of function (LOF) scenario. We then selected parameter combinations that generated BMP protein distributions that were less than 8% different to our experimentally measured P-Smad5 gradient at 5.7 hpf, henceforth referred to as "solutions" (Fig. 2.4B). We also eliminated parameter combinations that have significantly different BMP distribution gradients when Noggin production was set to 0, as the loss of Noggin does not affect DV patterning in zebrafish or *Xenopus* (Fig. 2.9) (Dal-Pra et al. 2006, Khokha M. K. et al. 2005).

All simulation results that fit our data were classified into categories based on the biophysical process that dominated formation of the gradient shape: shuttling, source-sink, counter-gradient, or transcriptional (Fig. 2.4C). We discerned between source-sink, counter-gradient, and transcriptional mechanisms by examining the balance of binding, diffusion, decay, and accumulation processes in the partial differential equation for the BMP species (Fig. 2.4C,C''). If 80% of the BMP ligand was degraded where it was produced or accumulated there, the solution was classified as transcriptional (Fig. 2.4C,C''). If the majority of BMP diffused away from its site of production rather than being bound by Chordin, the solution was considered to have a source-sink mechanism (Fig. 2.4C,C'). Conversely, if the majority of BMP was bound at its site of production by Chordin, the solution was classified as a Chordin counter-gradient mechanism (Fig. 2.4C,C'). We classified a solution as shuttling if the ventral-most point in the predicted *chordin*-/- BMP profile was at least 20% lower than in WT, as shuttling is a process

whereby the antagonist leads to a net accumulation of ligand in the ventral-most region (Fig. 2.4C,C''). By Comparison, Drosophila shuttling has a much more significant effect on the peak level, with a 50% decrease in the peak P-Mad level observed when the *chordin* homolog *sog* is deficient (Mizutani et al. 2005, Peluso et al. 2011, Sutherland et al. 2003). Shuttling of 20% is over one standard deviation greater than our measured embryo to embryo variability for peak P-Smad signaling levels (Fig 2.2B).

Multiple classes of mechanisms generated solutions fitting our WT data, including an antagonist counter-gradient, source-sink, and shuttling. Out of 1,000,000 randomly picked parameter combinations, 15,142 fit the experimentally measured WT signaling gradient (Fig. 2.4D'). 13,382 of these were classified as source-sink, 1,710 as counter-gradient, and 50 as shuttling (Fig. 2.4D"). Notably, no transcriptional solutions were found, because our selected *bmp* expression profile (Fig. 2.4H) did not exactly match our measured WT BMP signaling gradient (Fig. 2.3), and therefore BMP needed to diffuse away or be bound by Chordin to fit our measured signaling gradient.

Even though the measured *bmp2b* expression profile (Fig. 2.3) did not precisely match the measured WT BMP signaling gradient (Fig. 2.2), we wanted to determine what type of *bmp* expression domain would permit a transcriptional mechanism to match the P-Smad gradient we measured (Fig. 2.2). When we matched the *bmp* expression domain to the BMP signaling gradient (Fig. 2.4E), we found that the transcriptional mechanism was the most abundant mechanism among the solutions (Fig. 2.4E',E''). No Counter-Gradient solutions were found, as Chordin binding to BMP would interfere with the shape of the BMP protein gradient, causing it to no longer match the measured BMP signaling gradient.

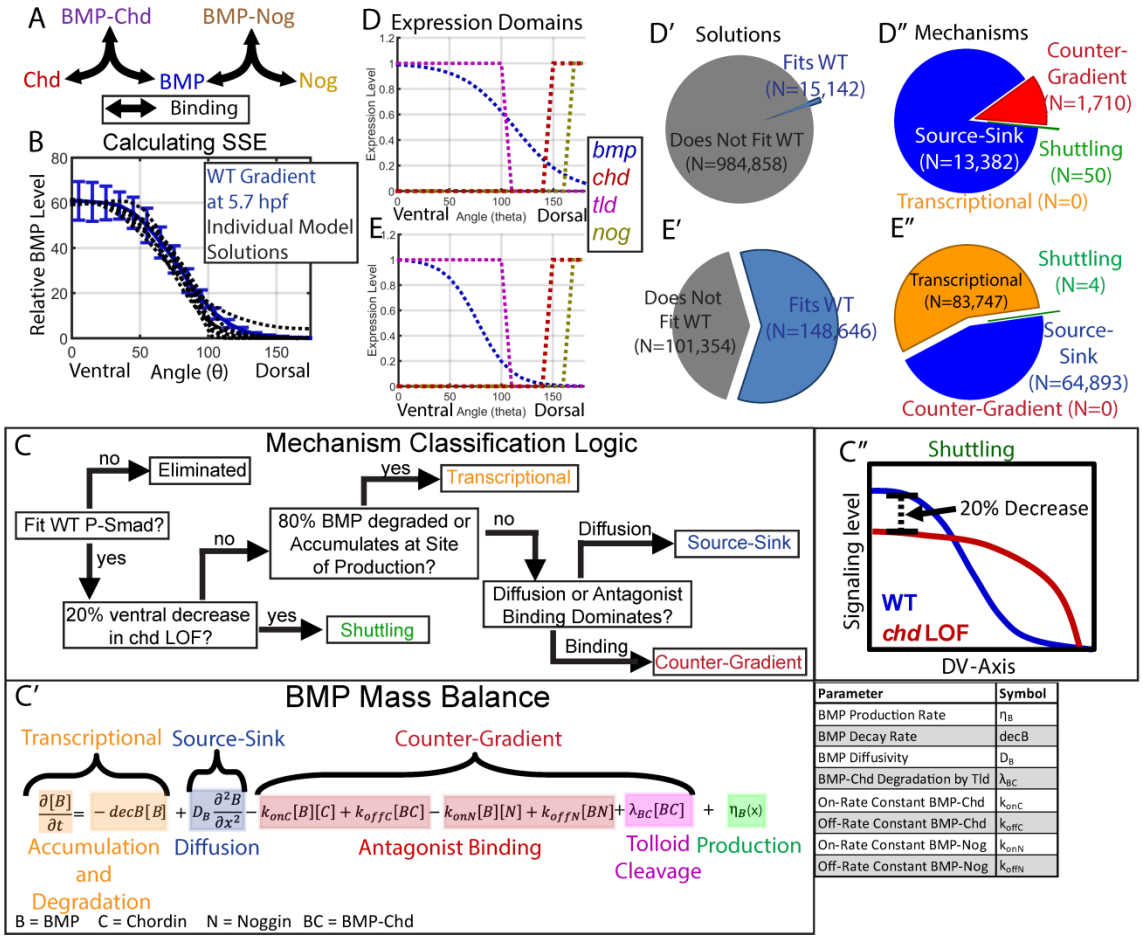

Figure 2.4: Creation of a system-scale mathematical model of BMP gradient formation. (A) Depiction of the species and binding possibilities modeled. (B) BMP distributions of 10 individual model solutions (black dotted lines) plotted against the WT 5.7 hpf P-Smad5 gradient (blue line). Error bars indicate standard deviation. (C) Flow-chart of model mechanism classification. (C') BMP mass balance from model labeled to indicate which terms contribute to the source-sink, counter-gradient, and transcriptional mechanisms at each point. (C") Shuttling mechanism was defined by a 20% decrease at the ventral-most point in chd LOF compared to WT. (D) Expression domains of bmp (blue), tld (purple), chd (red), and nog (yellow) used in the model. (E) Expression domains of bmp (blue), tld (purple), chd (red), and nog (yellow) used for the alternative

scenario where the bmp expression domain mirrors the measured P-Smad gradient. (D', E') Pie chart showing how many parameter combinations fit the WT data (blue) and how many failed to do so (grey). (D", E") Pie chart showing how many parameter combinations were classified to have a source-sink (blue), counter-gradient (red), transcriptional (orange), or shuttling (green) mechanism.

Subsection 2.4: Constraints on biophysical parameters imposed by the WT gradient

Each mechanism required specific biophysical parameters to fit the experimentally measured DV signaling gradient. The source-sink mechanism required BMP to have a high diffusion rate and low decay rate so BMP could diffuse to a dorsally localized sink of antagonists (Fig. 2.5A). The counter-gradient mechanism required Chordin to have a high diffusion rate and low decay rate so Chordin could diffuse ventrally to set up an antagonist gradient (Fig. 2.5B). When BMP and Chordin range are plotted on the same axis, the segregation of the source-sink and counter-gradient mechanisms based on range is readily apparent (Fig. 2.5C). The shuttling mechanism required that BMP-Chordin have a high diffusion rate and low decay rate in order to freely diffuse ventrally where Tolloid cleaves Chordin, which then releases BMP (Fig. 2.5D).

For the simulations performed where the *bmp* expression domain was set to match the signaling gradient, distinct biophysical requirements were also observed for each mechanism. The source-sink mechanism required BMP to have a high range, while the transcriptional mechanism required BMP to have a low range or a very low diffusivity ($<0.05\ \mu m^2/s$) (Fig. 2.5G,I). Neither of these mechanisms constrained Chordin range (Fig.

2.5H,I). The shuttling mechanism required BMP-Chordin range to be high and its decay rate to be low (Fig. 2.5J). The shuttling mechanism also required BMP range to be high (Fig. 2.5G), because Chordin cannot move ventrally to bind BMP in this scenario since that would interfere with the *bmp* expression gradient matching the BMP signaling gradient. BMP needs to move dorsally to form the BMP-Chordin species that ultimately is then shuttled back ventrally. The remaining parameters required for shuttling were similar for the two simulations (Fig. 2.5,F,K,L). Intriguingly, the WT distributions of P-Smad5 data alone did not eliminate any of these gradient formation mechanisms in the simulations.

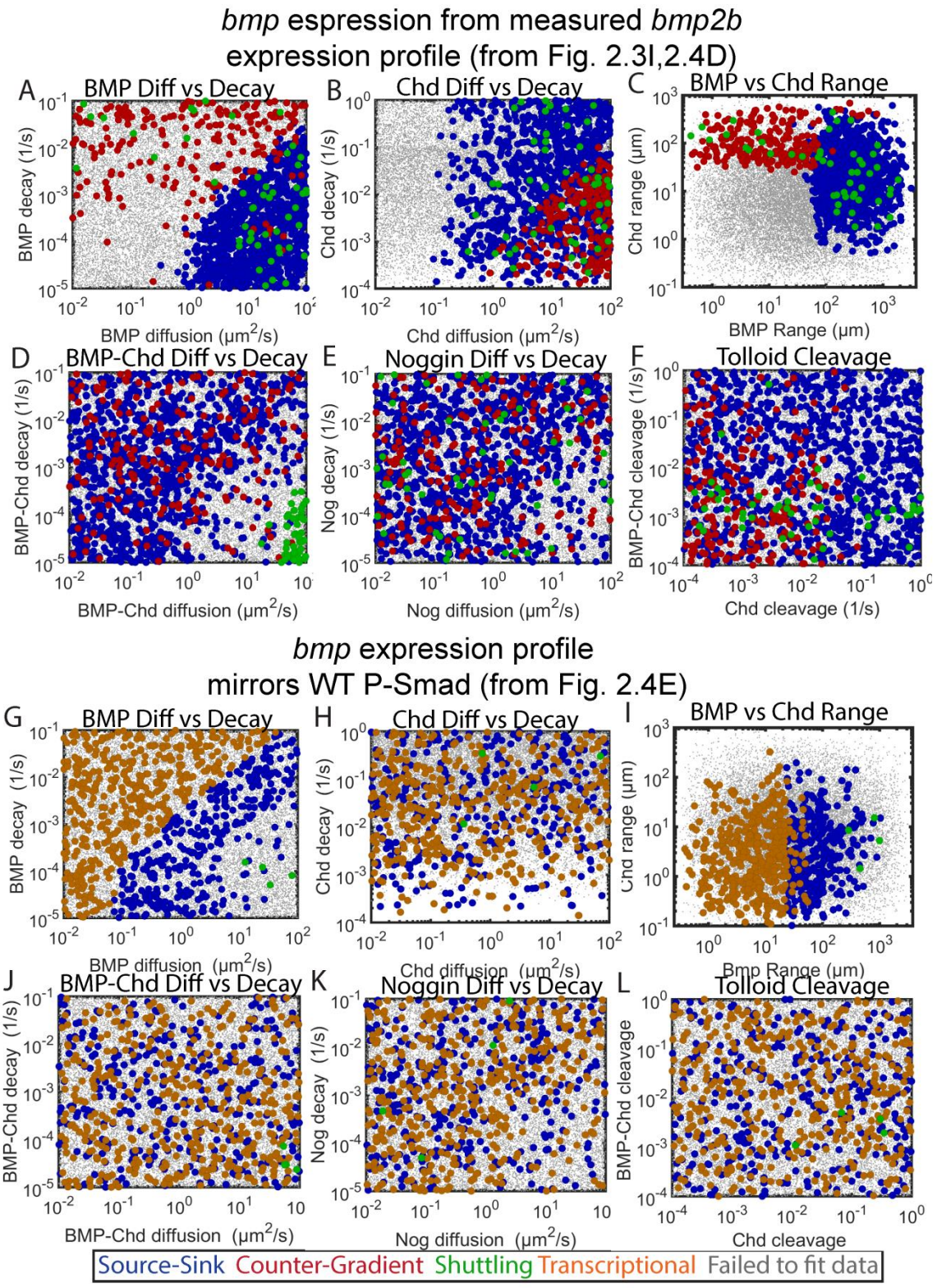
bmp espression from measured *bmp2b* expression profile (from Fig. 2.3I,2.4D)
A
BMP Diff vs Decay
BMP decay (1/s)
BMP diffusion (μm²/s)
B
Chd Diff vs Decay
Chd decay (1/s)
Chd diffusion (μm²/s)
C
BMP vs Chd Range
Chd range (μm)
BMP Range (μm)
D
BMP-Chd Diff vs Decay
BMP-Chd decay (1/s)
BMP-Chd diffusion (μm²/s)
E
Noggin Diff vs Decay
Nog decay (1/s)
Nog diffusion (μm²/s)
F
Tolloid Cleavage
BMP-Chd cleavage (1/s)
Chd cleavage (1/s)
bmp expression profile mirrors WT P-Smad (from Fig. 2.4E)
G
BMP Diff vs Decay
BMP decay (1/s)
BMP diffusion (μm²/s)
H
Chd Diff vs Decay
Chd decay (1/s)
Chd diffusion (μm²/s)
I
BMP vs Chd Range
Chd range (μm)
Bmp Range (μm)
J
BMP-Chd Diff vs Decay
BMP-Chd decay (1/s)
BMP-Chd diffusion (μm²/s)
K
Noggin Diff vs Decay
Nog decay (1/s)
Nog diffusion (μm²/s)
L
Tolloid Cleavage
BMP-Chd cleavage
Chd cleavage
Source-Sink
Counter-Gradient
Shuttling
Transcriptional
Failed to fit data

Figure 2.5: Biophysical values of individual simulations that fit the WT P-Smad5 gradient. (A-L) Scatter plots comparing biophysical parameters of 1,000 solutions classified by mechanism that fit the WT data. Combinations that failed to fit the WT P-Smad5 gradient are small grey dots. We plot solutions as large circles colored according to their mechanism, which is based on definitions outlined in Figure 4C: counter-gradient (red), source-sink (blue), transcriptional (orange), or shuttling (green). We plotted additional shuttling solutions in order to better illustrate trends. (A-F) Simulations using domains displayed in Fig. 4D. (G-L) Simulations using domains displayed in Fig. 4E. (A,G) BMP diffusivity vs. BMP decay rate. (B,H) Chd diffusivity vs. Chd decay rate plus the rate of Chd cleavage by Tld. (C,I) Range was estimated as sqrt(diffusivity/decay). (D,J) Diffusivity of BMP bound to Chd vs. decay rate of BMP bound to Chd. (E,K) Range of Nog protein. (F,L) Chd and BMP-Chd cleavage rate by Tld.

Subsection 2.5: The *chordin* mutant gradient shows no evidence of shuttling

To determine whether Chordin shuttling of BMP ligand plays a functionally relevant role in generating the ventral P-Smad5 peak in zebrafish, as it does in *Drosophila*, we quantified the P-Smad5 gradient of *chordin* mutant embryos over a developmental time series (Fig. 2.6A,B). If it does play a role, then we would expect the ventral P-Smad5 peak to be reduced in *chordin* mutants compared to WT embryos. We found that the P-Smad5 gradient in *chordin* mutants showed a statistically significant increase in lateral regions of the embryo at the four time-points examined from 4.7 to 6.3 hpf (Fig. 2.6C-F,4.2B). Importantly, no decrease in P-Smad5 was observed in the ventral region of *chordin* mutant embryos, nor in any region of the gradient. These results indicate that, unlike the *Drosophila* homolog Sog, Chordin plays no significant BMP

shuttling role during zebrafish DV patterning. It is worth noting that in many solutions, small amounts of BMP ligand are shuttled short distances but do not impact the gradient significantly, and thus are not classified as shuttling. The P-Smad5 gradient in the *chordin* mutants shows, however, that this is minimal in zebrafish.

Interestingly, the loss of *chordin* did not cause an increase in the ventral-most P-Smad5 peak level either (Fig 2.6C-F,4.2B), suggesting that Chordin does not actively block BMP signaling there. However, Smad5 could be limiting and already saturated as P-Smad5 in the ventral-most cells of WT embryos, rendering them unresponsive to further increases in free ligand. To investigate this possibility, I overexpressed Bmp2/7 ligand in WT embryos at a level that fully ventralizes (V5) them at 24 hpf (Fig. 2.6G,H). We quantified P-Smad5 at 5.7 and 6.5 hpf and found that the gradient showed a significant increase in signaling embryo-wide over WT siblings, including in the ventral-most region (Fig. 2.6I). These results indicate that BMP signaling in ventral regions is not near saturation in WT embryos and that Chordin does not regulate the peak P-Smad5 levels by promoting or inhibiting signaling at these stages.

We next tested whether the P-Smad gradient is robust to the heterozygosity of *chordin*. The *Drosophila* P-Mad gradient shows some small changes in *sog* heterozygotes (*sog* is a *chordin* homologue) compared to wildtype (Eldar et al. 2002, Umulis et al. 2010). Similarly, zebrafish heterozygous for *chordin* do not show any DV patterning phenotype at 24 hpf (Matthias Hammerschmidt 1996). We found that the *chordin* heterozygous and WT signaling gradients were indistinguishable at 5.7 hpf (Fig. 2.6J). Therefore, we show that the BMP signaling gradient in zebrafish is robust to a 50% decrease in Chordin levels, but not to the complete loss of Chordin.

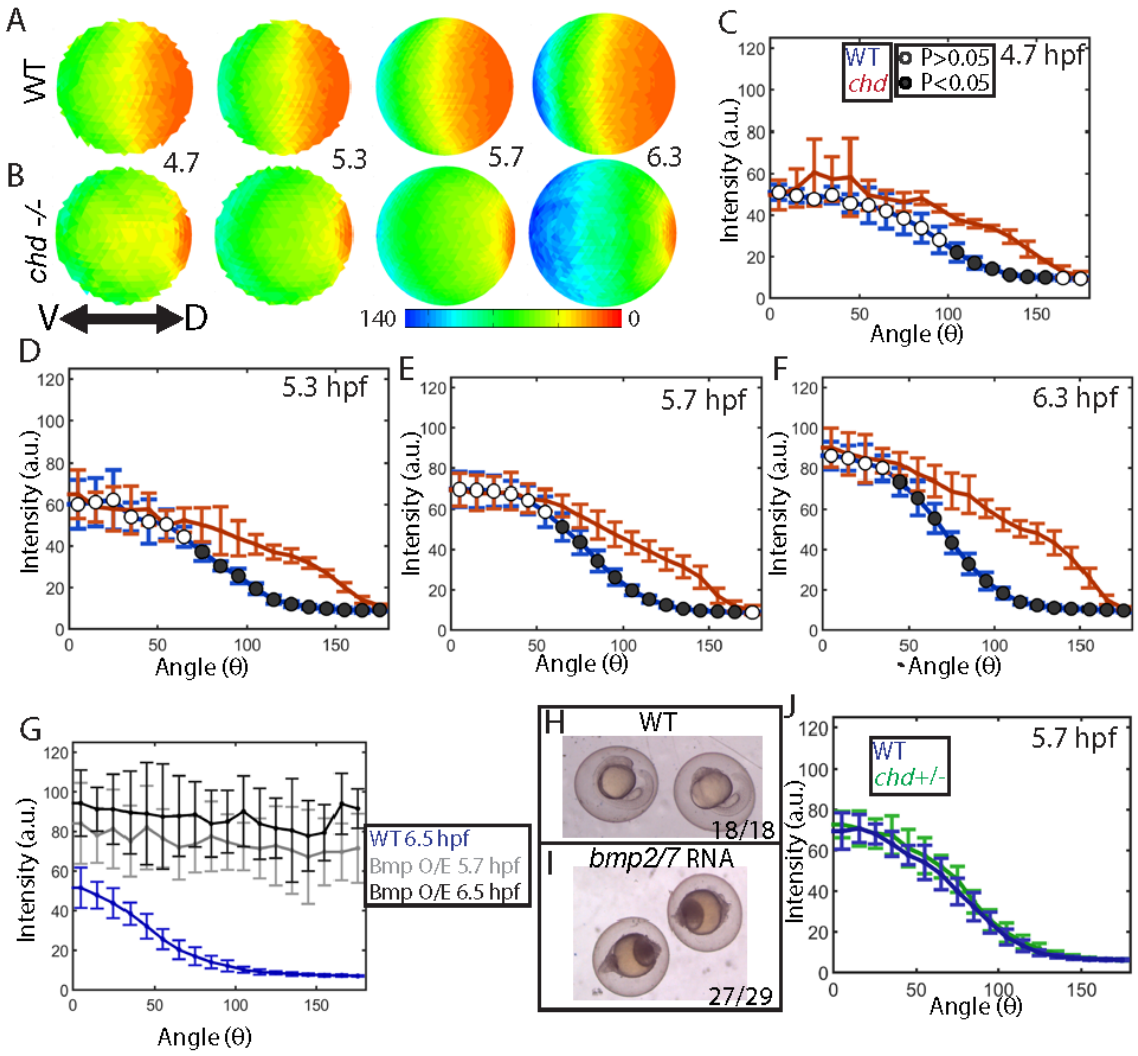

Figure 2.6: Effect of Chd on gradient shape and ligand shuttling. (A,B) Animal views of average intensities from each time-point in (A) WT (4.7: N=3, 5.3: N=4, 5.7: N=13, 6.3: N=11) and (B) *chd* mutant (4.7: N=3, 5.3: N=5, 5.7: N=11, 6.3: N=9) embryos. (C-F) Average marginal intensities for WT (blue) and *chd* mutant (red) embryos from 5.7-6.3 hpf. (G) Average marginal intensities for WT (blue, N=4) and *bmp2/7* RNA injected embryos (grey, N=4) at 5.7 and 6.3 hpf (black, N=5). Error bars indicate standard deviation. (H) Fully ventralized (V5) embryos injected with 6 pg of *bmp7a* RNA and 12

pg of *bmp2b* RNA vs (I) uninjected WT siblings. (J) WT (N=9) vs *chd*+/- (N=10) at 5.7 hpf.

Subsection 2.6: Constraints on computational models imposed by the *chordin* mutant gradient

We then constrained the computational model-based screen with both the WT and the *chordin* mutant and heterozygote P-Smad5 gradients at 5.7 hpf to determine which mechanisms and parameter combinations would remain compatible (Fig. 2.7A,B). We eliminated individual simulations that deviated by more than 8% from the *chordin* heterozygous or homozygous P-Smad gradients (Fig. 2.7C-D). Many mathematical model solutions that fit the WT BMP signaling gradient did not fit our *chordin* heterozygous and homozygous mutant data. Of the 15,142 parameter combinations that fit the WT gradient alone, only 4,059 fit both the WT and *chordin* mutant gradients (Fig. 2.7E-E'). Of those, all were either source-sink or counter-gradient mechanisms (Fig. 2.7E'). All parameter combinations classified as shuttling had *chordin* LOF BMP distributions that deviated from the measured *chordin* mutant P-Smad (Fig. 2.6) gradient by more than 17% (Fig. 2.7C). Many, but not all, parameter combinations classified as counter-gradient had *chordin* heterozygous BMP distributions that deviated from the measured *chordin* heterozygous mutant P-Smad (Fig. 2.6J) gradient by more than 8% (Fig. 2.7D).

These remaining mechanisms required different and specific combinations of biophysical parameters. The source-sink solutions required a high BMP range of 60+ μm with a diffusivity above 1 $\mu m^2/s$ (Fig. 2.7F,G). The counter-gradient mechanism required

a lower BMP range, less than 60 µm, and a high Chordin range above 40 µm with a diffusivity above 2 $\mu m^2/s$ (Fig. 2.7G,H). A low rate of Chordin cleavage by Tolloid was also required for the counter-gradient mechanism to facilitate a high Chordin range (Fig. 2.7I).

We then tested whether the transcriptional mechanism could also fit the *chordin* mutant data. We used our previously discussed simulation in which the *bmp* expression domain exactly matched the WT P-Smad5 gradient (Fig. 2.4E). Of the 64,893 parameter combinations identified as having a source-sink mechanism that fit the WT data alone, 227 fit both WT and *chordin* mutant gradients (Fig. 2.7J,J'). These source-sink solutions required a high BMP diffusivity (Fig. 2.7K) and range similar to what was observed in the simulation with a broader *bmp* expression domain (Fig. 2.7L). However, while 83,747 parameter combinations identified as having a transcriptional mechanism fit the WT data alone, none fit both the WT and *chordin* mutant gradients (Fig. 2.6H,H'). This is because only a change in the *bmp* expression domain in the *chordin* mutant could allow a transcriptional mechanism to fit both the WT and *chordin* mutant data.

The *bmp* expression domain is known to become responsive to BMP signaling, creating a positive feedback loop during gastrulation (Matthias Hammerschmidt 1996, Nguyen et al. 1998, Schmid et al. 2000a). Gastrulation begins in zebrafish at 6 hpf. While the initial *bmp* expression domains are established independently of BMP feedback, a BMP feedback loop becomes active with reported onset times ranging from ~5.5 to 6.5 hpf (Kishimoto et al. 1997, Miller-Bertoglio et al. 1999, Ramel and Hill 2013, Schmid et al. 2000b). To test whether the *bmp* expression domain changes in *chordin* mutants at 4.7 to 5.7 hpf, we compared the *bmp2b* domain size in sibling *chordin-/-* and *chordin+/-*

embryos (Fig. 2.3D,E). *chordin* heterozygotes display a WT phenotype (Matthias Hammerschmidt 1996, Miller-Bertoglio et al. 1999) and we found also display a WT P-Smad5 gradient (Fig. 2.6J). There was no discernable difference in the *bmp2b* domain size at 4.7, 5.3, or 5.7 hpf, indicating that *bmp* transcriptional feedback is not active before 5.7 hpf (Fig. 2.3D,E). Similarly, the *chordin* expression domain did not change in size before 5.7 hpf (Fig. 2.3B). Therefore, the increase in BMP signaling activity observed in *chordin* mutants precedes the change in *bmp* expression, showing that the transcriptional mechanism cannot account for the P-Smad5 gradient profiles prior to 5.7 hpf. We observed a change in *bmp2b* expression by 7 hpf, consistent with previous findings that *bmp* transcriptional feedback activates after gastrulation begins (Fig 2.3D’’’,E’’’) (Kishimoto et al. 1997, Miller-Bertoglio et al. 1999, Ramel and Hill 2013, Schmid et al. 2000b).

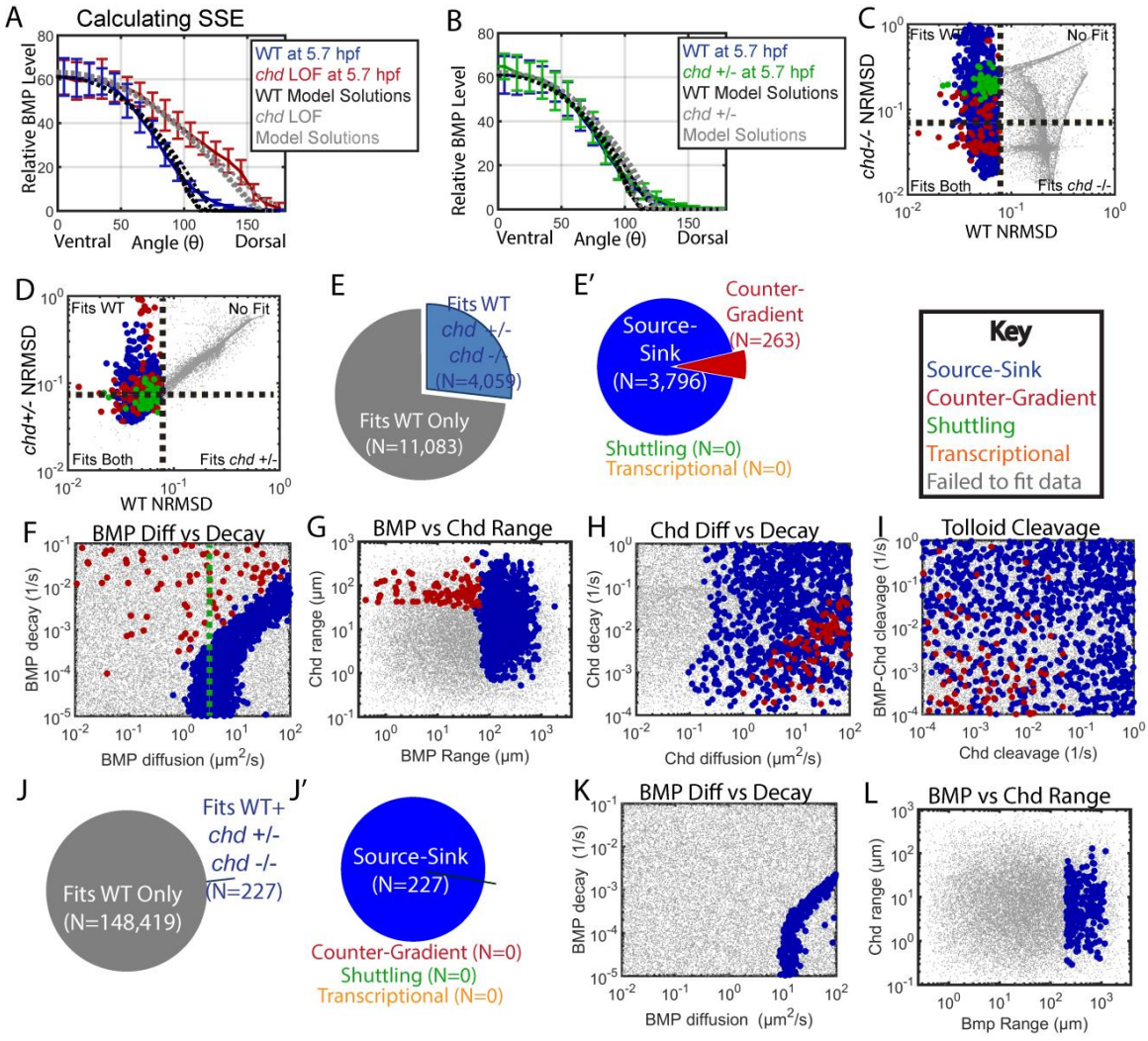

Figure 2.7: Biophysical values of individual simulations that fit both the WT and *chd* LOF P-Smad gradients. (A) BMP distributions of 5 individual modeling solutions (WT: black dotted lines, chd LOF: grey dotted lines) plotted against WT (blue line) and chd LOF (red line) 5.7 hpf P-Smad5 gradients. Error bars indicate standard deviation of experimental P-Smad intensity. (B) BMP distributions of 5 individual modeling solutions (WT: black dotted lines, chd +/-: grey dotted lines) plotted against WT (blue line) and chd +/- (green line) 5.7 hpf P-Smad5 gradients. Error bars indicate standard deviation of experimental P-Smad intensity. (C,D,F-I,K,L) 1,000 randomly selected parameter

combinations capable of fitting both the WT data, chd +/-, chd LOF data classified by mechanism. Larger circular points fit the WT P-Smad gradient and are colored based on their mechanism according to the definitions outlined in figure 4C: counter-gradient (red), sink-source (blue), transcriptional (orange), or shuttling (green). Combinations that failed to fit the WT P-Smad gradient are small grey dots. (C-D) Normalized Root Mean Squared Deviation (NRMSD) between the measured P-Smad and the model BMP distributions. Black dotted lines mark the 8% threshold. (C) Comparing WT and chd LOF. (D) Comparing WT and chd +/-. (E) Parameter combinations fit both the WT data and chd LOF data (blue) and how many failed to do so (grey). (E') parameter combinations were classified to have a source-sink (blue), counter-gradient (red), or shuttling (green) mechanism. (F-I) Simulation using the bmp expression domain displayed in Fig. 4D. (K,L) Simulation using the bmp expression domain displayed in Fig. 4E. (F,K) BMP diffusivity vs. BMP decay rate. Green dotted line marks the BMP diffusivity we measured using FRAP (4.4 μm2/s). (G,L) Range was estimated as sqrt(diffusivity/decay). (H) Chd diffusivity vs. Chd decay rate plus the rate of Chd cleavage by Tld. (I) Rate of Chd cleavage by Tld vs. rate of BMP-Chd cleavage by Tld. (J) Pie chart showing the parameter combinations that fit the WT data (blue) or failed to do so (grey) for the alternative scenario where the bmp expression domain mirrors the measured P-Smad5 gradient (Fig. 3I). (J') Pie chart of how many solutions had a source-sink (blue), counter-gradient (red), transcriptional (orange), or shuttling (green) mechanism.

Subsection 2.7: Fluorescence Recovery After Photobleaching (FRAP) to measure BMP diffusivity

The combination of WT and *chordin* mutant P-Smad5 gradients limits the number of computationally-derived model solutions and, importantly, reduces the number of mechanisms to two: source-sink and counter-gradient. We and others have largely purported the counter-gradient mechanism as acting in vertebrate DV patterning (Blitz et al. 2000, Hama and Weinstein 2001, Little and Mullins 2006, Sasai and De Robertis 1997, Thomsen 1997). To our surprise, the source-sink modeling solutions emerged more frequently within our computational screen than the counter-gradient solutions (Fig 2.7B'). In the source-sink mechanism, BMP ligand must exhibit high diffusivity (Fig 2.7C). To test if BMP diffusivity excludes or supports the source-sink mechanism, we measured the effective diffusivity of the Bmp2b ligand using fluorescence recovery after photobleaching (FRAP).

Our collaborator Ye Bu tagged Bmp2b by inserting the fluorescent protein Venus between the pro- and mature domains of *bmp2b*. He was able to detect both the the pro- and mature domains of Bmp2b with Venus protein (Fig. 2.8A, black arrows). The Venus tag did not interfere with Bmp2b activity, as injections of 50 or 100 pg of the mRNA at the 1-cell stage significantly ventralized the embryos (Fig. 2.8B, Rows 1-2). To further assess the activity and range of the Bmp2b-Venus chimera, I tested if Bmp2b-Venus could rescue embryos lacking Bmp2b, as it has been previously reported that embryos lacking *bmp2b* can be rescued using *bmp2b* RNA (Nguyen et al. 1998). I was able to rescue *bmp2b* LOF embryos to a WT phenotype by injecting *bmp2b-venus* RNA (Fig. 2.8B, Rows 6-8).

To perform the FRAP, we injected *bmp2b-Venus* mRNA into a single blastomere at the 8-cell stage (Fig. 2.8B, Row 3) and then photobleached a 160 μm cube of cells in 4.3 hpf embryos (Fig 2.8C). We then measured recovery of fluorescence over one hour. To ensure we only recorded extracellular Bmp2b-Venus, we photobleached a region away from the cells producing Bmp2b-Venus. The bleached region recovered fluorescence to its initial level in ~30 mins (Fig. 2.8C,E), corresponding to a measured Bmp2b-Venus effective diffusivity of 4.4 +/- 0.4 $\mu m^2/s$ (SEM, n=5). To ensure that we were only measuring the diffusivity of Bmp2b-Venus alone and not Bmp2b-Venus bound to Chordin, we repeated the FRAP experiment in Chordin LOF embryos (Fig 2.8B Row 4-5). Again, The bleached region recovered fluorescence to its initial level in ~30 mins (Fig. 2.8F), corresponding to a measured Bmp2b-Venus effective diffusivity of 4.0 +/- 0.5 $\mu m^2/s$ (SEM, n=5). To determine the extent to which Bmp2b was limiting diffusion, we measured the diffusivity of Venus alone. The bleached region recovered fluorescence much more rapidly, reaching its initial level in under 5 mins (Fig. 2.8D,G), corresponding to a measured Venus effective diffusivity of 16.3 +/- 2.2 $\mu m^2/s$ (SEM, n=5).

A measured BMP diffusivity of ~4 $\mu m^2/s$ fits with a large portion of the source-sink modeling solutions. In fact, 1,421 source-sink solutions have diffusivities within 2 $\mu m^2/s$ of our measured diffusivity (Fig 6F, Green Line). In contrast, only 31 counter-gradient solutions were within 2 $\mu m^2/s$ of our measured diffusivity, and these solutions all have very high BMP decay rates (above $10^{-3}/s$)(Fig 6F, green Line). A decay rate of that magnitude would cause the half-life of BMP ligand in the embryo to be very short, less than 10 minutes for decay rates above $1x10^{-3}/s$, suggesting that a source-sink

mechanism more likely establishes the BMP signaling gradient patterning the zebrafish DV axis.

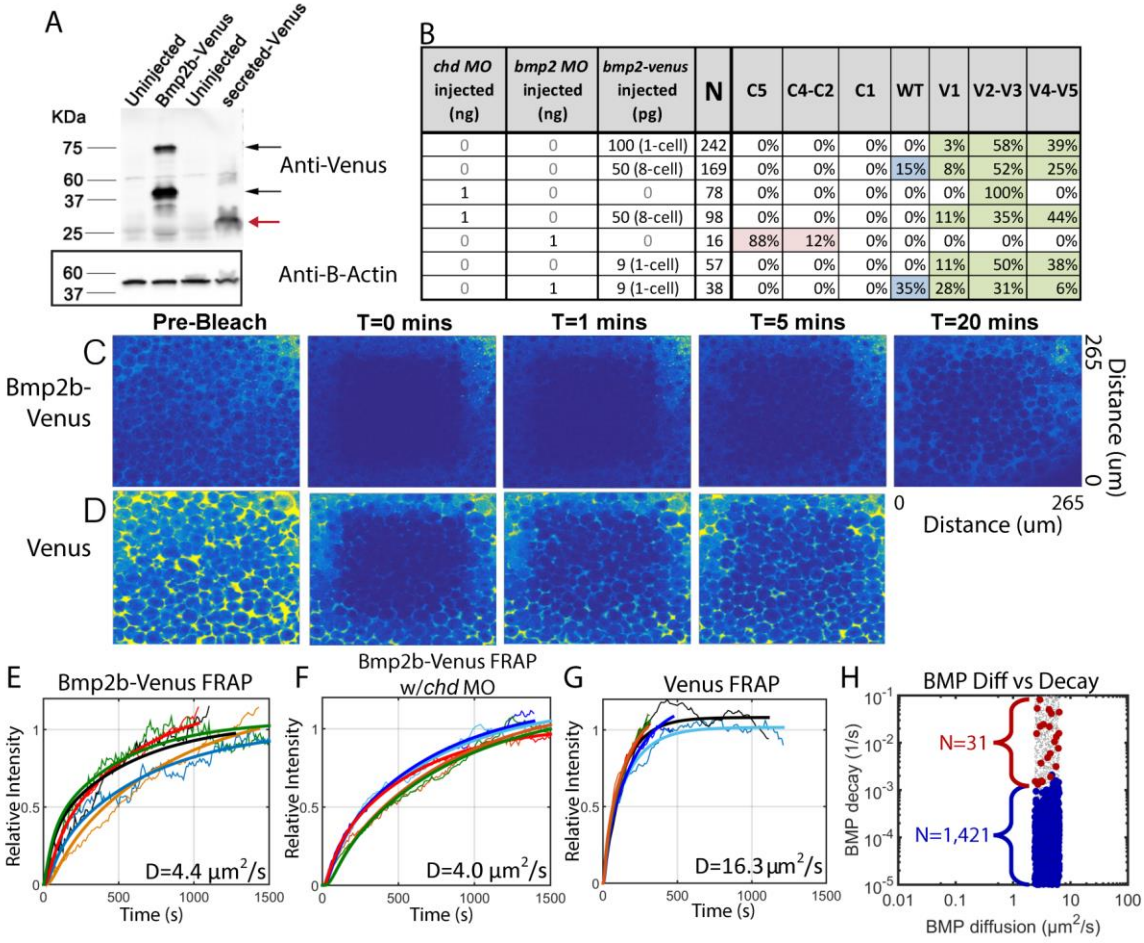

Figure 2.8: Measuring Bmp2b-Venus diffusivity via FRAP. (A) Detection of Bmp2b-Venus and secreted Venus proteins by western blot. Embryos were injected with bmp2b-venus mRNA (250pg) or secreted-Venus mRNA (200pg) at the one-cell stage. Protein lysates were prepared at late blastula stage. In the Bmp2b-Venus overexpression sample, two major protein bands were detected by Venus antibody (black arrows). The larger molecular weight protein is the pro- and mature domains of Bmp2b with Venus protein (669AA, ~74KDa). The smaller protein is the mature domain of Bmp2b with Venus

protein (376AA, ~41KDa). The secreted Venus protein (248AA, ~27KDa) is also detected in the secreted-Venus overexpression sample (red arrow). β-actin was used as a loading control. (B) 24 hpf phenotypes of embryos injected with the bmp2b-venus construct used for FRAP experiments, controls, and rescue. Dorsalization was classified as C5: Loss of all ventral structures; C4-C3: Loss of, or truncated tail; C2-C1: Loss of ventral tail fin. Ventralization is classified as V1: reduction is eye size; V2-V3: the eyes, notochord, and anterior brain are partially or completely absent; or V4-V5: complete loss of all dorsal structures. Fluorescent BMP-Venus (C) or Venus (D) recovery after photobleaching for 20 minutes. (E-G) Plots of fluorescent intensity recovery in the extracellular region. Bold lines are mean curves, thin lines are raw intensity data. (H) BMP diffusivity vs. BMP decay rate for simulations that fit WT, chd +/-, and chd -/- P-Smad profiles and were within 2 μm2/s of 4.4 μm2/s. Large blue circles are simulations classified as source-sink, red are counter-gradient, and small grey dots failed to fit the measured P-Smad profiles. *FRAP and Western Blot were performed by Ye Bu in the lab of David Umulis. Rescue experiments were performed by the author.*

Subsection 2.8: How Noggin and Follistatin affect the BMP gradient

During zebrafish DV patterning, two additional antagonists, Noggin and Follistatin act together with Chordin to repress BMP signaling dorsally (Dal-Pra et al. 2006, Schulte-Merker et al. 1997). Noggin and Follistatin differ from Chordin in their expression domains, phenotype, and interaction with the metalloprotease Tolloid. *chordin* is expressed in a larger domain than *noggin* or *follistatin* (Fig. 2.3,A,B) (Dal-Pra et al. 2006), and Chordin has been shown to diffuse more rapidly than Noggin in the Xenopus gastrula (Inomata et al. 2013). Most importantly, Noggin and Follistatin are not cleaved

by Tolloid or Bmp1, and they bind to BMP with a higher affinity than Chordin (Bayramov et al. 2011, Geng et al. 2011, Glister et al. 2004, Glister et al. 2015, Groppe et al. 2002, Groppe et al. 2003, Iemura et al. 1998, Jay Groppe and Affolter 1998, Sidis et al. 2006, Zimmerman et al. 1996). Therefore, when BMP is bound by Noggin or Follistatin, it is removed from the system with little chance of being freed to re-enter.

Despite their strong BMP binding and immunity to metalloprotease degradation, the loss of *noggin* or *follistatin* by themselves or together does not show a DV patterning phenotype at 24 hpf (Fig. 2.9A) (Dal-Pra et al. 2006). However, when Noggin and Follistatin are depleted in *chordin* mutants, the embryo becomes further ventralized (Fig. 2.9B,C) (Dal-Pra et al. 2006), showing that Noggin and Follistatin play a partially redundant role with Chordin.

To better understand the role that Noggin and Follistatin play during DV axis patterning, we quantified the BMP signaling gradient in embryos depleted of Noggin and Follistatin. The depletion of Noggin and Follistatin together via morpholino injection did not significantly alter the p-Smad gradient at 5.7 hpf (Fig. 2.9D,E,H), consistent with the lack of phenotype seen at 24 hpf (Fig. 2.9A). Surprisingly, the depletion of Noggin and Follistatin in a *chordin* mutant embryo showed little change from the *chordin* mutant P-Smad gradient, except for a small but significant increase of BMP signaling in the dorsal organizer at 5.7 hpf (Fig. 2.9F,G,I,J). Intriguingly, this suggests that Noggin and Follistatin may be responsible for safeguarding the dorsal organizer from receiving any BMP signaling. The dorsal organizer is responsible for secreting numerous BMP antagonists (Niehrs 2004, Nieto 1999, Thisse and Thisse 2015), and BMP signaling is

known to repress antagonist expression after the onset of gastrulation (Miller-Bertoglio et al. 1997).

There are a few explanations as to how the small dorsal increase in BMP signaling seen in Chordin, Noggin, and Follistatin depleted embryos at 5.7 hpf (Fig. 2.9F,G,I,J) could account for the decrease in head structures seen at 24 hpf (Fig 2.9B,C). In both WT and *chordin* mutant embryos, P-Smad is never observed in the dorsal organizer. Though the loss of some head tissue and the notochord could be explained by elevated signaling in the dorsal organizer, much of the midbrain and diencephalon is derived from more animal cells above the organizer where no change in signal is seen at 5.7 hpf. It is possible that increased signaling in the dorsal organizer begins to diminish antagonist expression after gastrulation begins, ultimately exacerbating the BMP signaling phenotype and elevating BMP signaling laterally. It is also worth noting that the *noggin* and *follistatin* morpholinos cause significant developmental delay which may alter patterning in unforeseen ways. For this reason, I recommend that further queries into the function of Noggin and Follistatin be done by generating mutant lines with CRISPR. I was unable to generate a *noggin* mutant using CRISPR due to time constraints.

Constraining the model with the Chordin, Noggin, and Follistatin triple LOF data did little to constrain any model variables or narrow down the solution set (Fig. 2.9K-N). Note that Noggin and Follistatin were combined into a single species (refered to as Noggin) for modeling purposes because their binding to BMP (Table 1), expression (Dal-Pra et al. 2006), and interaction with Tolloid are similar. I eliminated any solutions that deviated from the Chordin, Noggin, and Follistatin LOF P-Smad data by more than 8% (Fig. 2.9K). Less than 1,000 source-sink solutions were eliminated, and it was not enough

to significantly alter the ratio of source-sink to counter-gradient solutions. The diffusivities and decay rates of BMP and Noggin were not constrained further by the addition of the triple loss of function data.

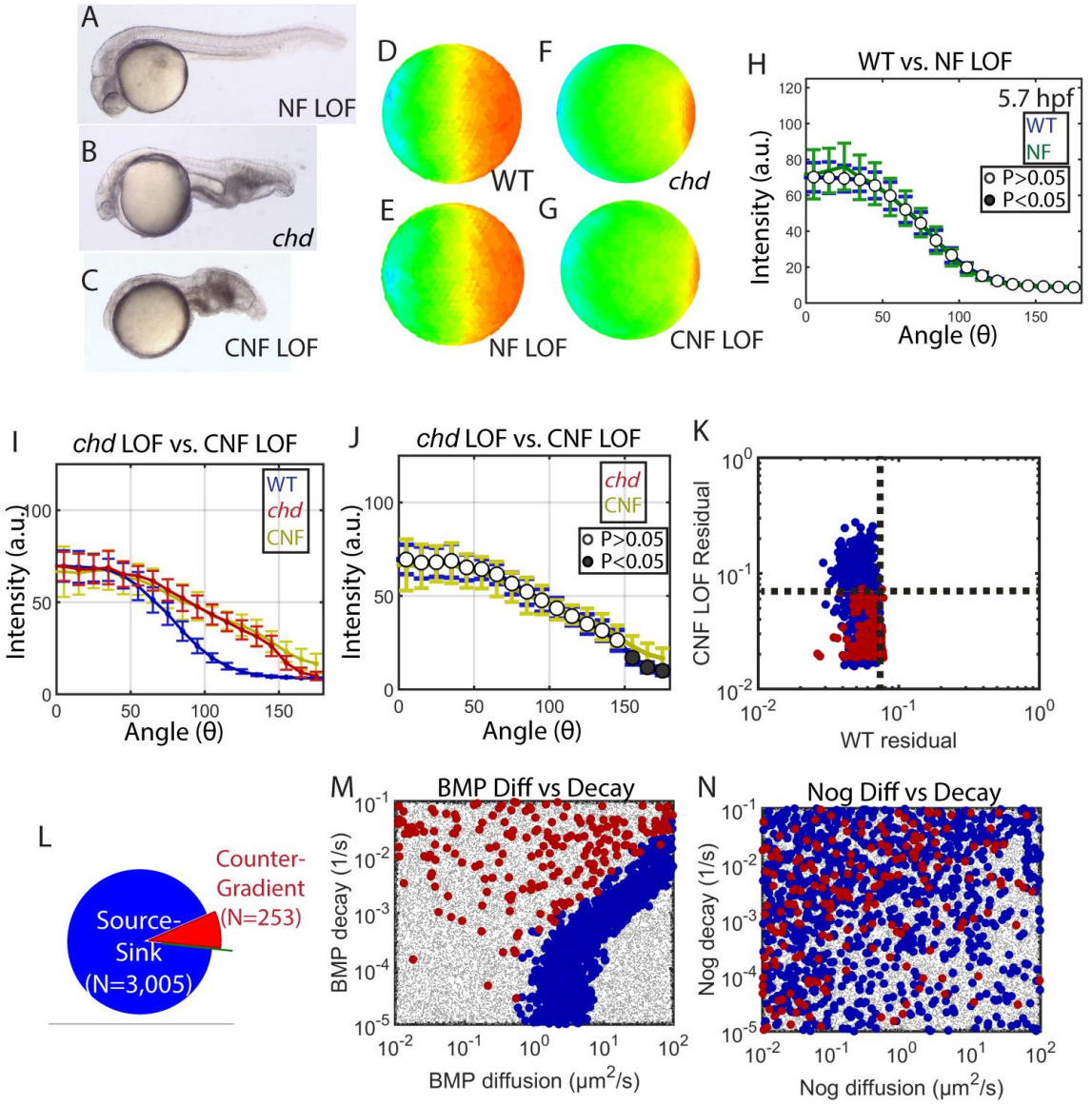

Figure 2.9: Effect of Noggin and Follistatin on gradient shape and ligand shuttling. (A-C) 24 hpf phenotypes of (A) embryos injected with *noggin* and *follistatin* morpholino, (B) *chordin* mutant embryos, (C) *chordin* mutant embryos injected with *noggin* and

follistatin morpholino. Animal views of average intensities at 5.7 hpf in (A) WT (N=9), (B) *chd* mutant (N=11), (C) *noggin* and *follistatin* morpholino injected (N=7), and (D) *chordin* mutant embryos injected with *noggin* and *follistatin* morpholino. (C-J) Average marginal intensities for WT (blue), *noggin* and follistatin morpholino injected (green), *chordin* mutant with *noggin* and *follistatin* morpholino injected (yellow), and *chordin* mutant (red) embryos from 5.7 hpf. Error bars indicate standard deviation. Black dots indicate rejection of the null hypothesis at the 5% significance level for a Two-tailed T-Test. (K) Mean relative error (residual) between the measured P-Smad and the model BMP distributions. Black dotted lines mark the 8% threshold. Grey dots did not fit. Blue dots are source-sink solutions, red dots are counter-gradient solutions, green dots are shuttling solutions. (M,N) parameter combinations capable of fitting the WT data, *chd* +/, *chd* LOF, Nog+Fstl LOF data and Chd+Nog+Fstl LOF data classified by mechanism. (M) BMP diffusivity vs. BMP decay rate. (N) Noggin diffusivity vs. Noggin decay rate.

Subsection 2.9: Comparing Zebrafish and *Drosophila* DV patterning

Our results show that the BMP signaling gradient patterning the zebrafish DV axis is markedly different from the one patterning the *Drosophila* DV axis. The zebrafish BMP signaling gradient is broad, reaching half of its maximum at ~40% of the total DV axis length (Fig. 2.2F). In contrast, the *Drosophila* gradient is incredibly steep, reaching half of its peak at only ~10% of the total embryo DV axis length (Fig. 2.10A) (Peluso et al. 2011, Sutherland et al. 2003). Similarly, the loss of the main BMP antagonist in either organism, Chordin or Sog, causes markedly different effects on the BMP signaling gradient (Fig. 2.10A) (Mizutani et al. 2005, Peluso et al. 2011, Sutherland et al. 2003).

Zebrafish and *Drosophila* DV patterning differ in both length-scale and time-scale. The *Drosophila* embryo has a 250 μm half-circumference, while the zebrafish embryo has a 700 μm half-circumference. The zebrafish gradient is established gradually in ~2-3 hours and maintained for several hours (Ramel and Hill 2013, Tucker et al. 2008), whereas the *Drosophila* BMP signaling gradient is established and patterns DV tissues in ~1 hour (Dorfman and Ben-Zion 2001, Wang and Ferguson 2005). Given these differences between the *Drosophila* and zebrafish systems, we sought to determine if *Drosophila*-like shuttling solutions could exist with zebrafish time- and length-scales, and if so, how the biophysical parameters of components would differ from those consistent with the WT and *chordin* mutant P-Smad5 gradients observed (Fig. 2.6).

In the 1,000,000 random simulations tested, we found many parameter combinations that could generate a steep gradient with extensive shuttling in zebrafish. Solutions were considered to be *Drosophila*-like if their WT gradient reached its half-maximum $\leq$10% of the total embryo circumference and the ventral peak of the *chordin* mutant was 50% lower than the ventral peak level of the WT curve (Fig. 2.10A) (Mizutani et al. 2005). We found 251 solutions that fit the *Drosophila*-like signaling gradients for both WT and *chordin* mutant conditions. We also excluded simulations with excessive BMP-Noggin interaction, as *Drosophila* does not possess *noggin* or *follistatin* homologs (Fig. 2.10B).

The *Drosophila*-like solutions required a very mobile Chordin and BMP-Chordin species. *Drosophila*-like solutions required Chordin to have a high range to move to encounter the BMP in the ventral region (Fig. 2.10C,E). Similarly, BMP-Chordin needed to have a high range so it could be shuttled a sufficient distance towards the ventral-most

region of the embryo (Fig. 2.10D,E). The cleavage of free Chordin by Tolloid needed to be low to allow Chordin range to remain high (Fig. 2.10F). Conversely, the cleavage of bound Chordin needed to be high to release the BMP from Chordin (Fig. 2.10F). Chordin range must be high to allow the formation of a counter-gradient to block signaling in the lateral regions of the embryo (Fig. 2.10E). Conversely, BMP range was relatively unrestricted in *Drosophila*-like solutions, as the shuttling mechanism relies more on BMP-Chordin mobility than BMP mobility (Fig. 2.10G).

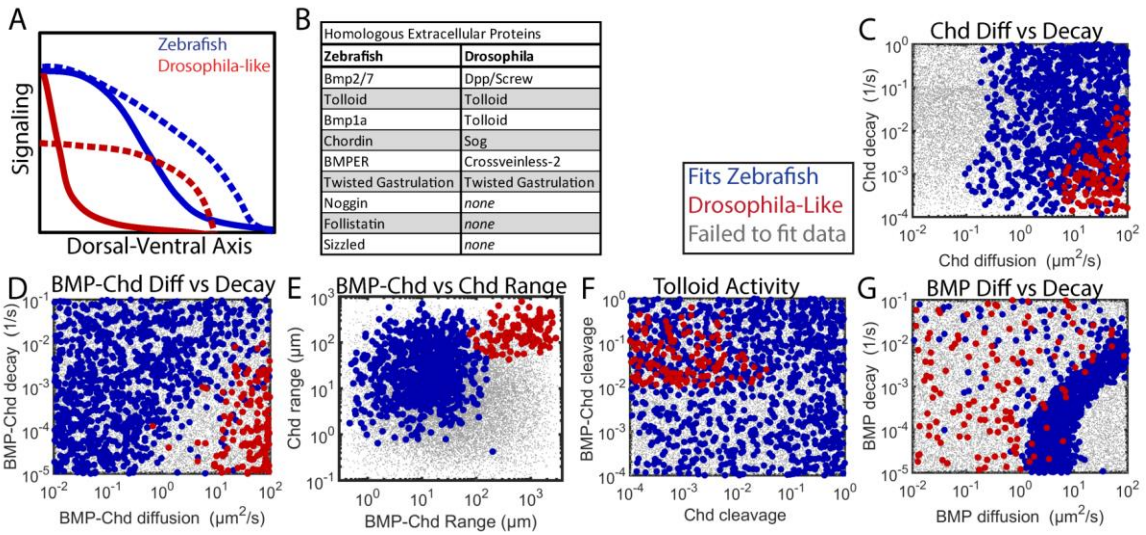

Homologous Extracellular Proteins	
Zebrafish	**Drosophila**
Bmp2/7	Dpp/Screw
Tolloid	Tolloid
Bmp1a	Tolloid
Chordin	Sog
BMPER	Crossveinless-2
Twisted Gastrulation	Twisted Gastrulation
Noggin	*none*
Follistatin	*none*
Sizzled	*none*

Figure 2.10: Comparing Zebrafish and Drosophila-like solutions. (A) Depiction the BMP gradients patterning the Drosophila and zebrafish DV axis. Drosophila DV axis has been flipped to match the zebrafish. Solid lines are WT. Dotted lines are chd or sog LOF. (B) List of homologous genes involved in DV patterning of zebrafish and Drosophila. (C-F) Solutions able to fit WT and chd LOF zebrafish data (blue) vs. solutions capable of fitting Drosophila-like WT and Drosophila-like chd LOF gradients (red). Parameter combinations that failed to fit either are represented as small grey dots. (C) Chd diffusivity vs. Chd decay rate plus the rate of Chd cleavage by Tld. (D) Diffusivity of

BMP bound to Chd vs. decay rate of BMP bound to Chd. (E) Range was estimated as sqrt(diffusivity/decay). (F) Cleavage rate of Chd and BMP-Chd by Tolloid. (G) BMP diffusivity vs. DMP decay rate.

Subsection 2.10: Discussion

Here we have quantified the BMP signaling gradient in WT and *chordin* zebrafish mutants by measuring with high precision the P-Smad5 immunofluorescence level in all ~8,000+ nuclei of an embryo, with high reproducibility within and between embryos at multiple developmental stages. We then used these data to inform a computational model-based screen of over 1,250,000 combinations of biophysical parameters of the major extracellular BMP modulators. We defined mathematical criteria to distinguish between four widely proposed mechanisms to set up the BMP signaling gradient. Our computational model-based screen excludes the shuttling and transcriptional mechanisms as possibilities for establishing our measured WT and *chordin* mutant P-Smad5 profiles, providing compelling evidence that the BMP signaling gradient patterning the zebrafish DV axis is established by either a counter-gradient or source-sink mechanism. We further determined that the effective diffusivity of the BMP ligand in the zebrafish embryo is relatively fast, consistent with 1,421 source-sink solutions but only 31 counter-gradient ones. Comparison of models that satisfy zebrafish or *Drosophila*-like profiles suggest that either the range of BMP-Chordin and/or degradation rate of BMP bound to Chordin/Sog by Tolloid differ between zebrafish and *Drosophila* BMP DV patterning.

Subsection 2.11: Fish vs. flies: a mechanism diverged

The shape of the BMP signaling gradient differs greatly between *Drosophila* and zebrafish DV patterning. The parameters that drive the most significant difference between the *Drosophila*-like and zebrafish solutions are the mobility and processing rates of BMP-Chordin (Fig. 2.5D,F, 2.10D,F). For all shuttling solutions, the BMP-Chordin needed to be sufficiently mobile to reach the ventral-most region of the embryo (Fig. 2.5D,J,9D) and Tolloid needed to cleave BMP-Chordin at a rate that released it close to the ventral-most point (Fig. 2.5F,L,2.10D). For shuttling to be possible in a system with a broad peak of signaling, as it is in zebrafish, the BMP-Chordin cleavage rate needed to be low enough to allow BMP-Chordin to move farther and distribute BMP over a larger region (Fig. 2.5F,L). For shuttling to be possible in a system with a tight peak of signaling as it is in *Drosophila*, BMP-Chordin cleavage needed to be rapid to release BMP-Chordin over a smaller region (Fig. 2.10F). We show that a shuttling mechanism is not functioning in zebrafish, indicating that this delicate balance of BMP-Chordin mobility and Tolloid cleavage has been lost or did not emerge in vertebrate DV patterning.

Sog and its vertebrate homolog Chordin differ in how they are processed by the metalloprotease Tolloid depending on whether it is bound to BMP ligand. Chordin can be cleaved by Tolloid whether bound to BMP ligand or not (Stefano Piccolo Eric Agius, Bin Lu, Shelley Goodman, Leslie Dale, and Eddy M. De Robertis 1997), while Sog is only cleaved when bound to BMP (Guillermo Marques 1997). Interestingly, when Sog is mutated to allow it to be processed by Tolloid regardless of BMP binding, the shuttling of BMP-Sog complexes in flies is greatly reduced (Peluso et al. 2011), suggesting that this

attribute of Sog is necessary for effective shuttling. However, surprisingly, we found numerous shuttling solutions in our zebrafish modeling-based screen with the opposite properties, high Chordin cleavage rates and low BMP-Chordin cleavage rates (Fig. 2.5F,L). The requirement for preferential cleavage of BMP-Chordin by Tolloid only emerged when we screened for *Drosophila*-like solutions, in which shuttling was generating a tight peak of BMP signal (Fig. 2.10A, F). This suggests that the preferential processing of BMP-Sog by Tolloid seen in *Drosophila* is not an inherent requirement of the shuttling mechanism, but may instead be a result of both the requirement to facilitate shuttling and to generate a steep gradient.

In *Drosophila* DV patterning, the BMP signaling gradient is so steep that its base falls well within the region of *bmp* expression, far from the *sog/chordin* expression domain (Fig. 2.10A) (Francois et al. 1994, Holley SA. et al. 1995). To suppress lateral BMP signaling and form the *Drosophila*-like solutions seen in our model-based screen (Fig. 9A), Sog/Chordin needed to have a high range to diffuse far from its site of expression to inhibit BMP signaling over most of the *bmp* expression domain (Fig. 2.10C,E). Therefore, the degradation of free Sog/Chordin by Tolloid needed to be low (Fig. 2.10F). However, to generate a small peak of BMP signaling (Fig. 2.10A), BMP-Chordin cleavage by Tolloid needed to be high (Fig. 2.10F). Therefore, the requirement to preserve the range of action of free Chordin, combined with the requirement to rapidly cleave BMP-Chordin to generate a steep peak of signaling may explain why the preferential cleavage of BMP-Sog by Tolloid is needed for shuttling in *Drosophila*.

Subsection 2.12: Comparing the source-sink and counter-gradient mechanisms

While the shuttling mechanism relies on the movement of the bound BMP-Chordin complex, the source-sink and counter-gradient mechanisms rely on the movement of unbound BMP and Chordin. The source-sink mechanism relies on BMP diffusing dorsally to bind Chordin. Conversely, the counter-gradient mechanism relies on Chordin diffusing ventrally to bind BMP. Consistent with this, we found that the majority of solutions consistent with the source-sink mechanism requires a high BMP range and a high BMP diffusivity (above 1 $\mu m^2/s$), while the counter-gradient mechanism requires a high Chordin range and high Chordin diffusion rate (above 1 $\mu m^2/s$) (Fig. 2.5,2.7).

To illustrate the distinct manners by which a source-sink and counter gradient mechanism would generate the zebrafish BMP signaling gradients observed, we graphically display in Fig. 2.11 the relative contributions of BMP and Chordin diffusion and BMP-Chordin binding to gradient formation. The primary differences between the source-sink and counter-gradient mechanisms manifest in the relative amount of Chordin protein that diffuses ventrally into the *bmp* expression domain and the primary role of Chordin in forming the BMP gradient. A counter-gradient mechanism leads to higher levels of Chordin that extend over a greater region of the ventral *bmp* expression domain compared to a source-sink mechanism (Fig. 2.11A). Counter-gradient and source-sink mechanisms also differ significantly in where Chordin binds and inhibits BMP ligand activity along the DV axis, which is consistent with the distinct Chordin protein distributions (Fig. 2.11A). In a counter-gradient mechanism Chordin binds BMPs in a broader domain, extending over a much greater extent of the DV axis than in a source-sink mechanism (Fig. 2.11B,C). In a source-sink mechanism, Chordin binds BMP largely in dorsal regions and extends little ventrally, effectively generating a driving force for

BMP diffusion (Fig. 2.11B,C). This dorsal sink of Chordin leads to a diffusive flux of BMP ligand down its concentration gradient (Fig. 2.11C) that largely shapes the BMP signaling profile in a source-sink mechanism but contributes far less to a counter-gradient mechanism (Fig. 2.11B).

Importantly, gradient formation by either of these mechanisms need not be exclusive, and instead characteristics of each can contribute to some extent in shaping sectors of the other's gradient. In the source-sink simulation in Fig. 2.11A,C, Chordin forms a small counter-gradient partially contributing to the gradient shape in this region. Thus, in some source-sink simulations, Chordin shaped the gradient by simultaneously binding ligand to block signaling in lateral positions and by establishing a sink that serves as a driving force for the diffusion of ligand from ventral positions dorsally towards the regions of higher Chordin. Though each solution is classified by the dominant mechanism, many share some aspects of both the source-sink and counter-gradient mechanisms.

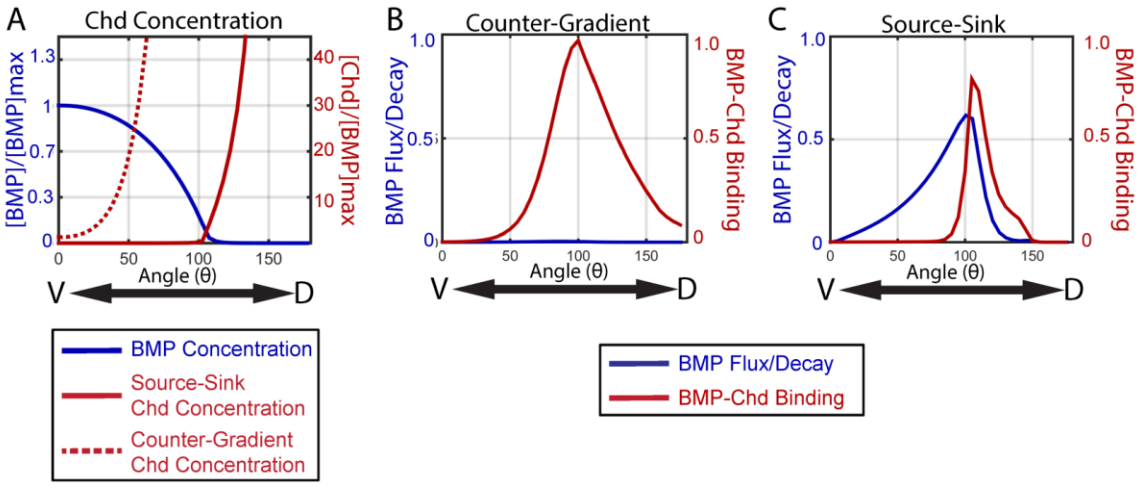

Figure 2.11: How the source-sink and counter-gradient mechanisms shape the gradient. (A) The mean Chd concentrations in all source-sink and counter-gradient solutions fitting WT, chd LOF, and chd heterozygous P-Smad data and within a diffusivity between 2.4 and 6.4 μm2/s. (B) The diffusive flux divided by the decay {(DBMP/decBMP)*(d[BMP]/dx)*(1/[BMP]max)} of BMP (blue) with units of 103*μm and rate of binding of BMP to Chd (kon*[BMP]*[Chd]) (red) with units of 3.6*10-2*sec-1 for representitive (B) Counter-Gradient and (C) Source-Sink solutions fitting WT, chd LOF, and chd heterozygous P-Smad data and within a diffusivity between 2.4 and 6.4 μm2/s (Fig. 7).

Subsection 2.13: BMP diffuses relatively freely

We measured BMP diffusivity for the first time in vertebrates. Using FRAP, we show that BMP can diffuse relatively freely with a diffusivity of 4.4 +/- 0.4 $\mu m^2/s$ (Fig. 2.8E), about 4-fold less than unhindered Venus diffusion in the zebrafish blastula (≈16 $\mu m^2/s$) (Fig. 2.8G). Our measured BMP diffusivity is comparable to the diffusivity of Squint (Ndr1, D=3.2 $\mu m^2/s$), another TGF-β ligand in the zebrafish blastula that acts as a

long-range mesoderm inducer (Muller et al. 2012). This high BMP diffusivity is consistent with previous BMP heterodimer protein injections into the extracellular space of BMP-deficient embryos, which could extend throughout the embryo and restore the WT P-Smad5 gradient within 1.5 hours, suggesting the BMP ligand can move rapidly (Little and Mullins 2009).

Our model-based screen found hundreds of solutions with a BMP diffusivity near 4.4 $\mu m^2/s$. The vast majority of those solutions were classified as having a source-sink mechanism by the definition we outlined in Fig. 2.4. The remaining few are classified as having a counter-gradient mechanism. This paucity of counter-gradient solutions is a reflection of the fine-tuning needed for this mechanism to work as compared to the source-sink mechanism. The counter-gradient mechanism requires a specific balance of Chordin diffusivity and decay as well as Tolloid degradation rate, while the source-sink mechanism does not (Fig. 2.7H,I). Together, this suggests that the source-sink mechanism is more robust to changes in biophysical parameters than the counter-gradient mechanism.

Subsection 2.14: BMP transcriptional feedback: a symptom not a cause

The recent observation that *bmp2b and bmp7a* are expressed in a graded manner in WT embryos has lead to the hypothesis that the BMP signaling gradient may largely reflect the *bmp* expression gradient (Ramel and Hill 2013). A similar hypothesis was made when Bicoid, the morphogen patterning the *Drosophila* AP axis, was also observed to have graded transcript localization (Spirov et al. 2009). However, the Bicoid protein

gradient was later found not to mirror its expression domain and to be set up predominantly by diffusion (Little et al. 2011).

We sought to determine if the BMP signaling gradient in zebrafish is predominantly established by mirroring a *bmp* expression gradient. We disproved this hypothesis three ways. First, we measured the relative shape of the bmp2b expression domain (Fig. 2.3) and found that it did not mirror the P-Smad gradient (Fig. 2.2). Second, we mathematically defined a gradient established by a transcriptional mechanism as one where 80% of the BMP accumulates or is degraded where it is produced, as opposed to binding antagonists or diffusing away. When we performed a computational model-based screen using a *bmp* expression profile that mirrored the P-Smad5 WT gradient, no tested parameter combination could fit both our measured WT and *chordin* LOF P-Smad5 gradients. For the transcriptional mechanism to work, the *bmp* expression domain would have to change in the *chordin* mutant condition to fit the mutant gradient profile.

Finally, we show that feedback by BMP signaling on *bmp* expression does not begin until after 5.7 hpf. This is likely because the initial *bmp* expression domain is established by maternal factors and repression from Bozozok, a transcription factor activated by maternal Wnt signaling (Koos and Ho 1999, Langdon and Mullins 2011, Leung 2003, Solnica-Krezel and Driever 2001). Fgf and Nodal signaling also repress *bmp* expression dorsally (Furthauer et al. 2004, Kuo et al. 2013, Maegawa et al. 2006, Shimizu et al. 2000, Varga et al. 2007). Importantly, BMP signaling does not play a role in the initial establishment of the *bmp* and *chordin* expression domains at 4 hpf, as both are unchanged prior to ~6 hpf in BMP pathway mutants (Kishimoto et al. 1997, Miller-Bertoglio et al. 1997, Schmid et al. 2000b). After ~6 hpf, the *bmp* expression domain

begins to respond to changes in BMP signaling level, as *bmp* expression decreases in BMP pathway mutants and increases in BMP antagonist mutants (Kishimoto et al. 1997, Miller-Bertoglio et al. 1999, Nguyen et al. 1998, Ramel and Hill 2013, Schmid et al. 2000b). We show that the *bmp2b* expression domain does not begin to shift in response to the loss of *chordin* until after 5.7 hpf (Fig. 2.3), while the P-Smad5 gradient shifts as early as 4.7 hpf (Fig. 2.6).

Subsection 2.15: Integrated approach reveals source-sink mechanism

Although in vertebrates we, and most others in the field, have contended that a Chordin (or BMP antagonist) counter-gradient drives formation of the BMP activity gradient in DV patterning, our studies here, intriguingly, suggest that an alternate source-sink mechanism may prevail. While the source-sink gradient mechanism is also modulated by Chordin, Chordin instead acts in a distinct manner as a sink, binding BMP ligand predominantly in dorsal regions, thus allowing a BMP diffusive gradient to form throughout most of the ventral half of the embryo. Key to deriving this alternate model was the integrated approach used that combined quantitative experimental analysis with computational modeling. Importantly, a role for Chordin in establishing a sink that drives gradient formation would not have been revealed to us had we not performed the computational model-based screen. By narrowing the modeling solutions successively with the P-Smad5 WT and then *chordin* mutant profiles, many source-sink models perdured, while most of the counter-gradient ones did not. Furthermore, the computational modeling also illuminated the BMP diffusivity parameter as one to test further the source-sink mechanism. Significantly, our measured Bmp2 diffusivity further supports the source-sink mechanism of gradient formation. Thus the seamless integration

of quantitative experimental analysis with computational model-based screens has proved to be a highly successful approach to elucidating mechanisms of BMP gradient formation. Future studies will be required to definitively determine the mechanism and further test the source-sink and counter gradient models of BMP gradient formation.

Subsection 2.16: Future studies on target gene response and cell to cell variability

Though the interpretation of the BMP signaling gradient by BMP target genes is a crucial step in patterning the DV axis, the relative level of P-Smad promoter binding needed to elicit a BMP target gene response *in vivo* is not yet known. The recent development of quantitative fluorescent *in situ* hybridization method by the RNAscope method and its application to whole mount zebrafish embryos may now allow us to quantify the response of BMP target genes by counting the number of transcript foci produced. By pairing this quantification of the transcriptional response with our method of quantifying the P-Smad response (Fig. 2.12A-F), we can determine the level of BMP signaling needed to induce target gene transcription in an actively patterning vertebrate morphogen gradient.

To determine the relative thresholds needed to activate BMP responsive genes, we could compare the P-Smad level (Fig. 2.12B,C,F) and gene domain size of direct targets of BMP signaling in WT and *chordin* mutant embryos. The genes *msxb*, *AP-2*, and *dlx3*, as well as the well characterized BMP response element (*BRE*), could be used for this analysis. By cloning the promoter regions of these genes into a reporter construct, we could determine which parts of their promoters impart different levels of responsiveness to BMP signaling.

How morphogen gradients create distinct regions of target gene expression in the presence of cell to cell and embryo to embryo variability is an ongoing area of research (Hironaka and Morishita 2012). Due the technical challenges of quantifying morphogen gradients, measurements of embryo to embryo variability have been limited to Drosophila anterior-posterior (AP) (Bahram Houchmandzadeh 2002, Gregor et al. 2007, He et al. 2008), DV (Gavin-Smyth et al. 2013, Umulis et al. 2010), and wing disc patterning (Bollenbach et al. 2008, O. Wartlick 2011). Cell to cell variability has only been measured for the Bicoid gradient patterning the Drosophila AP axis (Gregor et al. 2007).

I provide the first measure of both cell to cell and embryo to embryo positional variability in a vertebrate morphogen gradient. I found that cell to cell variability ranged from ≈10% dorsally to 24% ventrally (Fig. 2.12G). Embryo to embryo variability followed a similar trend, ranging from ≈6%-18% (Fig. 2.12H). I then determined how this cell to cell and embryo to embryo variability translates into positional variability (σ_x). σ_x is defined as the variability divided by the slope of the gradient in a given region. Regions of the embryo that have a high slope and low variability are capable of patterning with greater precision. Using the measured variability and gradient slope, we show that σ_x is lowest between ≈±125˚ and ≈±85˚ of the embryo at all time-points, averaging ≈4% of the embryos length over that range for both cell to cell (Fig. 2.12I) and embryo to embryo (fig. 2.12J) variability. At this stage, cells are ≈1.4% of embryo length in diameter, meaning $\sigma_x \approx 3$ cell lengths in both cases. When thresholded to an absolute intensity of 23, the precision of these boundaries can be observed (Fig 2.12A,C,E).

I then determined whether the loss of Chordin affects cell to cell variability. The loss of *chordin* increases cell to cell variability in dorsolateral regions (Fig 2.12K). However, this increase in variability is due to the overall increase in BMP signaling level seen in *chordin* mutants, as cells with higher signaling levels in both mutant and WT embryos have higher variability (Fig. 2.12L). Therefore, while the loss of *chordin* increases BMP signaling dorsolaterally, it does not increase the cell to cell variability of cells with equivalent signaling levels.

It is unknown whether BMP responsive genes also have similar cell to cell and embryo to embryo variability in expression as the P-Smad gradient. We could use quantitative fluorescent *in situ* hybridization on BMP responsive genes in conjunction with our quantitative measure of BMP signaling activity to determine if the expression of these genes also varies predictably. If they show less variability than the P-Smad gradient, it would indicate that cells are using other mechanisms to supplement their ability to sense positional information. Together, the ability to quantify BMP signaling activity and gene expression in zebrafish embryos offers an important opportunity to move studies of BMP morphogen gradient interpretation into the vertebrate embryo for the first time.

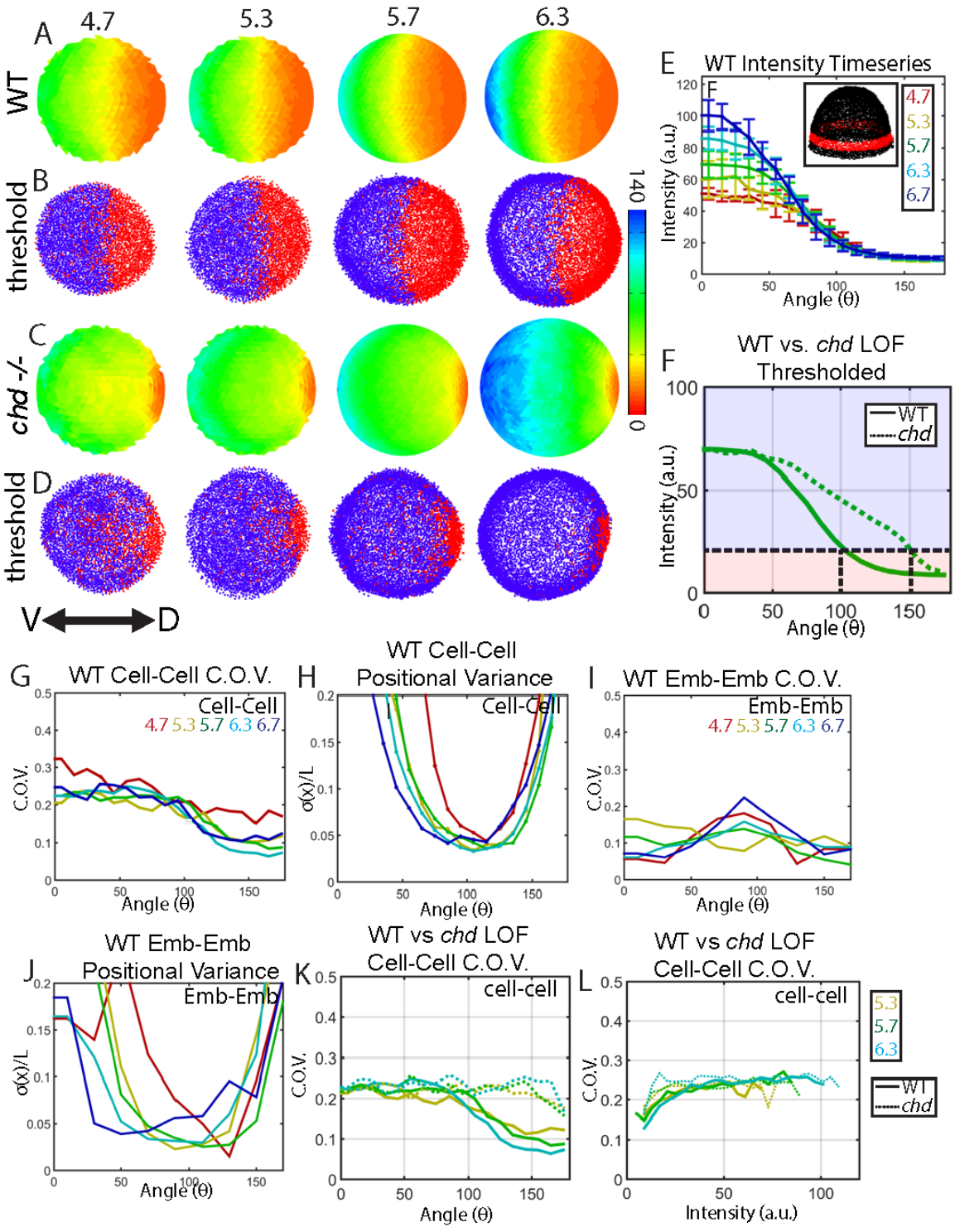

Figure 2.12: Cell to cell and embryo to embryo variability in WT and *chd* embryos.

(A,C) Animal view of the average P-Smad intensities for (A) WT or (C) *chd* LOF

embryos from 4.7-6.3 hpf. (B,D) Individual embryos with a threshold for the absolute intensity set to 23 marks cells above that value blue and below that value as red. (E) Marginal relative P-Smad intensity of a WT time series from 4.7-6.7 hpf. (F) Average relative P-Smad intensity with a threshold set at the absolute intensity of 23 (horizontal black dotted line). The horizontal black dotted lines mark the shift in position of the given threshold in WT vs *chd* mutant embryos. (G) The cell to cell coefficient of variance in WT embryos. (H) The positional cell to cell variance in WT embryos. (I) The embryo to embryo coefficient of variance in WT embryos. (J) The positional embryo to embryo variance in WT embryos. (K) Comparing the cell to cell coefficient of variance in WT and *chd* LOF embryos from 5.3-6.3 hpf. (L) The intensity vs the coefficient of variance in WT and *chd* LOF embryos from 5.3-6.3 hpf.

Chapter 3: The role of Bmper in DV patterning

Subsection 3.1: Background

Bmper has been reported to play a pro-BMP role during zebrafish DV patterning, but morpholino knockdown induces a wide range of dorsalized and ventralized phenotypes (Ambrosio et al. 2008, Rentzsch et al. 2006, Zhang J. L. et al. 2010). This range of phenotypes may be attributed to the ability of Bmper to bind Chordin, in addition to BMP ligand itself, as well as HSPGs and Tsg (Figure 3.1A, Table 1.1) (Ambrosio et al. 2008, Rentzsch et al. 2006, Serpe et al. 2008). Bmper has been reported to act as both an BMP agonist and antagonist in different systems, presumably because of a different environment of proteins present. For example, in Xenopus, Bmper inhibits BMP by forming a ternary complex with it and Tsg (Ambrosio et al. 2008), while in mouse kidney and vertebral field formation, Bmper plays a pro-BMP role that is suppressed by the loss of Tsg (Ikeya et al. 2010, Zakin et al. 2008). In zebrafish, Bmper can enhance BMP signaling only when Chd is present (Zhang J. L. et al. 2010), but can inhibit BMP signaling even in the absence of Chd (Zhang J. L. et al. 2010). However, all studies on Bmper to date in zebrafish have relied on morpholino knockdown, which may account for some of the variability in phenotype.

Subsection 3.2: The *bmper* mutant phenotype

Because Bmper interacts with key extracellular components of the DV patterning system, we considered it an important regulator in shaping the BMP signaling gradient. To test the role of Bmper in quantitatively shaping the BMP signaling gradient, I used TALEN targeted mutagenesis to create a 2 and 5 bp deletion at base pair 669/2004 (AA

223/668) in exon 8 of 16 total exons. Both mutations create a premature stop codon in the same exon (Fig. 3.1A). This premature stop codon disrupts the last two CR domains, as well as the partial von Willebrand Factor D domain at the C-terminus of the protein responsible for HSPG binding (Serpe et al. 2008). Because the mutation creates a stop before the last exon, it likely also induces nonsense mediated decay, thereby preventing translation of Bmper . We also obtained a nonsense mutation at amino acid 545 of 668 total in exon 12 from the Sanger Zebrafish Mutation Project (Fig. 3.1A). The sa108 allele does not disrupt the CR domains, but it may still induce non-sense mediated decay.

To our surprise, none of the *bmper* mutant alleles showed any overt DV phenotype at 24 or 48 hours after fertilization. The *bmper*Δ2 and *bmper*Δ5 alleles were consistently WT at 24 and 48 hpf (Fig. 3.1B). The *sa108* allele fish were predominantly WT, but they did show some mild dorsalization and tail problems (Fig. 3.1B). The most consistent phenotype displayed by *sa108* mutant incrosses was a vein bulge which often blocked the tail vein and caused heart edema (Fig. 3.1B, Vein Bulge). It is unclear whether the mild dorsalization and vein phenotype seen in the sa108 line is from the disruption of *bmper* or from another mutation in a different gene induced by the Zebrafish Mutation Project mutagenesis screen. The lack of a DV phenotype in the *bmper*Δ2 and *bmper*Δ5 alleles, which cause a stop codon far earlier in the gene than the *sa108* allele, suggests that Bmper may not be playing as prominent a role in DV patterning as was originally thought. It also suggests that the previous phenotypes observed in *bmper* morpholino injected fish were artifacts of morpholino injection (Rentzsch et al. 2006, Zhang J. L. et al. 2010).

The *bmper*Δ2, *bmper*Δ5, and *sa108* all share the same larval and adult ear defects that are not related to body axis patterning. This ear defect was initially missed by my analysis until Tanya T. Whitfield from the Bateson Centre and Department of Biomedical Science contacted our lab to request our help in analyzing the DV phenotype of the *sa108* allele. She had noticed a defect in the developing ear anterior and posterior canal duct epithelia. She has found that this defect results in a malformation of the semi-circular canal, and that the adult fish present with vestibular behavioral deficits. After examining my *bmper*Δ2 and *bmper*Δ5 alleles, I found the same ear malformation as seen in the *sa108* allele fish (Fig. 3.1C,D). Both the *sa108* and *bmper*Δ2 homozygous mutants show an enlarged posterior semicircular canal pillar with a diminished posterior semicircular canal pillar (Fig. 3.1D). The ear defect was 100% penetrant, observed in all *sa108* and *bmper*Δ2 larval fish. Interestingly, this suggests that the *bmper*Δ2 and *sa108* mutations both disrupt Bmper function, likely via non-sense mediated decay.

What role Bmper plays in zebrafish ear development is not yet known. BMP signaling is known to play a role in cochlear development and sensory cell formation (Basch et al. 2016). While zebrafish do not possess a cochlea, they instead show defects in semi-circular canal formation (Fig. 3.1D). *bmper* is directly positively regulated by *dlx5*, a gene associated with human split-hand/split-foot type 1 malformation associated with sensorineural hearing loss and mouse inner ear development (Sajan et al. 2011). Dr. Whitfield and colleagues will continue to investigate the role of Bmper in regulating BMP signaling in this new context.

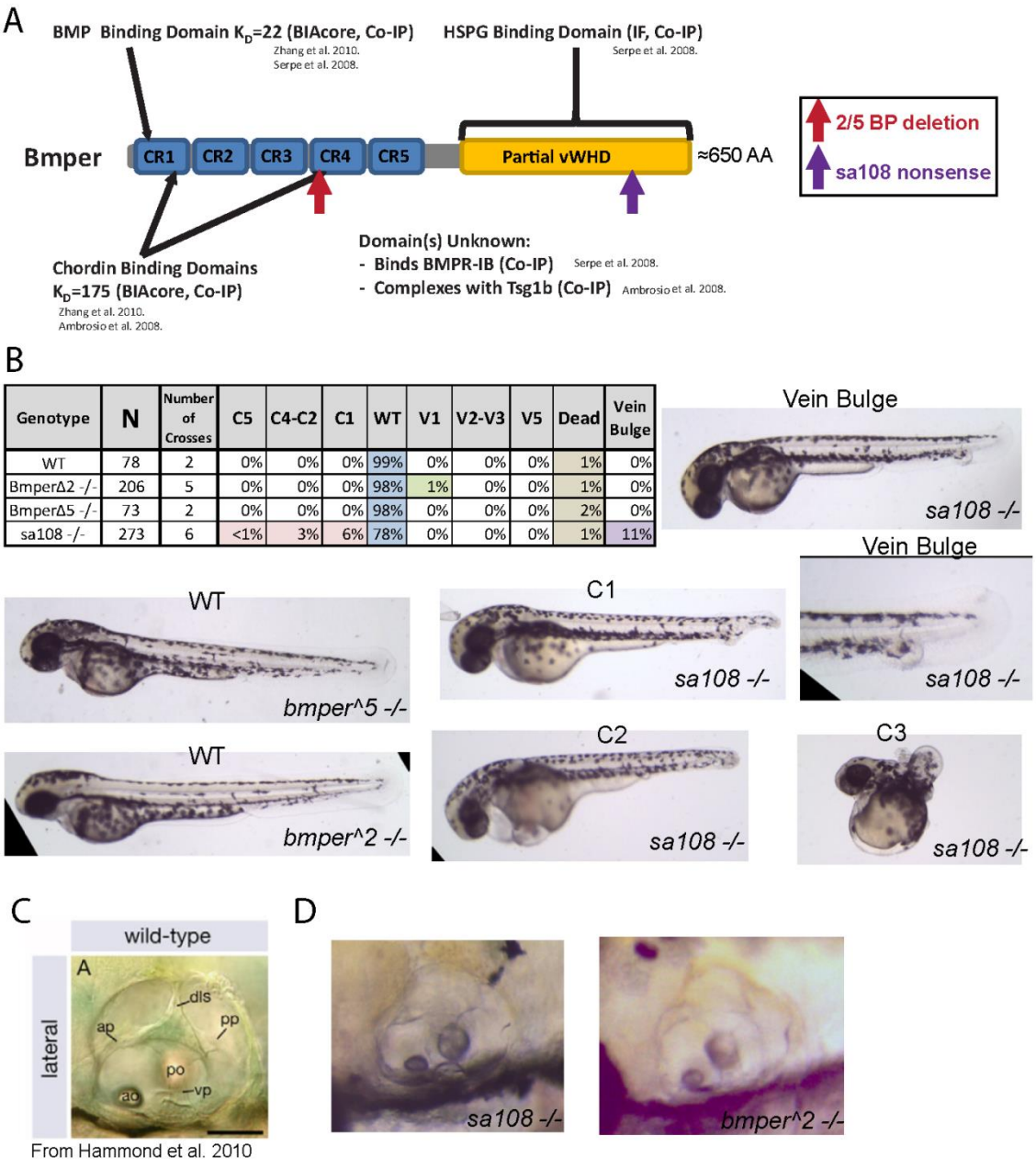

Genotype	N	Number of Crosses	C5	C4-C2	C1	WT	V1	V2-V3	V5	Dead	Vein Bulge
WT	78	2	0%	0%	0%	99%	0%	0%	0%	1%	0%
BmperΔ2 -/-	206	5	0%	0%	0%	98%	1%	0%	0%	1%	0%
BmperΔ5 -/-	73	2	0%	0%	0%	98%	0%	0%	0%	2%	0%
sa108 -/-	273	6	<1%	3%	6%	78%	0%	0%	0%	1%	11%

Figure 3.1: The phenotype of the *bmper*Δ2, *bmper*Δ5, and *sa108* alleles. (C) lateral view of a WT ear bud at 48 hpf from (Hammond et al. 2010), (ap) anterior semicircular canal pillar; (ao) anterior otolith; (dls) dorsolateral septum; (po) posterior otolith; (pp) posterior semicircular canal pillar; (vp) ventral semicircular canal pillar. (D) Lateral view of *sa108* and *bmper*Δ2 mutant ear buds at 48 hpf.

Subsection 3.3: Future studies on Bmper

Though the *bmper*Δ*2* and *bmper*Δ5 show no obvious DV phenotypes at 24 hpf (Fig. 3.1B), they may still play a role in DV patterning. We have not yet quantified the P-Smad gradient during DV patterning or looked for changes in BMP target gene expression during DV patterning. Such analysis may reveal a more subtle BMP signaling phenotype that does not drastically affect the zebrafish at 24 hpf.

The loss of *bmper* in conjunction with *tsg* may reveal a role in DV patterning and exacerbate the observed ear defects. The loss of *tsg* dorsalizes zebrafish embryos, playing a pro-BMP role (Little and Mullins 2004). Tsg has been proposed to enhance the degradation of Chordin by Tolloid during gastrulation in zebrafish (Xie and Fisher 2005). Bmper has also been proposed to play a pro-BMP role in zebrafish by binding to Chordin, but the mechanism by which it does so is not clear (Rentzsch et al. 2006, Zhang J. L. et al. 2010). Bmper has been shown not only to bind to Tsg, but to form a ternary complex with Tsg and Chordin (Ambrosio et al. 2008). Tsg modulates Bmper function during DV patterning in Xenopus (Ambrosio et al. 2008), during vertebral field patterning in mouse (Zakin et al. 2008), and during kidney formation in mouse (Ikeya et al. 2010).

I am currently generating *bmper*Δ2;*tsg* double mutants to determine if these two genes function together or partially redundantly in zebrafish. I used TALEN targeted mutagenesis to induce a 7-bp deletion at base pair 243/720 (AA 81/220) at the beginning of exon 4 of 7 that induces a premature stop in the same exon (Fig. 3.2A). This mutation removes the region of Tsg predicted to bind Chordin and may induce non-sense mediated

decay of the transcript. I currently have *bmper*Δ*2*;*tsg*Δ*7* double heterozygotes and will be making *bmper*Δ*2*;*tsg*Δ*7* double mutants.

Finally, both the *bmper*Δ2 and *bmper*Δ5 mutant fish eventually develop mild skeletal defects which shorten the lifespan of the fish, with very few living past 2 years. The female fish become hunched in posture, and analysis via X-Ray reveals a sharp bend between the 10^{th} and 11^{th} vertebrae (Fig. 3.2B-E). In mice, the loss of *bmper* causes defects in vertebral column development (Zakin et al. 2010, Zakin et al. 2008), as well as eye and kidney defects (Ikeya et al. 2006). The mice die at birth. While the defects caused by the loss of Bmper in zebrafish are much milder, it is possible that the vertebrae of *bmper* mutant fish do not form properly or degrade later in life due to deficient BMP signaling. To determine if BMP signaling plays a role in the skeletal defects caused by *bmper* mutant alleles, further tracking the progression of skeletal defects as well as measuring BMP signaling activity in the vertebral column of larval and adult fish is needed. Additionally, the combinatorial knockout of *bmper* along with *tsg* may exacerbate these skeletal defects.

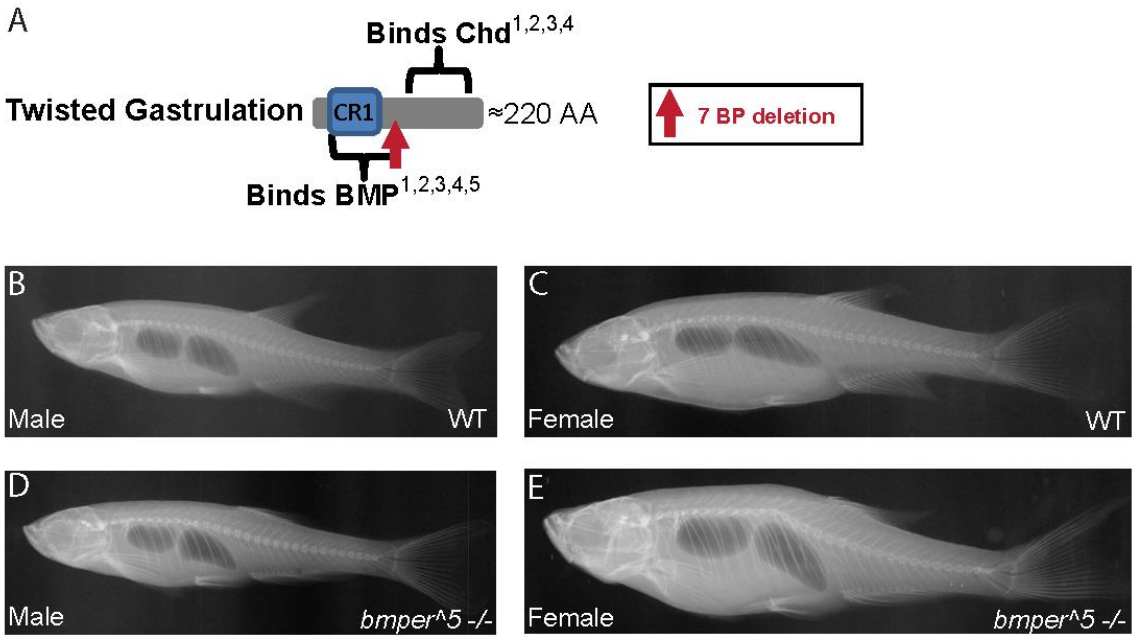

Figure 3.2: *tsg* mutant generation and *bmper* mutant skeletal phenotype. (A) The location of the 7-bp deletion generated relative to the important binding domains in the Tsg protein. (B-E) Lateral X-Rays of 2-year-old WT and *bmper*Δ5 fish. References: 1. (Chang Chenbei et al. 2003) ; 2. (Oelgeschlager et al. 2000); 3. (Oelgeschlager 2003); 4. (Shibata et al. 2005); 5. (Troilo et al. 2016)

Chapter 4: Materials and Methods

mRNA injection for BMP overexpression

Embryos were injected with mRNA at the 1-cell stage. *bmp2b* and *bmp7a* RNA were made using the SP6 MMessage Machine (Life Technologies AM1340). *bmp2b* cDNA in a pBluescript II KS- construct was linearized with NotI. *bmp7a* cDNA in a pCS2+ construct was linearized with NotI. To overexpress BMP, 6 pg of *bmp7a* RNA and 12 pg of *bmp2b* RNA were injected. Resulting embryos had a V5 fully ventralized phenotype at 24 hpf (Fig. 5H,I).

I*n situ* hybridization and domain size analysis

Whole-mount in situ hybridizations were performed using RNA DIG probes as described using: *chordin* (Miller-Bertoglio et al. 1997) and *noggin1* (Dal-Pra et al. 2006). RNA probes were generated using the Roche DIG RNA labeling kit (11277073910). Embryos were cleared in glycerol, and photographed using a Leica IC80 HD. Images were processed using ImageJ and MATLAB. In situs were stained with Anti-DIG-Alkaline Phosphatase (Roche 11093274910) and developed using BM Purple (Roche Life Sciences).

The sizes of the *chordin* and *noggin* expression domains was determined by image processing with MATLAB. Centerpoints of animal views of each embryo were determined by thresholding. The boundaries of the *noggin* and *chordin* expression domains relative to the center of the animal view were determined by a second threshold. These points were connected by line segments, and the angle was measured (Fig. 5C).

TALEN Mutagenesis

Plamids containing TALENs against bmper were ordered from Timothy Dahlem, PhD from the Mutation Generation and Detection Core at the University of Utah. Plasmids targeted 'T ATGATAACTGCACCACCT' and 'T CTTCCTGCAGAGCACTGT' with a 'gcacctgtgtggactcc' spacer region in a PCSII plasmid. Plasmids were linearized using NotI and synthesized from the Sp6 promoter to make RNA for injection. The tsg1b TALEN was prepared the same way, but its target sequences were 'T GTAACCCGCGCAGCAT' and 'ACGGGCAGGAGTACGGTGG A' with a 'gagtgagtctccagcg' spacer. 50 pg of RNA was injected of both the left and the right TALEN.

Single molecule fluorescence *in situ* hybridization and image analysis

Two-color Single molecule fluorescence *in situ* hybridization (smFISH) was performed on fixed cryosections using a RNAscope Fluorescent Multiplex Kit (Advanced Cell Diagnostics(ACD)). Embryos were fixed with 4% paraformaldehyde in PBS at 4°C overnight. Embryos equilibrate in 30% sucrose until they sink and incubated in fresh 30% sucrose for 3 days at 4°C. Cryosections (20μm) at the marginal region were collected on slides, followed by air drying for 30min at −20°C. *In situ* hybridization were performed according to the manufacturer's instructions(ACD). A custom C2 probe was designed for *bmp2b* (#456471-C2). *chd* probe was purchased from the ACD catalog(#440081). *bmp2b* and *chd* probes were mixed at 1:10 dilution. Sections are stained for DAPI and images are acquired at 63× oil objective using a Zeiss 800 upright confocal.

Relative intensity quantification of mRNA levels were performed maximum intensity projections of 20μm sections. *chd* mRNA expression was used to determine the dorsal region. Marginal cells were grouped into 10 degree intervals along the marginal circumference. Average intensity was quantified in each section using MATLAB image analysis toolbox. Averaged *bmp2b* mRNA levels in 2.5hpf embryos were used to measure background. We found equivalent intensity levels and distributions in the 2.5 hpf embyros and the dorsal bmp2b signal in wt 5.7 hpf embryo suggesting limited to zero bmp2b expression in the dorsal region. For each cross-section, the right and left side of the distributions were averaged into a single ventral to dorsal profile.

Immunostaining

Embryos were fixed overnight in 4% paraformaldehyde at 4^{o}C, blocked in NCS-PBST (10% fetal bovine serum, 1% DMSO, 0.1% Tween 20 in PBS), and probed overnight with a 1:100 dilution of anti-phosphoSmad1/5/8 antibody (Cell Signaling Technology), followed by a 1:500 dilution of goat anti-rabbit Alexa Fluor 647-conjugated antibody (Molecular Probes). Embryos were mounted in BABB (benzyl alcohol (Sigma B-1042) and benzyl benzoate (Sigma B-6630), 1:2 ratio) and scanned using a Zeiss LSM 710 confocal microscope with a LD LCI Plan-Achromat 25x/0.8 Imm Corr DIC M27 multi-immersion lens. The oil-immersion setting was used to reduce Mie scattering distortion, spherical aberrations, and chromatic aberrations by minimizing refractive index (R.I.) mismatch between the lens oil (R.I.=1.518), the coverslip, BABB (R.I.≈1.56), and the light scattering particles in the embryo (R.I.≈1.56). Fluorophore bleaching was greatly reduced by precise embryo orientation, reducing sample thickness, and by high scan

speeds using a Zeiss LSM 710 confocal microscope. Nuclei were visualized with Sytox Orange (Molecular Probes) or Sytox Green (Molecular Probes).

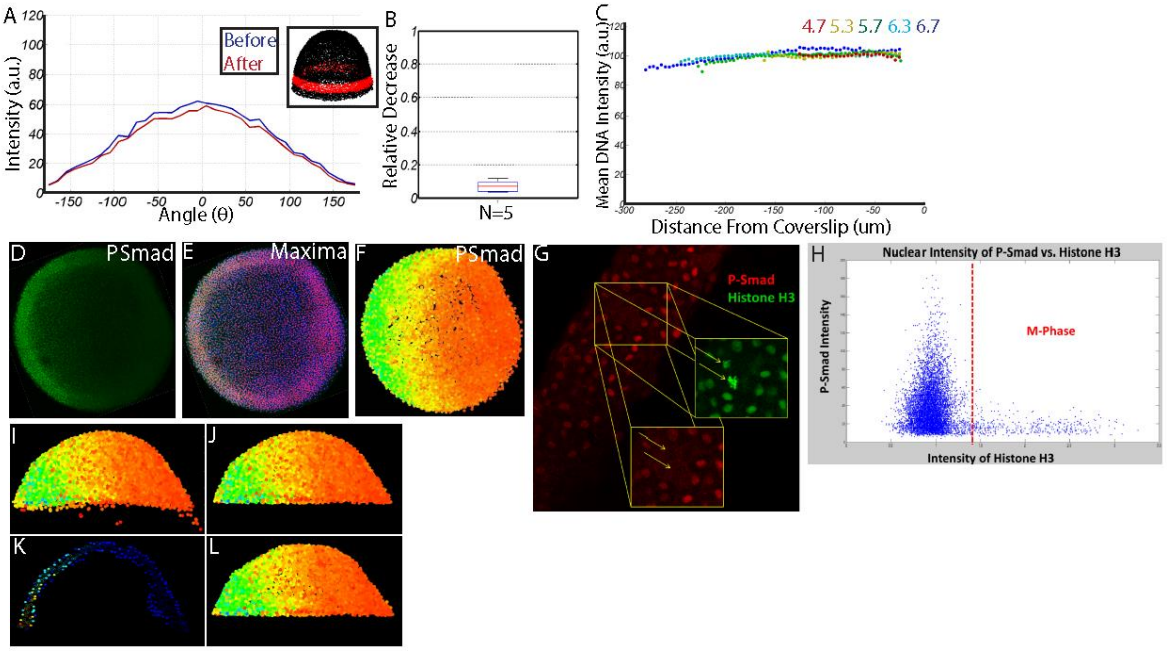

Figure 4.1: Quantifying nuclear P-Smad intensities embryo-wide. (A) Marginal P-Smad intensity from a *chd* LOF embryo imaged twice. (B) Average P-Smad intensity drop-off from photo-bleaching of all nuclei in embryos imaged twice (N=5). (C) There is minimal intensity drop-off due to spherical aberration, as shown by the average intensity of the nuclear DNA stain (Sytox Orange) versus distance from the coverslip (4.7: N=3, 5.3: N=4, 5.7: N=13, 6.3: N=11, 6.7: N=4). (D) Maximum projection of an animal view of a single embryo. (E) Nuclei centerpoints (red dots) identified from the sytox nuclear stain (blue). (F) Measured centerpoint nuclear intensities displayed as a heatmap. (G) P-Smad is absent in dividing cells (red stain, yellow arrows). Dividing cells have bright condensed chromatin (green stain, yellow arrows). (H) Bright condensed chromatin was used to identify dividing cells. Cells above a certain threshold (red line) were eliminated

from the analysis. (I) Lateral view of a single embryo. (J) Sparse Yolk Syncytial Layer nuclei below the margin are eliminated. (K) Single lateral slice depicting the elimination of remaining Yolk Syncytial Layer nuclei and Enveloping Layer Nuclei by subtracting the outer 15% of all nuclei (filled in circles) to leave only deep cell nuclei (open circles). (L) Lateral view of embryo after outer 15% has been eliminated.

Summary of imaging and processing

Immunostained P-Smad5 embryos were processed and imaged as described above. We observed minimal photo-bleaching and spherical aberration (Fig. 11A-C). We wrote a Matlab algorithm capable of identifying all 8000+ nuclei centerpoints in each embryo in 3D, removing populations unresponsive to P-Smad (such as yolk syncytial nuclei and dividing cells), and extracting the P-Smad intensities associated with each nucleus (Fig. 11D-L). The resulting individual digital embryos (Fig. 3A'-E') from each condition were averaged together to generate large datasets from embryo-wide P-Smad levels could be quantified in WT and mutant conditions (Fig. 5A-B).

Image Processing

Nuclear intensities of P-Smad were extracted from the stacks of images generated using Matlab algorithms (source code in supplemental files).

The centerpoints of all the nuclei were located using the Sytox DNA stain. The '.lsm' files were converted to '.tif' files using ImageJ, and then imported into Matlab as 1024 X 1024 X Z multidimensional arrays. XY pixels were 0.55 um, Z pixels were 2.3 um. The images were then smoothed using a 9 x 9 x 3 kernel (most nuclei are 15 x 15 x 4 pixels large). Local minima and maxima were removed using the 'imhmax' and 'imhmin'

functions. The remaining maxima were found using the 'imregionalmax' function on the entire 1024 X 1024 X Z array. Maxima closer together than 6 pixels were assumed to be in the same nucleus, and were combined. The remaining maxima were assumed to be the centerpoints of the nuclei (Fig. 11E).

These centerpoints were used to extract P-Smad intensities on the P-Smad channel. P-Smad distribution in each nucleus was approximately uniform, so a small sphere within each nucleus was averaged to attain the P-Smad intensity. On the P-Smad channel, pixels within within a spherical 6 x 6 x 3 kernel of each maxima were averaged.

Cell types unresponsive to Bmp signaling were removed. P-Smad appears to be uniformly distributed throughout the cytoplasm during cell division, making measurement impractical (Fig. 11G). In dividing cells, chromatin condenses making DNA stains such as Sytox concentrated and bright. Cells with a bright DNA fluorescence staining above 140% of the mean DNA fluorescence were considered dividing and eliminated from the analysis. Extra-embryonic cells such as the Enveloping Layer (EVL) and the Yolk Syncytial Layer (YSL) did not appear to respond to BMP ligand the same way as the deep cells. These cell types are not patterned along the DV axis by BMP, and were eliminated from our analysis. To do so, sparse EVL cells located below the vegetal margin were eliminated by hand (Fig. 11J). Next, the inner and outer layer of approximately 15% of the total cells was eliminated (Fig. 11K,L). The remaining cells were assumed to be non-dividing deep cells.

Embryos of similar stages were then aligned and conformed to a template embryo of the same stage using Coherent Point Drift (CPD)(Song 2010). Embryos were aligned in the

AP direction by fitting them to a sphere, finding a plane that spanned the marginal region, and rotating until that plane was aligned with the XY axis. Embryos were aligned in the DV direction using the embryonic shield as a morphological marker. Before 6 hpf, when the shield is not present, the embryos were aligned in the DV direction by fitting a polynomial regression to the P-Smad gradient around the margin and rotating until the max peak was ventral. Next, embryos were all aligned to a template using an affine CPD (Song 2010). This corrected for any distortions in embryo shape that may have occurred during fixation and staining.

Embryos from the same set were subjected to no normalization. Embryos stained and imaged on different days with different settings were normalized by multiplying the entire set by a single scalar value. To determine this normalization scalar, control WT embryos were always imaged in conjunction with each experimental condition. The scalar normalization value was determined by minimizing the sum of the error between the control WT embryos imaged on different days.

Generating and comparing P-Smad profiles around the margin of the embryo

To generate marginal profiles, a 40 um thick band of cells around the dorsal margin was chosen for each embryo. Cells within that band were grouped into 10 degree intervals and averaged together to form 36 individual points. The left and right side of the gradient were averaged together into a single ventral to dorsal profile. For 3-D embryo-wide averages, all nuclei were projected onto a sphere fitting the embryo. The sphere was then divided into 4800 approximately equilateral triangles. All nuclei falling within each triangle were averaged together. Slopes were obtained by fitting a lowess fit to the

averaged 3-D data's spherical coordinates phi and theta using the 'fit' function in Matlab. To determine if the marginal gradients of WT and *chordin* mutant embryos were significantly different, two-tailed T-Tests were performed with a rejection of the null hypothesis at the 5% significance level (Fig. 1, S1B).We observed a difference in WT vs. *chordin* mutant embryos that was much larger than our observed embryo to embryo variability (Fig. 1). Our t-tests confirmed that our sample sizes are sufficient to discern differences between the WT and *chordin* mutant embryos (Fig. 1, S1B).

A

$$\frac{d[B]}{dt} = D_B\frac{\partial^2 B}{\partial x^2} - k_{onC}[B][C] + k_{offC}[BC] - k_{onN}[B][N] + k_{offN}[BN] - decB[B] + \eta_B + \lambda_{BC}[BC]$$

$$\frac{d[C]}{dt} = D_C\frac{\partial^2 C}{\partial x^2} - k_{onC}[B][C] + k_{offC}[BC] - decC[C] + \eta_C - \lambda_C[C]$$

$$\frac{d[N]}{dt} = D_N\frac{\partial^2 N}{\partial x^2} - k_{onN}[B][N] + k_{offN}[BN] - decN[N] + \eta_N$$

$$\frac{d[BC]}{dt} = D_{BC}\frac{\partial^2 BC}{\partial x^2} + k_{onC}[B][C] - k_{offC}[BC] - decBC[BC] - \lambda_{BC}[BC]$$

$$\frac{d[BN]}{dt} = D_{BN}\frac{\partial^2 BN}{\partial x^2} + k_{onN}[B][N] - k_{offN}[BN] - decBN[BN]$$

1. Production Terms
2. Decay Terms
3. Diffusion Terms
4. Binding Terms
5. Tolloid Degradation Terms

B = BMP
C = Chordin
N = Noggin
BC = Bound Chordin

B

P values WT vs. chd-/- comparison																		
	P value at x degrees:																	
Hours Post Fertilization	0	10	20	30	40	50	60	70	80	90	100	110	120	130	140	150	160	170
4.7	8.0E-01	5.4E-01	2.3E-01	3.2E-01	3.2E-01	5.6E-01	4.4E-01	3.0E-01	7.9E-02	5.2E-02	2.0E-02	4.3E-03	2.3E-04	1.8E-03	8.0E-03	3.2E-03	1.7E-01	2.9E-01
5.3	5.6E-01	7.1E-01	6.2E-01	6.3E-01	3.6E-01	9.0E-01	6.5E-02	2.4E-02	2.5E-02	5.5E-03	8.9E-05	7.2E-06	4.0E-06	1.1E-06	4.0E-07	3.8E-05	1.4E-03	3.1E-03
5.7	9.6E-01	7.0E-01	8.1E-01	6.9E-01	7.7E-01	5.0E-02	4.0E-04	1.7E-05	2.0E-07	2.6E-10	5.7E-13	3.1E-14	7.6E-14	6.6E-13	8.4E-11	6.5E-08	4.2E-04	7.8E-02
6.3	3.0E-01	5.9E-01	5.7E-01	2.0E-01	6.6E-03	5.6E-03	3.4E-05	1.9E-07	3.6E-09	4.1E-13	1.3E-13	2.7E-16	5.4E-15	1.0E-12	4.3E-12	5.0E-09	3.3E-06	8.1E-03

Figure 4.2: Model-based screen of DV patterning in zebrafish. (A) System of differential equations used for model-based screen. (B) P-Values of WT vs. *chd* mutant embryo margin comparison. P values less than 0.05 are highlighted in green.

Model-Based Screen Method

For each set of parameters defined in the parameter vector, we solved the five non-linear reaction-diffusion partial differential equations (PDEs) for BMP ligand, Chordin, Noggin, and the complexes of BMP-Chordin, BMP-Noggin in MATLAB (Fig. S1A). Equations

were solved on the half-circumference, with 'symmetry' boundary conditions imposed on the first and last node-point in the spatial discretization. The half-circumference was discretized into 55 node points with equidistant spacing and the 2^{nd} order spatial derivative is discretized via the finite difference method. The production regions of BMP ligand, Chordin, Noggin, are specified along the nodes by mapping the spatial position to subsequent node position (Fig. 3,4D,E, Table 1). Tld is treated parametrically as a function of position according to its domain of expression (Fig. 4D,E,Table 1). Time-stepping of the solution is handled by the adaptive solver ode15s with a relative tolerance set to 1e-9. The model is solved for the developmental window that spans from 3.5 to 5.7 hpf and all measurements of model error are calculated at 5.7 hpf.

For each parameter vector, the model is initially solved against WT conditions and subsequent simulations for mutant conditions are carried out for the same parameter vector by setting the corresponding production rates for the mutant to zero and re-simulating. Error between the model results and the fluorescent data are calculated via a two-step process. First, the amplitude of the pSMAD fluorescent-intensity data and model peak levels for free BMP are normalized as commonly done when calculating a residual with fluorescent intensity data (Hengenius et al. 2014, Pargett and Umulis 2013). This approximation is valid considering that 1) BMP ligands are not saturating receptors and 2) SMAD activity is not saturated (Fig. 5G). The scaling parameter determined for model-fitness against pSMAD is then applied to the remaining model results to capture any changes in BMP levels in the mutant simulations. Residuals are calculated for WT and mutant conditions independently and solutions are scored for passing the WT and

mutant conditions independently as opposed to using an aggregate residual. Solutions are classified as transcriptional, source-sink, counter-gradient, or shuttling.

Fluorescence Recovery After Photobleaching

Constructs

Sequence encoding fluorescent protein Venus was amplified from pBSK12-*her1:Ub2-Venus* (a gift from Sharon L. Amacher, Ohio State University, OH) (Delaune et al. 2012). This sequence was inserted between the pro- and mature domains of Bmp2b two amino acids downstream of the proprotein convertase (PC) cleavage site (REKR) with a GSTGTTGGG linker separating the prodomain and the fluorescent protein and a GS linker (GGGGSGGGGS) separating the fluorescent protein from the mature domain. This fusion construct was modified from pCS2(+)-HA-Bmp2b (Little and Mullins 2009). Sequences encoding Venus protein were also fused to the pro-domain of Bmp2b two amino acids downstream of the proprotein convertase (PC) cleavage site (REKR) with a GSTGTTGGG linker, to generate the secreted-Venus plasmid.

mRNA synthesis

Capped mRNA was synthesized using the mMessage mMachine Kit (Ambion) with SP6 RNA polymerase according to the manufacturer's protocol. Vectors were linearized by digestion with NotI.

RNA and morpholino Injection

mRNA encoding the Bmp2b-Venus or secreted-Venus, was injected into one- or eight-cell stage embryos. For rescue experiments, 1 ng of *bmp2b* morpholino

(GTCTGCGTTCCCGTCGTCTCCTAAG) was injected along with 9 pg of b*mp2b-venus* RNA from a different needle. To perform FRAP in the absence of Chordin, we injected embryos at the 1-cell stage with 1 ng of *chordin* morpholino (ATCCACAGCAGCCCCTCCATCATCC). Next, *bmp2b-venus* RNA was injected into a single blastomere at the eight-cell stage. Associated injection phenotypes are shown in Figure 8B.

Western Blot

Zebrafish embryos were lysed in Pierce RIPA buffer (89900, Thermo Scientific) supplemented with Halt Protease Inhibitor Cocktail (1862209, Thermo Scientific) and Phosphatase inhibitor Cocktail (1862495, Thermo Scientific). Protein samples mixed with Laemmli sample buffer (Bio-rad) were denatured by incubation for 5min at 98o, and resolved by SDS-PAGE using Mini-PROTEAN TGX Gels (10%, Bio-rad) and transferred to PVDF membranes (Bio-rad). The membranes were blocked with 5% non-fat milk (Bio-rad) in PBST 1 hour at room temperature, and incubated with primary antibodies in 2% BSA (Sigma) in PBST at 4℃ overnight. After that, the membranes were incubated with HRP-coupled secondary antibodies 1 hour at room temperature. Chemiluminescence was detected using Clarity Western ECL Substrate (Bio-rad) to get the image. Using stripping buffer (46430, Thermo Scientific), the membranes were reused to detect β-Actin as loading controls.

Subheading XX: Fluorescence Recovery After Photobleaching (FRAP)

mRNA encoding the Bmp2b-Venus fusion protein (50pg) was injected at the one-cell stage to test the activity of the mRNA in a ventralization assay. Embryos used for FRAP

were injected in one cell at the eight-cell stage. Embryos were mounted in 1% low melting temperature agarose (Sigma) in glass bottom microwell dishes (MatTek Corporation). FRAP experiments were performed using a LSM 800 confocal microscope (Zeiss) with a W Plan-Apochromat 20×/1.0 objective (D=0.17 M27 75mm). Photobleaching in a square region (160.4μm × 160.4μm) was performed through the depth of the blastoderm with 100% laser power in ~10 min. Recovery of fluorescence was monitored every 10s in the same imaging plane.

Processing of FRAP data

In 8-cell stage injected embryos, regions lacking Bmp2b-Venus producing cells (visualized by high intensity signaling throughout the cytoplasm) were identified. Cells displayed characteristic higher intensity signals in the intercellular space and no signal was detected intracellularly in the non-producing cells. Images are taken before the FRAP experiment commences, and saved every 10s during acquisition. All files are exported in lossless TIFF format for subsequent quantification in MATLAB. To measure the recovery, all TIFF files are imported into MATLAB and the FRAP region is identified for subsequent measurements. Internal FRAP region is scaled from 8-bit [0 255] to [0, 1] and an extracellular mask is generated by removing background with a minimum threshold level set at 1% of the image maximum value. This excludes the intracellular compartments from biasing the average intensity calculations for the extracellular recovery. With background removed, recovery is calculated as the average fluorescence intensity of the extracellular fluorescence within the masked region.

Calculation of diffusion coefficients from FRAP data

The FRAP region is modeled using a finite-difference equation for diffusion in the FRAP region. Diffusion is estimated by measuring model recovery starting from zero initial conditions and constant concentration boundary conditions. Masked region dimensions for measurement are mapped directly to node-points and distances in the finite difference model to compare and optimize recovery in the mask region. A steepest-descent optimizer with multiple starts was used to estimate the diffusion coefficient for each FRAP experiment. We do not explicitly model the occlusion and tortuosity of the diffusion process caused by the arrangement of cells, nor does it account explicitly for binding and unbinding to HSPGs and other immobile binding components. The impact of binding and the role of occlusions in the diffusion path are very well known (Cussler 2009, Maxwell-Garnett 1904). Therefore our measured diffusion coefficients are the effective diffusion coefficients in zebrafish and not an intrinsic measurement of the diffusion coefficient in a free environment.

Citations

Abe G, Lee SH, Chang M, Liu SC, Tsai HY, Ota KG. 2014. The origin of the bifurcated axial skeletal system in the twin-tail goldfish. Nat Commun 5:3360.

Abe G, Lee SH, Li IJ, Chang CJ, Tamura K, Ota KG. 2016. Open and closed evolutionary paths for drastic morphological changes, involving serial gene duplication, sub-functionalization, and selection. Sci Rep 6:26838.

Agius E, Oelgeschlager M, Wessely O, Kemp C, De Robertis EM. 2000. Endodermal Nodal-related signals and mesoderm induction in Xenopus. Development 127:1173-1183.

Ambrosio AL, Taelman VF, Lee HX, Metzinger CA, Coffinier C, De Robertis EM. 2008. Crossveinless-2 Is a BMP feedback inhibitor that binds Chordin/BMP to regulate Xenopus embryonic patterning. Dev Cell 15:248-260.

Andriy Myronenko XS, Miguel A . Carreira-Perpinan. 2010. Non-rigid point set registration: Coherent Point Drift. IEEE Trans Pattern Anal Mach Intell. 32:2262-2275.

Aykul S, Martinez-Hackert E. 2016. New Ligand Binding Function of Human Cerberus and Role of Proteolytic Processing in Regulating Ligand-Receptor Interactions and Antagonist Activity. J Mol Biol 428:590-602.

Aykul S, Ni W, Mutatu W, Martinez-Hackert E. 2015. Human Cerberus prevents nodal-receptor binding, inhibits nodal signaling, and suppresses nodal-mediated phenotypes. PLoS One 10:e0114954.

Bachiller D. 2003. The role of chordin/Bmp signals in mammalian pharyngeal development and DiGeorge syndrome. Development 130:3567-3578.

Bachiller D, et al. 2000. The organizer factors Chordin and Noggin are required for mouse forebrain development. Nature 403.

Bahram Houchmandzadeh EW, Stanislas Leibler. 2002. Establishment of developmental precision and proportions in the early Drosophila embryo. Nature 415:798-802.

Bakkers J, Hild M, Kramer C, Furutani-Seiki M, Hammerschmidt M. 2002. Zebrafish ・Np63 Is a Direct Target of Bmp Signaling and Encodes a Transcriptional Repressor Blocking Neural Specification in the Ventral Ectoderm. Developmental Cell 2.

Basch ML, Brown RM, 2nd, Jen HI, Groves AK. 2016. Where hearing starts: the development of the mammalian cochlea. J Anat 228:233-254.

Bates TJ, Vonica A, Heasman J, Brivanlou AH, Bell E. 2013. Coco regulates dorsoventral specification of germ layers via inhibition of TGFbeta signalling. Development 140:4177-4181.

Bayramov AV, Eroshkin FM, Martynova NY, Ermakova GV, Solovieva EA, Zaraisky AG. 2011. Novel functions of Noggin proteins: inhibition of Activin/Nodal and Wnt signaling. Development 138:5345-5356.

Beddington R, Robertson E. 1999. Axis Development and Early Asymmetry in Mammals. Cell 96.

Bell E. 2003. Cell fate specification and competence by Coco, a maternal BMP, TGFbeta and Wnt inhibitor. Development 130:1381-1389.

Belo JA, Bachiller D, Agius E, Kemp C, Borges AC, Marques CL, Piccolo S, De Robertis EM. 2000. Cerberus-like is a secreted BMP and nodal antagonist not essential for mouse development. Genesis 26.

Ben-Zvi D, Shilo BZ, Fainsod A, Barkai N. 2008. Scaling of the BMP activation gradient in Xenopus embryos. Nature 453:1205-1211.

Bier E, De Robertis EM. 2015. EMBRYO DEVELOPMENT. BMP gradients: A paradigm for morphogen-mediated developmental patterning. Science 348:aaa5838.

Bijakowski C, et al. 2012. Sizzled is unique among secreted frizzled-related proteins for its ability to specifically inhibit bone morphogenetic protein-1 (BMP-1)/tolloid-like proteinases. J Biol Chem 287:33581-33593.
Blader P. 1997. Cleavage of the BMP-4 Antagonist Chordin by Zebrafish Tolloid. Science 278:1937-1940.
Blitz IL, Cho KW, Chang C. 2003. Twisted gastrulation loss-of-function analyses support its role as a BMP inhibitor during early Xenopus embryogenesis. Development 130:4975-4988.
Blitz IL, Shimmi O, Wunnenberg-Stapleton K, O'Connor MB, Cho KW. 2000. Is chordin a long-range- or short-range-acting factor? Roles for BMP1-related metalloproteases in chordin and BMP4 autofeedback loop regulation. Dev Biol 223:120-138.
Bokel C, Brand M. 2013. Generation and interpretation of FGF morphogen gradients in vertebrates. Curr Opin Genet Dev 23:415-422.
Bollenbach T, Pantazis P, Kicheva A, Bokel C, Gonzalez-Gaitan M, Julicher F. 2008. Precision of the Dpp gradient. Development 135:1137-1146.
Branam AM, Hoffman GG, Pelegri F, Greenspan DS. 2010. Zebrafish chordin-like and chordin are functionally redundant in regulating patterning of the dorsoventral axis. Dev Biol 341:444-458.
Briscoe J, Small S. 2015. Morphogen rules: design principles of gradient-mediated embryo patterning. Development 142:3996-4009.
Canty EG, Garrigue-Antar L, Kadler KE. 2006. A complete domain structure of Drosophila tolloid is required for cleavage of short gastrulation. J Biol Chem 281:13258-13267.
Carron C, Shi DL. 2016. Specification of anteroposterior axis by combinatorial signaling during Xenopus development. Wiley Interdiscip Rev Dev Biol 5:150-168.
Cha YR, Takahashi S, Wright CV. 2006. Cooperative non-cell and cell autonomous regulation of Nodal gene expression and signaling by Lefty/Antivin and Brachyury in Xenopus. Dev Biol 290:246-264.
Chang C, Eggen BJL, Weinstein DC, Brivanlou AH. 2003. Regulation of nodal and BMP signaling by tomoregulin-1 (X7365) through novel mechanisms. Developmental Biology 255:1-11.
Chang C, Holtzman D, Chau S, Chickering T, Woolf A, Holmgren L, Bodorova J, Gearing D, Holmes W, Brivanlou AH. 2001a. Twisted gastrulation can function as a BMP antagonist. Nature 410.
Chang C, Holtzman D, Chau S, Chickering T, Woolf E, Holmgren L, Bodorova J, Gearing D, Holmes W, Brivanlou AH. 2001b. Twisted Gastrulation can function as a BMP antagonists. Nature 410.
Chen C, Shen MM. 2004. Two modes by which Lefty proteins inhibit nodal signaling. Curr Biol 14:618-624.
Cheng SK, Olale F, Brivanlou AH, Schier AF. 2004. Lefty blocks a subset of TGFbeta signals by antagonizing EGF-CFC coreceptors. PLoS Biol 2:E30.
Chiodelli P, Mitola S, Ravelli C, Oreste P, Rusnati M, Presta M. 2011. Heparan sulfate proteoglycans mediate the angiogenic activity of the vascular endothelial growth factor receptor-2 agonist gremlin. Arterioscler Thromb Vasc Biol 31:e116-127.
Cho GS, Choi SC, Han JK. 2013. BMP signal attenuates FGF pathway in anteroposterior neural patterning. Biochem Biophys Res Commun 434:509-515.
Church RH, et al. 2015. Gremlin1 preferentially binds to bone morphogenetic protein-2 (BMP-2) and BMP-4 over BMP-7. Biochem J 466:55-68.
Cohen M, Briscoe J, Blassberg R. 2013. Morphogen interpretation: the transcriptional logic of neural tube patterning. Curr Opin Genet Dev 23:423-428.
Collavin L. 2003. The secreted Frizzled-related protein Sizzled functions as a negative feedback regulator of extreme ventral mesoderm. Development 130:805-816.
Connors S, Trout J, Ekker M, Mullins M. 1999. The role of tolloid mini fin in dorsoventral pattern formation of the zebrafish embryo. Development 126:3119-3130.

Connors SA, Tucker JA, Mullins MC. 2006. Temporal and spatial action of tolloid (mini fin) and chordin to pattern tail tissues. Dev Biol 293:191-202.
Crick F. 1970. Diffusion in embryogenesis. Nature 225:420-422.
Cussler. 2009. Diffusion: Mass Transfer in Fluid Systems, 3rd edition.
Dal-Pra S, Furthauer M, Van-Celst J, Thisse B, Thisse C. 2006. Noggin1 and Follistatin-like2 function redundantly to Chordin to antagonize BMP activity. Dev Biol 298:514-526.
Dale L, Evans W, Goodman S. 2002. Xolloid-related: a novel BMP1/Tolloid-related metalloprotease is expressed during early Xenopus development. Mechanisms of Development 119.
De Robertis EM, Kuroda H. 2004. Dorsal-ventral patterning and neural induction in Xenopus embryos. Annu Rev Cell Dev Biol 20:285-308.
De Robertis EM, Moriyama Y. 2016. The Chordin Morphogenetic Pathway. Curr Top Dev Biol 116:231-245.
De Robertis EM, Sasai Y. 1996. A common plan for dorso-ventral patterning in bilateria. Nature 380.
Degenkolbe E, et al. 2013. A GDF5 point mutation strikes twice--causing BDA1 and SYNS2. PLoS Genet 9:e1003846.
Deglincerti A, Haremaki T, Warmflash A, Sorre B, Brivanlou AH. 2015. Coco is a dual activity modulator of TGFbeta signaling. Development 142:2678-2685.
Delaune EA, Francois P, Shih NP, Amacher SL. 2012. Single-cell-resolution imaging of the impact of Notch signaling and mitosis on segmentation clock dynamics. Dev Cell 23:995-1005.
Di-Gregorio A, Sancho M, Stuckey DW, Crompton LA, Godwin J, Mishina Y, Rodriguez TA. 2007. BMP signalling inhibits premature neural differentiation in the mouse embryo. Development 134:3359-3369.
Dionne MS, Skarnes WC, Harland RM. 2001. Mutation and analysis of Dan, the founding member of the Dan family of transforming growth factor beta antagonists. Mol Cell Biol 21:636-643.
Dorfman R, Ben-Zion S. 2001. Biphasic activation of the BMP pathway in drosophila embryonic dorsal region. Development 128:965-972.
Dutko JA, Mullins MC. 2011. SnapShot: BMP signaling in development. Cell 145:636, 636 e631-632.
Eldar A, Dorfman R, Weiss D, Ashe H, Shile B-Z, Barkai N. 2002. Robustness of the BMP morphogen gradient in Drosophila embryonic patterning. Nature 419:300-304.
Esteves FF, Springhorn A, Kague E, Taylor E, Pyrowolakis G, Fisher S, Bier E. 2014. BMPs regulate msx gene expression in the dorsal neuroectoderm of Drosophila and vertebrates by distinct mechanisms. PLoS Genet 10:e1004625.
Feldman B, Concha ML, Saude L, Parsons M, Adams R, Wilson SW, Stemple DL. 2002. Lefty Antagonism of Squint Is Essential for Normal Gastrulation. Current Biology 12:2129-2135.
Fisher S, Amacher SL, Halpern M. 1997. Loss of cerebum function ventralizes the zebrafish embryo. Development 124.
Francois V, Solloway M, O'Neill JW, Emery J, Bier E. 1994. Dorsal-ventral patterning of the Drosophila embryo depends on a putative negative growth factor encoded by the short gastrulation gene. Genes & Development 8:2602-2616.
Furthauer M, Van Celst J, Thisse C, Thisse B. 2004. Fgf signalling controls the dorsoventral patterning of the zebrafish embryo. Development 131:2853-2864.
Garcia Abreu J, Coffinier C, Larrain J, Oelgeschlager M, De Robertis EM. 2002. Chordin-like CR domains and the regulation of evolutionarily conserved extracellular signaling systems. Genes 287.

Gavin-Smyth J, Wang YC, Butler I, Ferguson EL. 2013. A genetic network conferring canalization to a bistable patterning system in Drosophila. Curr Biol 23:2296-2302.
Geach TJ, Dale L. 2008. Molecular determinants of Xolloid action in vivo. J Biol Chem 283:27057-27063.
Geng Y, et al. 2011. Follistatin-like 1 (Fstl1) is a bone morphogenetic protein (BMP) 4 signaling antagonist in controlling mouse lung development. PNAS 108.
Genikhovich G, Fried P, Prunster MM, Schinko JB, Gilles AF, Fredman D, Meier K, Iber D, Technau U. 2015. Axis Patterning by BMPs: Cnidarian Network Reveals Evolutionary Constraints. Cell Rep.
Gerhart J. 2000. Inversion of the chordate body axis: are there alternatives? Proc Natl Acad Sci U S A 97.
Glister C, Kemp CF, Knight PG. 2004. Bone morphogenetic protein (BMP) ligands and receptors in bovine ovarian follicle cells: actions of BMP-4, -6 and -7 on granulosa cells and differential modulation of Smad-1 phosphorylation by follistatin. Reproduction 127:239-254.
Glister C, Sunderland SJ, Boland MP, Ireland JJ, Knight PG. 2015. Comparison of bioactivities, binding properties and intrafollicular levels of bovine follistatins. Reproduction 150:85-96.
Goodman S, Albano R, Wardle FC, Matthews G, Tannahill D, Dale L. 1998. BMP1-related metalloproteinases promote the development of ventral mesoderm in early Xenopus embryos. Developmental Biology 195:144-157.
Gourronc F, Ahmad N, Nedza N, Eggleston T, Rebagliati M. 2007. Nodal activity around Kupffer's vesicle depends on the T-box transcription factors Notail and Spadetail and on Notch signaling. Dev Dyn 236.
Gregor T, Tank DW, Wieschaus EF, Bialek W. 2007. Probing the limits to positional information. Cell 130:153-164.
Groppe JC, Greenwald J, Wiater E, Rodriguez-Leon J, Economides AN, Kwiatkowski W, Affolter M, Vale W, Belmonte J, Choe S. 2002. Structural basis of BMP signalling inhibition by the cystine knot protein Noggin. Nature 420.
Groppe JC, et al. 2003. Structural basis of BMP signaling inhibition by Noggin, a novel twelve-membered cystine knot protein. THE JOURNAL OF BONE & JOINT SURGERY 85.
Guillermo Marques MM, Mary Jane Shimell, Katrin Wunnenberg-Stapleton, Ken W. Y. Cho, and Michael B. O'Connor. 1997. Production of a DPP Activity Gradient in the Early Drosophila Embryo through the Opposing Actions of the SOG and TLD Proteins. Cell 91:417-426.
Hama J, Weinstein DC. 2001. Is Chordin a Morphogen? BioEssays 23:121-124.
Hammond KL, van Eeden FJ, Whitfield TT. 2010. Repression of Hedgehog signalling is required for the acquisition of dorsolateral cell fates in the zebrafish otic vesicle. Development 137:1361-1371.
Hans S, Christison J, Liu D, Westerfield M. 2007. Fgf-dependent otic induction requires competence provided by Foxi1 and Dlx3b. BMC Dev Biol 7:5.
Harms PW, Chang C. 2003. Tomoregulin-1 (TMEFF1) inhibits nodal signaling through direct binding to the nodal coreceptor Cripto. Genes Dev 17:2624-2629.
Hashiguchi M, Mullins MC. 2013. Anteroposterior and dorsoventral patterning are coordinated by an identical patterning clock. Development 140:1970-1980.
Hata A, Seoane J, Lagna G, Montalvo E, Hemmati-Brivanlou A, Massague J. 2000. OAZ uses distinct DNA- and protein-binding zinc fingers in separate BMP-Smad and Olf signaling pathways. Cell 100.
He F, Wen Y, Deng J, Lin X, Lu LJ, Jiao R, Ma J. 2008. Probing intrinsic properties of a robust morphogen gradient in Drosophila. Dev Cell 15:558-567.
Hengenius JB, Gribskov M, Rundell AE, Umulis DM. 2014. Making models match measurements: model optimization for morphogen patterning networks. Semin Cell Dev Biol 35:109-123.

Henningfeld KA, Friedle H, Rastegar S, Knochel W. 2002. Autoregulation of Xvent-2B; direct interaction and functional cooperation of Xvent-2 and Smad1. J Biol Chem 277:2097-2103.
Hironaka K, Morishita Y. 2012. Encoding and decoding of positional information in morphogen-dependent patterning. Curr Opin Genet Dev 22:553-561.
Holley S, Jackson P, Sasai Y, Bin L, De Robertis EM, Hoffman M, Ferguson EL. 1995. A conserved system for DV patterning in insects and vertebrates involving sog and chordin. Nature 376.
Holley S, Neul J, Attisano L, Wrana J, Sasai Y, O'Connor MB, De Robertis EM, Ferguson EL. 1996. The Xenopus dorsalizing factor noggin ventralizes Drosophila embryos by preventing DPP from activating its receptor. Cell 86:607-617.
Iemura S, Yamamoto T, Takagi C, Uchiyama H, Natsume T, Shimasaki S, Sugino H, Ueno N. 1998. Direct binding of follistatin to a complex of bone-morphogenetic protein and its receptor inhibits ventral and epidermal cell fates in early Xenopus embryo. Proc. Natl. Acad. Sci. USA 95:9337–9342.
Ikeya M, Fukushima K, Kawada M, Onishi S, Furuta Y, Yonemura S, Kitamura T, Nosaka T, Sasai Y. 2010. Cv2, functioning as a pro-BMP factor via twisted gastrulation, is required for early development of nephron precursors. Dev Biol 337:405-414.
Ikeya M, Kawada M, Kiyonari H, Sasai N, Nakao K, Furuta Y, Sasai Y. 2006. Essential pro-Bmp roles of crossveinless 2 in mouse organogenesis. Development 133:4463-4473.
Ikeya M, Nosaka T, Fukushima K, Kawada M, Furuta Y, Kitamura T, Sasai Y. 2008. Twisted gastrulation mutation suppresses skeletal defect phenotypes in Crossveinless 2 mutant mice. Mech Dev 125:832-842.
Inomata H, Haraguchi T, Sasai Y. 2008. Robust stability of the embryonic axial pattern requires a secreted scaffold for chordin degradation. Cell 134:854-865.
Inomata H, Shibata T, Haraguchi T, Sasai Y. 2013. Scaling of dorsal-ventral patterning by embryo size-dependent degradation of Spemann's organizer signals. Cell 153:1296-1311.
Jasuja R, Allen BL, Pappano WN, Rapraeger AC, Greenspan DS. 2004. Cell-surface heparan sulfate proteoglycans potentiate chordin antagonism of bone morphogenetic protein signaling and are necessary for cellular uptake of chordin. J Biol Chem 279:51289-51297.
Jasuja R, Voss N, Ge G, Hoffman GG, Lyman-Gingerich J, Pelegri F, Greenspan DS. 2006. bmp1 and mini fin are functionally redundant in regulating formation of the zebrafish dorsoventral axis. Mech Dev 123:548-558.
Jay Groppe KR, Aris N. Economides, Neil Stahl, Walter Sebald,, Affolter aM. 1998. Biochemical and Biophysical Characterization of Refolded Drosophila DPP, a Homolog of Bone Morphogenetic Proteins 2 and 4. THE JOURNAL OF BIOLOGICAL CHEMISTRY 273:29052–29065.
Karaulanov E, Knochel S, Niehrs C. 2004. Transcriptional regulation of BMP4 synexpression in transgenic Xenopus. The EMBO Journal 23.
Katsu K, Tokumori D, Tatsumi N, Suzuki A, Yokouchi Y. 2012. BMP inhibition by DAN in Hensen's node is a critical step for the establishment of left-right asymmetry in the chick embryo. Dev Biol 363:15-26.
Kelley R, et al. 2009. A concentration-dependent endocytic trap and sink mechanism converts Bmper from an activator to an inhibitor of Bmp signaling. J Cell Biol 184:597-609.
Khokha M, Hsu D, Brunet L, Dionne M, Harland R. 2003. Gremlin is the BMP antagonist required for maintenance of Shh and Fgf signals during limb patterning. Nat Genetics 34.
Khokha MK, Yeh J, Grammer TC, Harland RM. 2005. Depletion of three BMP antagonists from Spemann's organizer leads to a catastrophic loss of dorsal structures. Dev Cell 8:401-411.
Kishigami S, Mishina Y. 2005. BMP signaling and early embryonic patterning. Cytokine Growth Factor Rev 16:265-278.

Kishimoto Y, Lee K, Zon L, Hammerschmidt M, Schulte-Merker S. 1997. The molecular nature of zebrafish swirl BMP2 function is essential during early dorsoventral patterning. Development 124:4457-4466.
Kisonaite M, Wang X, Hyvonen M. 2016. Structure of Gremlin-1 and analysis of its interaction with BMP-2. Biochem J 473:1593-1604.
Kobayashi K, et al. 2009. Secreted Frizzled-related protein 2 is a procollagen C proteinase enhancer with a role in fibrosis associated with myocardial infarction. Nat Cell Biol 11:46-55.
Koos D, Ho R. 1999. The nieuwkoid dharma homeobox gene is essential for bmp2b repression in the zebrafish pregastrula. Developmental Biology 215:190–207.
Kuo CL, Lam CM, Hewitt JE, Scotting PJ. 2013. Formation of the embryonic organizer is restricted by the competitive influences of Fgf signaling and the SoxB1 transcription factors. PLoS One 8:e57698.
Kuraku S, Kuratani S. 2011. Genome-wide detection of gene extinction in early mammalian evolution. Genome Biol Evol 3:1449-1462.
Kurata T, Nakabayashi J, Yamamoto TS, Mochii M, Ueno N. 2001. Visualization of endogenous BMP signaling during Xenopus development. Differentiation 67:33-40.
Kuroda H, Wessely O, De Robertis EM. 2004. Neural induction in Xenopus: requirement for ectodermal and endomesodermal signals via Chordin, Noggin, beta-Catenin, and Cerberus. PLoS Biol 2:E92.
Kwon HJ, Bhat N, Sweet EM, Cornell RA, Riley BB. 2010. Identification of early requirements for preplacodal ectoderm and sensory organ development. PLoS Genet 6:e1001133.
Lana-Elola E, Tylzanowski P, Takatalo M, Alakurtti K, Veistinen L, Mitsiadis TA, Graf D, Rice R, Luyten FP, Rice DP. 2011. Noggin null allele mice exhibit a microform of holoprosencephaly. Hum Mol Genet 20:4005-4015.
Langdon YG, Mullins MC. 2011. Maternal and zygotic control of zebrafish dorsoventral axial patterning. Annu Rev Genet 45:357-377.
Lapraz F, Besnardeau L, Lepage T. 2009. Patterning of the dorsal-ventral axis in echinoderms: insights into the evolution of the BMP-chordin signaling network. PLoS Biol 7:e1000248.
Larrain J, Bachiller D, Bin L, Agius E, Piccolo S, De Robertis EM. 2000. BMP-binding modules in chordin a model for signalling regulation in the extracellular space. Development 127:821-830.
Larrain J, Oelgeschlager M, Ketpura N, Reversade B, Zakin L, De Robertis EM. 2001. Proteolytic cleavage of Chordin as a switch for the dual activities of Twisted gastrulation in BMP signaling. Development 128:4439-4447.
Lee HS, et al. 2011. Direct response elements of BMP within the PV.1A promoter are essential for its transcriptional regulation during early Xenopus development. PLoS One 6:e22621.
Lee HS, et al. 2002. Transcriptional regulation of Xbr-1a/Xvent-2 homeobox gene: analysis of its promoter region. Biochem Biophys Res Commun 298.
Lee HX, Ambrosio AL, Reversade B, De Robertis EM. 2006. Embryonic dorsal-ventral signaling: secreted frizzled-related proteins as inhibitors of tolloid proteinases. Cell 124:147-159.
Lee HX, Mendes FA, Plouhinec JL, De Robertis EM. 2009. Enzymatic regulation of pattern: BMP4 binds CUB domains of Tolloids and inhibits proteinase activity. Genes Dev 23:2551-2562.
Leung T. 2003. bozozok directly represses bmp2b transcription and mediates the earliest dorsoventral asymmetry of bmp2b expression in zebrafish. Development 130:3639-3649.
Little SC, Mullins MC. 2004. Twisted gastrulation promotes BMP signaling in zebrafish dorsal-ventral axial patterning. Development 131:5825-5835.
---. 2006. Extracellular modulation of BMP activity in patterning the dorsoventral axis. Birth Defects Res C Embryo Today 78:224-242.

---. 2009. Bone morphogenetic protein heterodimers assemble heteromeric type I receptor complexes to pattern the dorsoventral axis. Nat Cell Biol 11:637-643.
Little SC, Tkacik G, Kneeland TB, Wieschaus EF, Gregor T. 2011. The formation of the Bicoid morphogen gradient requires protein movement from anteriorly localized mRNA. PLoS Biol 9:e1000596.
Maeda R, Kobayashi A, Sekine RL, J., Kung H, Maeno M. 1997. Xmsx-1 modifies mesodermal tissue pattern along dorsoventral axis in Xenopus laevis embryo. Development 124.
Maegawa S, Varga M, Weinberg ES. 2006. FGF signaling is required for {beta}-catenin-mediated induction of the zebrafish organizer. Development 133:3265-3276.
Marques CL, Borges AC, Silva AC, Freitas S, Cordenonsi M, Belo JA. 2004. The activity of the Nodal antagonist Cerl-2 in the mouse node is required for correct L/R body axis. Genes & Development 18:2342–2347.
Matthias Hammerschmidt FP, Mary C. Mullins, Donald A. Kane, Fredericus J. M. van Eeden, Michael Granato, Michael Brand, Makoto Furutani-Seiki, Pascal Haffter, Carl-Philipp Heisenberg, Yun-Jin Jiang, Robert N. Kelsh§, Jörg Odenthal, Rachel M. Warga and Christiane Nüsslein-Volhard. 1996. dino and mercedes, two genes regulating dorsal development in the zebrafish embryo. Development 123:95-102.
Matzuk MM, Lu N, Hannes V, Sellheyer K, Roop D, Bradley A. 1995. Multiple Defects and Periatal Death in Mice Deficient in Follistatin. Nature 374.
Maxwell-Garnett JC. 1904. Phil. Trans. R. Soc. London 203.
McMahon J, Takada S, Zimmerman L, Fan C, Harland R, McMahon A. 1998. Noggin-mediated antagonism of BMP signaling is required for growth and patterning of the neural tube and somite. Genes Dev 12.
Michos O, Panman L, Vintersten K, Beier K, Zeller R, Zuniga A. 2004. Gremlin-mediated BMP antagonism induces the epithelial-mesenchymal feedback signaling controlling metanephric kidney and limb organogenesis. Development 131:3401-3410.
Mii Y, Taira M. 2009. Secreted Frizzled-related proteins enhance the diffusion of Wnt ligands and expand their signalling range. Development 136:4083-4088.
Miller-Bertoglio V, Carmany-Rampey A, Furthauer M, Gonzales E, Thisse B, Thisse C, Halpern M, Solnica-Krezel L. 1999. Maternal and zygotic activity of the zebrafish ogon locus antagonizes BMP signaling. Developmental Biology 214:72-86.
Miller-Bertoglio V, Fisher S, Sanchez A, Mullins M, Halpern M. 1997. Differential Regulation of chordin Expression domains in mutant zebrafish. Developmental Biology 192:537-550.
Mitola S, Ravelli C, Moroni E, Salvi V, Leali D, Ballmer-Hofer K, Zammataro L, Presta M. 2010. Gremlin is a novel agonist of the major proangiogenic receptor VEGFR2. Blood 116:3677-3680.
Mizutani CM, Nie Q, Wan FY, Zhang YT, Vilmos P, Sousa-Neves R, Bier E, Marsh JL, Lander AD. 2005. Formation of the BMP activity gradient in the Drosophila embryo. Dev Cell 8:915-924.
Moser M, Binder O, Wu Y, Aitsebaomo J, Ren R, Bode C, Bautch VL, Conlon FL, Patterson C. 2003. BMPER, a Novel Endothelial Cell Precursor-Derived Protein, Antagonizes Bone Morphogenetic Protein Signaling and Endothelial Cell Differentiation. Molecular and Cellular Biology 23:5664-5679.
Muller P, Rogers KW, Jordan BM, Lee JS, Robson D, Ramanathan S, Schier AF. 2012. Differential diffusivity of Nodal and Lefty underlies a reaction-diffusion patterning system. Science 336:721-724.
Muller P, Rogers KW, Yu SR, Brand M, Schier AF. 2013. Morphogen transport. Development 140:1621-1638.
Muraoka O, Shimizu T, Yabe T, Nojima H, Bae YK, Hashimoto H, Hibi M. 2006. Sizzled controls dorso-ventral polarity by repressing cleavage of the Chordin protein. Nat Cell Biol 8:329-338.

Nakamura T, Sugino K, Titani K, Sugino H. 1991. Follistatin, an activin-binding protein, associates with heparan sulfate chains of proteoglycans on follicular granulosa cells. THE JOURNAL OF BIOLOGICAL CHEMISTRY 266.
Nakayama N, et al. 2001. A novel chordin-like protein inhibitor for bone morphogenetic proteins expressed preferentially in mesenchymal cell lineages. Dev Biol 232:372-387.
Nakayama N, et al. 2004. A novel chordin-like BMP inhibitor, CHL2, expressed preferentially in chondrocytes of developing cartilage and osteoarthritic joint cartilage. Development 131:229-240.
Nesterenko AM, Orlov EE, Ermakova GV, Ivanov IA, Semenyuk PI, Orlov VN, Martynova NY, Zaraisky AG. 2015. Affinity of the heparin binding motif of Noggin1 to heparan sulfate and its visualization in the embryonic tissues. Biochem Biophys Res Commun 468:331-336.
Nguyen VH, Schmid B, Trout J, Conners S, Ekker M, Mullins M. 1998. Ventral and lateral regions of the zebrafish gastrula are established by a bmp2b swirl pathway of genes. Developmental Biology 199:93-110.
Nicoli S, Gilardelli CN, Pozzoli O, Presta M, Cotelli F. 2005. Regulated expression pattern of gremlin during zebrafish development. Gene Expr Patterns 5:539-544.
Niehrs C. 2004. Regionally specific induction by the Spemann-Mangold organizer. Nat Rev Genet 5:425-434.
Nieto A. 1999. Reorganizing the Organizer 75 Years On. Cell 98.
Nosaka T, et al. 2003. Mammalian Twisted Gastrulation Is Essential for Skeleto-Lymphogenesis. Molecular and Cellular Biology 23:2969-2980.
O'Connor MB, Umulis D, Othmer HG, Blair SS. 2006. Shaping BMP morphogen gradients in the Drosophila embryo and pupal wing. Development 133:183-193.
O. Wartlick PM, A. Kicheva, T. Bittig, C. Seum, F. Jülicher, M. González-Gaitán. 2011. Dynamics of Dpp Signaling and Proliferation Control. Science 331:1154-1159.
Oelgeschlager M. 2003. The pro-BMP activity of Twisted gastrulation is independent of BMP binding. Development 130:4047-4056.
Oelgeschlager M, Kuroda H, Reversade B, De Robertis EM. 2003. Chordin Is Required for the Spemann Organizer Transplantation Phenomenon in Xenopus Embryos. Developmental Cell 4:219-230.
Oelgeschlager M, Larrain J, Geissert D, De Robertis EM. 2000. The evolutionarily conserved BMP-binding protein Twisted gastrulation promotes BMP signalling. Nature 405.
Otsuka F, Moore RK, Iemura S, Ueno N, Shimasaki S. 2001. Follistatin inhibits the function of the oocyte-derived factor BMP-15. Biochem Biophys Res Commun 289:961-966.
Paine-Saunders S, Viviano BL, Economides AN, Saunders S. 2002. Heparan sulfate proteoglycans retain Noggin at the cell surface: a potential mechanism for shaping bone morphogenetic protein gradients. J Biol Chem 277:2089-2096.
Pappano WN, Steiglitz BM, Scott IC, Keene DR, Greenspan DS. 2003. Use of Bmp1/Tll1 Doubly Homozygous Null Mice and Proteomics To Identify and Validate In Vivo Substrates of Bone Morphogenetic Protein 1/Tolloid-Like Metalloproteinases. Molecular and Cellular Biology 23:4428-4438.
Pargett M, Umulis DM. 2013. Quantitative model analysis with diverse biological data: applications in developmental pattern formation. Methods 62:56-67.
Peluso CE, Umulis D, Kim YJ, O'Connor MB, Serpe M. 2011. Shaping BMP morphogen gradients through enzyme-substrate interactions. Dev Cell 21:375-383.
Pera EM, De Robertis EM. 2000. A direct screen for secreted proteins in Xenopus embryos identifies distinct activities for the Wnt antagonists Crescent and Frzb-1. Mechanisms of Development 96.

Pfirrmann T, et al. 2015. Molecular mechanism of CHRDL1-mediated X-linked megalocornea in humans and in Xenopus model. Hum Mol Genet 24:3119-3132.
Pi X, et al. 2012. LRP1-dependent endocytic mechanism governs the signaling output of the bmp system in endothelial cells and in angiogenesis. Circ Res 111:564-574.
Piccolo S, Agius E, Leyns L, Bhattacharyya S, Grunz H, Bouwmeester T, De Robertis EM. 1999. The head inducer Cerberus is a multifunctional antagonist of Nodal, BMP and Wnt signals. Nature 397.
Ploper D, Lee HX, De Robertis EM. 2011. Dorsal-ventral patterning: Crescent is a dorsally secreted Frizzled-related protein that competitively inhibits Tolloid proteases. Dev Biol 352:317-328.
Plouhinec JL, Zakin L, Moriyama Y, De Robertis EM. 2013. Chordin forms a self-organizing morphogen gradient in the extracellular space between ectoderm and mesoderm in the Xenopus embryo. Proc Natl Acad Sci U S A 110:20372-20379.
Ramel MC, Hill CS. 2013. The ventral to dorsal BMP activity gradient in the early zebrafish embryo is determined by graded expression of BMP ligands. Dev Biol 378:170-182.
Rentzsch F, Zhang J, Kramer C, Sebald W, Hammerschmidt M. 2006. Crossveinless 2 is an essential positive feedback regulator of Bmp signaling during zebrafish gastrulation. Development 133:801-811.
Reversade B, De Robertis EM. 2005. Regulation of ADMP and BMP2/4/7 at opposite embryonic poles generates a self-regulating morphogenetic field. Cell 123:1147-1160.
Robertis EMD. 2008. Evo-Devo: Variations on Ancestral Themes. Cell 132:185–195.
Rogers KW, Schier AF. 2011. Morphogen gradients: from generation to interpretation. Annu Rev Cell Dev Biol 27:377-407.
Ross J, Osamu S, Vilmos P, Petryk A, Kim H, Gaudenz K, Hermanson S, Ekker S, O'Connor MB, Marsh JL. 2001. Twisted gastrulation is a conserved extracellular BMP antagonist. Nature 410.
Rushlow CA, Shvartsman SY. 2012. Temporal dynamics, spatial range, and transcriptional interpretation of the Dorsal morphogen gradient. Curr Opin Genet Dev 22:542-546.
Sajan SA, Rubenstein JL, Warchol ME, Lovett M. 2011. Identification of direct downstream targets of Dlx5 during early inner ear development. Hum Mol Genet 20:1262-1273.
Salic A, Kroll K, Evans L, Kirschner M. 1997. Sizzled a secreted Xwnt8 antagonist expressed in the ventral marginal zone of Xenopus embryos. Development 124.
Sander K, Schmidt-Ott U. 2004. Evo-devo aspects of classical and molecular data in a historical perspective. J Exp Zool B Mol Dev Evol 302:69-91.
Sansom SN, Livesey FJ. 2009. Gradients in the brain: the control of the development of form and function in the cerebral cortex. Cold Spring Harb Perspect Biol 1:a002519.
Sasai Y, De Robertis EM. 1997. Ectodermal patterning in vertebrate embryos. Dev Biol 182:5-20.
Schier AF, Talbot WS. 2005. Molecular genetics of axis formation in zebrafish. Annu. Rev. Genet 39:561-613.
Schilling TF, Nie Q, Lander AD. 2012. Dynamics and precision in retinoic acid morphogen gradients. Curr Opin Genet Dev 22:562-569.
Schmid B, Furthauer M, Conners S, Trout J, Thisse B, Thisse C. 2000a. Equivalent genetic roles for bmp7snailhouse and bmp2bswirl in dorsoventral pattern formation. Development 127.
Schmid B, Furthauer M, Conners S, Trout J, Thisse B, Thisse C, Mullins M. 2000b. Equivalent genetic roles for bmp7snailhouse and bmp2bswirl in dorsoventral pattern formation. Development 127:957-967.
Schneyer AL, Rzucidlo D, Sluss P, Cowley W. 1994. Characterization of unique binding kinetics of follistatin and activin or inhibin in serum. Endocrinology 135:667-674.

Schohl A, Fagotto F. 2003. A role for maternal beta-catenin in early mesoderm induction in Xenopus. The EMBO Journal 22:3303-3313.
Schuler-Metz A, Knochel S, Kaufmann E, Knochel W. 2000. The homeodomain transcription factor Xvent-2 mediates autocatalytic regulation of BMP-4 expression in Xenopus embryos. J Biol Chem 275:34365-34374.
Schulte-Merker S, Lee K, McMahon A, Hammerschmidt M. 1997. The zebrafish organizer requires chordino. Nature 387:861-863.
Schweickert A, Vick P, Getwan M, Weber T, Schneider I, Eberhardt M, Beyer T, Pachur A, Blum M. 2010. The nodal inhibitor Coco is a critical target of leftward flow in Xenopus. Curr Biol 20:738-743.
Scott IC, et al. 1999. Mammalian BMP-1/Tolloid-Related Metalloproteinases, Including Novel Family Member Mammalian Tolloid-Like 2, Have Differential Enzymatic Activities and Distributions of Expression Relevant to Patterning and Skeletogenesis. Developmental Biology 213:283-300.
Scott IC, Blitz IL, Pappano WN, Maas S, Cho KW, Greenspan DS. 2001. Homologues of Twisted gastrulation are extracellular cofactors in antagonism of BMP signalling. Nature 410.
Seemann P, et al. 2009. Mutations in GDF5 reveal a key residue mediating BMP inhibition by NOGGIN. PLoS Genet 5:e1000747.
Serpe M, Umulis D, Ralston A, Chen J, Olson DJ, Avanesov A, Othmer H, O'Connor MB, Blair SS. 2008. The BMP-binding protein Crossveinless 2 is a short-range, concentration-dependent, biphasic modulator of BMP signaling in Drosophila. Dev Cell 14:940-953.
Shibata M, Itoh M, Hikasa H, Taira S, Taira M. 2005. Role of crescent in convergent extension movements by modulating Wnt signaling in early Xenopus embryogenesis. Mech Dev 122:1322-1339.
Shilo BZ, Haskel-Ittah M, Ben-Zvi D, Schejter ED, Barkai N. 2013. Creating gradients by morphogen shuttling. Trends Genet 29:339-347.
Shimizu T, Yamanaka Y, Seung-Lim R, Hashimoto H, Yabe T, Hirata T, Bae YK, Hibi M, Hirano T. 2000. Cooperative roles of Bozozok/Dhama and Nodal-Related protein in the formation of the dorsal organizer in zebrafish. Mech Dev 91:293-303.
Shimmi O, Umulis D, Othmer H, O'Connor MB. 2005. Facilitated transport of a Dpp/Scw heterodimer by Sog/Tsg leads to robust patterning of the Drosophila blastoderm embryo. Cell 120:873-886.
Sidis Y, Mukherjee A, Keutmann H, Delbaere A, Sadatsuki M, Schneyer A. 2006. Biological activity of follistatin isoforms and follistatin-like-3 is dependent on differential cell surface binding and specificity for activin, myostatin, and bone morphogenetic proteins. Endocrinology 147:3586-3597.
Solnica-Krezel L, Driever W. 2001. The role of the homeodomain protein Bozozok in Zebrafish axis formation. Int J Dev Biol 45:299-310.
Song AMaX. 2010. Point Set Registration: Coherent Point Drift. IEEE TRANSACTIONS ON PATTERN ANALYSIS AND MACHINE INTELLIGENCE 32.
Spirov A, Fahmy K, Schneider M, Frei E, Noll M, Baumgartner S. 2009. Formation of the bicoid morphogen gradient: an mRNA gradient dictates the protein gradient. Development 136:605-614.
Stafford DA, Monica SD, Harland RM. 2014. Follistatin interacts with Noggin in the development of the axial skeleton. Mech Dev 131:78-85.
Stefano Piccolo EA, Bin Lu, Shelley Goodman, Leslie Dale, and Eddy M. De Robertis. 1997. Cleavage of Chordin by Xolloid Metalloprotease Suggests a Role for Proteolytic Processing in the Regulation of Spemann Organizer Activity. Cell 91:407-416.

Stefano Piccolo YS, Bin Lu, Eddy M. De Robertis. 1996. Dorsoventral Patterning in Xenopus: Inhibition of Ventral Signals by Direct Binding of Chordin to BMP-4. Cell 86:589-598.
Sun J, Zhuang FF, Mullersman JE, Chen H, Robertson EJ, Warburton D, Liu YH, Shi W. 2006. BMP4 activation and secretion are negatively regulated by an intracellular gremlin-BMP4 interaction. J Biol Chem 281:29349-29356.
Sutherland DJ, Li M, Liu XQ, Stefancsik R, Raftery LA. 2003. Stepwise formation of a SMAD activity gradient during dorsal-ventral patterning of the Drosophila embryo. Development 130:5705-5716.
Suzuki N, Labosky PA, Furuta Y, Hargett L, Dunn R, Fogo A, Takahara K, Peters D, Greenspan DS, Hogan BL. 1996. Failure of ventral body wall closure in mouse embryos lacking a procollagen C-proteinase encoded by Bmp1. Development 122.
Sylva M, Moorman AF, van den Hoff MJ. 2013. Follistatin-like 1 in vertebrate development. Birth Defects Res C Embryo Today 99:61-69.
Takehara-Kasamatsu Y, et al. 2007. Characterization of follistatin-related gene as a negative regulatory factor for activin family members during mouse heart development. The Journal of Medical Investigation 54.
Tanegashima K, Haramoto Y, Yokota C, Takahashi S, Asashima M. 2004. Xantivin suppresses the activity of EGF-CFC genes to regulate nodal signaling. Int J Dev Biol 48:275-283.
TC. L. 1995. DorsoVentral Axis Inversion. Nature 373.
Thisse B, Thisse C. 2015. Formation of the vertebrate embryo: Moving beyond the Spemann organizer. Semin Cell Dev Biol 42:94-102.
Thompson TB, Lerch TF, Cook RW, Woodruff TK, Jardetzky TS. 2005. The structure of the follistatin:activin complex reveals antagonism of both type I and type II receptor binding. Dev Cell 9:535-543.
Thomsen G. 1997. Antagonism within and around the organizer: BMP inhibitrs in vertebrate body patterning. TIG 13.
Tribulo C, Aybar MJ, Nguyen VH, Mullins MC, Mayor R. 2003. Regulation of Msx genes by a Bmp gradient is essential for neural crest specification. Development 130:6441-6452.
Troilo H, et al. 2016. Structural characterization of twisted gastrulation provides insights into opposing functions on the BMP signalling pathway. Matrix Biol.
Troilo H, Zuk AV, Tunnicliffe RB, Wohl AP, Berry R, Collins RF, Jowitt TA, Sengle G, Baldock C. 2014. Nanoscale structure of the BMP antagonist chordin supports cooperative BMP binding. Proc Natl Acad Sci U S A 111:13063-13068.
Tuazon FB, Mullins MC. 2015. Temporally coordinated signals progressively pattern the anteroposterior and dorsoventral body axes. Semin Cell Dev Biol 42:118-133.
Tucker JA, Mintzer KA, Mullins MC. 2008. The BMP signaling gradient patterns dorsoventral tissues in a temporally progressive manner along the anteroposterior axis. Dev Cell 14:108-119.
Umulis DM, Shimmi O, O'Connor MB, Othmer HG. 2010. Organism-scale modeling of early Drosophila patterning via bone morphogenetic proteins. Dev Cell 18:260-274.
Varga M, Maegawa S, Bellipanni G, Weinberg ES. 2007. Chordin expression, mediated by Nodal and FGF signaling, is restricted by redundant function of two beta-catenins in the zebrafish embryo. Mech Dev 124:775-791.
Vitt U, Sheau H, Hsueh A. 2001. Evolution and Classification of Cystine Knot-Containing Hormones and Related Extracellular Signaling Molecules. Molecular Endocrinology 15.
Viviano BL, Paine-Saunders S, Gasiunas N, Gallagher J, Saunders S. 2004. Domain-specific modification of heparan sulfate by Qsulf1 modulates the binding of the bone morphogenetic protein antagonist Noggin. J Biol Chem 279:5604-5611.

Vonica A, Brivanlou AH. 2007. The left-right axis is regulated by the interplay of Coco, Xnr1 and derriere in Xenopus embryos. Dev Biol 303:281-294.
Wang Y, Ferguson EL. 2005. Spatial bistability of Dpp–receptor interactions during Drosophila dorsal–ventral patterning. Nature 434:225-229.
Wardle FC, Welch JV, Dale L. 1999. Bone morphogenetic protein 1 regulates dorsal-ventral patterning in early Xenopus embryos by degrading chordin, a BMP4 antagonist. Mech Dev 86:75-85.
Winstanley J, Sawala A, Baldock C, Ashe HL. 2015. Synthetic enzyme-substrate tethering obviates the Tolloid-ECM interaction during Drosophila BMP gradient formation. Elife 4.
Xie J, Fisher S. 2005. Twisted gastrulation enhances BMP signaling through chordin dependent and independent mechanisms. Development 132:383-391.
Xue Y, Zheng X, Huang L, Xu P, Ma Y, Min Z, Tao Q, Tao Y, Meng A. 2014. Organizer-derived Bmp2 is required for the formation of a correct Bmp activity gradient during embryonic development. Nat Commun 5:3766.
Yabe SI. 2003a. FRL-1, a member of the EGF-CFC family, is essential for neural differentiation in Xenopus early development. Development 130:2071-2081.
Yabe T. 2003b. Ogon/Secreted Frizzled functions as a negative feedback regulator of Bmp signaling. Development 130:2705-2716.
Zakin L, Chang EY, Plouhinec JL, De Robertis EM. 2010. Crossveinless-2 is required for the relocalization of Chordin protein within the vertebral field in mouse embryos. Dev Biol 347:204-215.
Zakin L, De Robertis EM. 2004. Inactivation of mouse Twisted gastrulation reveals its role in promoting Bmp4 activity during forebrain development. Development 131:413-424.
Zakin L, Metzinger CA, Chang EY, Coffinier C, De Robertis EM. 2008. Development of the vertebral morphogenetic field in the mouse: interactions between Crossveinless-2 and Twisted Gastrulation. Dev Biol 323:6-18.
Zhang F, Beaudet JM, Luedeke DM, Walker RG, Thompson TB, Linhardt RJ. 2012. Analysis of the interaction between heparin and follistatin and heparin and follistatin-ligand complexes using surface plasmon resonance. Biochemistry 51:6797-6803.
Zhang JL, Huang Y, Qiu LY, Nickel J, Sebald W. 2007a. von Willebrand factor type C domain-containing proteins regulate bone morphogenetic protein signaling through different recognition mechanisms. J Biol Chem 282:20002-20014.
Zhang JL, Patterson LJ, Qiu LY, Graziussi D, Sebald W, Hammerschmidt M. 2010. Binding between Crossveinless-2 and Chordin von Willebrand factor type C domains promotes BMP signaling by blocking Chordin activity. PLoS One 5:e12846.
Zhang YT, Lander AD, Nie Q. 2007b. Computational analysis of BMP gradients in dorsal-ventral patterning of the zebrafish embryo. J Theor Biol 248:579-589.
Zimmerman L, Jesus-Escobar J, Harland RM. 1996. The Spemann organizer signal noggin binds and inactivates bone morphogenetic protein 4. Cell 86:599-606.